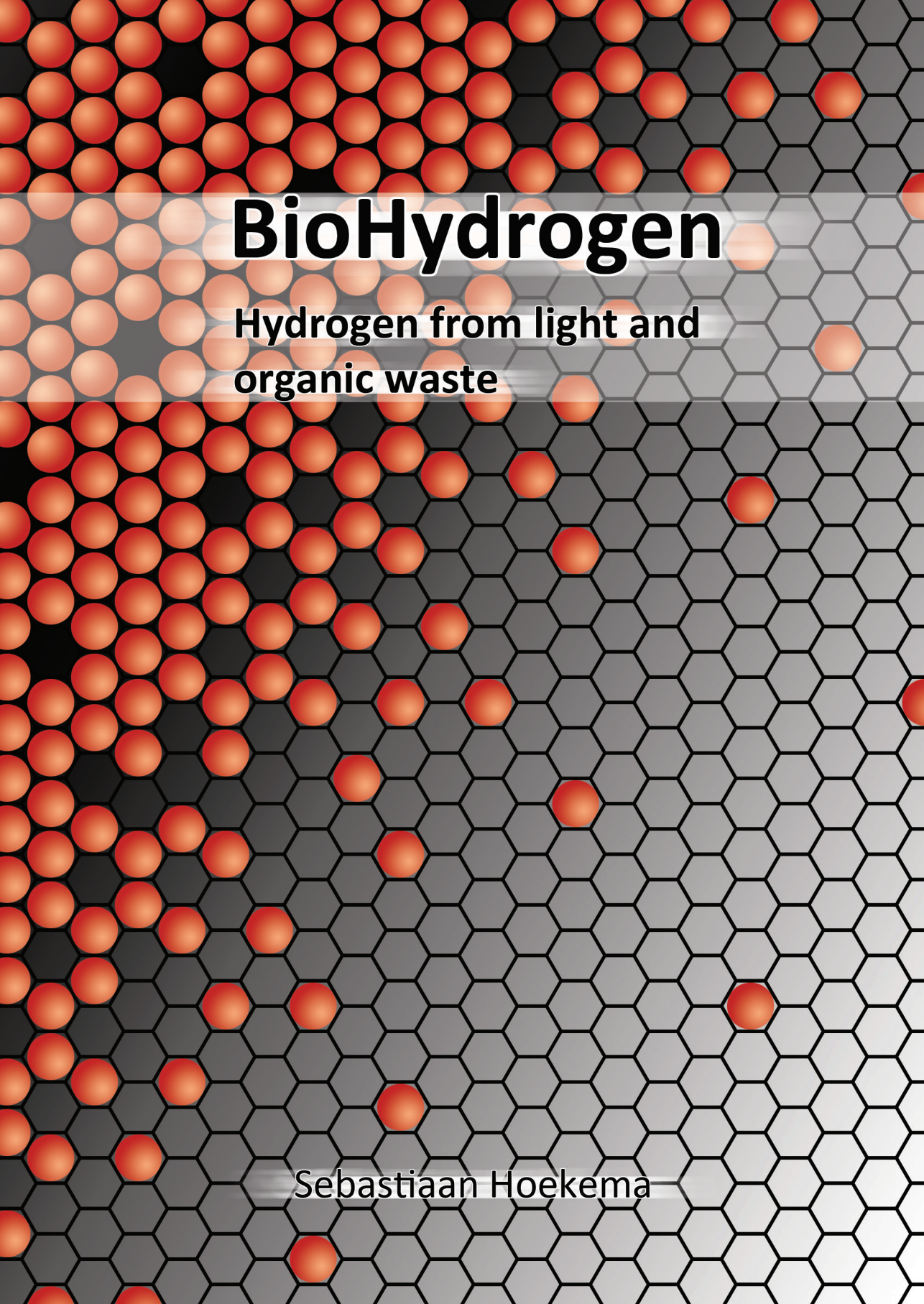

BioHydrogen

Hydrogen from light and organic waste

Sebastiaan Hoekema

BioHydrogen

Hydrogen from light and organic waste

Sebastiaan Hoekema

Thesis committee

Promotor
Prof. Dr R. H. Wijffels
Professor of Bioprocess Engineering
Wageningen University

Co-promotors
Dr. M.G.J. Janssen
Assistent professor of Bioprocess Engineering
Wageningen University

Prof. Dr J. Tramper
Professor of Bioprocess Engineering
Wageningen University

Other members
Prof. P. Lindblad, Uppsala University, Sweden
Prof. Dr J.H. Bitter, Wageningen University
Prof. Dr A.J.M. Stams, Wageningen University
Dr. A.E. Mars, Wageningen University

This research was conducted under the auspices of the Graduate School VLAG (Advanced studies in Food Technology, Agrobiotechnology, Nutrition and Health Sciences).

BioHydrogen

Hydrogen from light and organic waste

Sebastiaan Hoekema

Thesis
submitted in fulfilment of the requirements for the degree of doctor
at Wageningen University
by the authority of the Rector Magnificus
Prof. Dr M.J. Kropff,
In the presence of the
Thesis Committee appointed by the Academic Board
to be defended in public
on Tuesday 14th of October 2014
at 4 p.m. in the Aula.

Hoekema, S.
BioHydrogen: Hydrogen from light and organic waste,
228 pages.

PhD thesis, Wageningen University, Wageningen, NL (2014)
With references, with summaries in Dutch and English.

ISBN 978-94-6257-105-1

Dit proefschrift is opgedragen aan
Jan en Joke Hoekema

Contents

Chapter 1

Introduction and thesis outline

1. Introduction and thesis outline

Introduction

With the rising global energy demand, the need for renewable alternatives to fossil fuels becomes more apparent. One class of renewable alternatives is energy derived from biological systems. In this thesis, one of the possibilities within this class, the bacteriological conversion of light and organic acids to hydrogen, is studied.

Global energy demand

The projected world energy demand will continue to rise while crude oil production capacity decreases, as natural reserves are rapidly wearing out (Birol 2010; Dudley 2011). In Figure 1.1, the total global energy demand in time is presented from 1990 to 2010, divided into its main resources. The total global energy demand has increased steadily in this time interval. The contribution of fossil fuels (oil, natural gas and coal) to the global energy supply has largely remained unaltered at around 88%. The contribution of renewable energies including hydroelectricity increased from 6.3 to 7.6%, of which 80-95% can be attributed to hydroelectricity (Dudley 2011).

Aside from an inevitable shortage in energy supply in the near future, other disadvantages of large-scale combustion of fossil fuels are the associated adverse effects on the air quality in the troposphere, acid deposition, the depletion of the stratospheric ozone layer and global warming, resulting largely from SO_x, NO_x and CO_2 -emissions.

The most efficient way of reducing this effect is by a reduction in energy consumption, but in view of the developments in world population increase and economic growth, the global energy demand is expected to rise fast, resulting in a requirement for alternatives for fossil fuels.

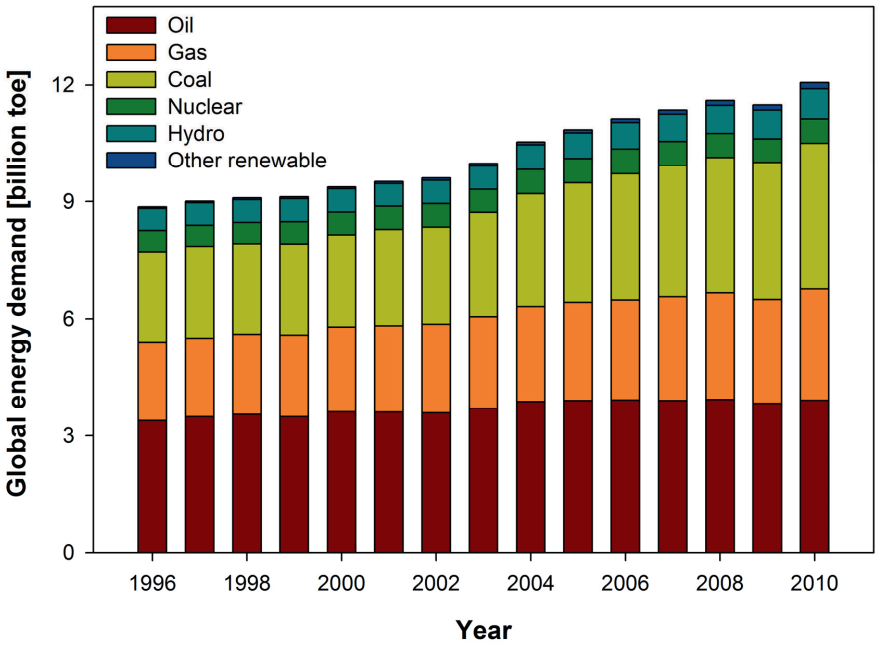

Figure 1.1 Development of the global energy consumption, divided into its main resources (data adapted from (Dudley 2011), toe = tonnes oil equivalent; 1 tonne oil equivalent = 41.85 GJ.)

Alternatives to fossil fuels

As the establishment of an alternate energy supply that can alleviate these drawbacks will take a considerable amount of time, much effort is invested in the development of promising near-future scenarios. In the current energy supply, a non-renewable, net CO_2 generating solid/liquid energy carrier mix is applied. It is generally accepted that scenarios for a stable future energy supply require the transition to renewable, carbon neutral

energy carriers, in order to limit the afore-mentioned disadvantages associated with the combustion of fossil fuels.

A vast array of alternative energy yielding technologies is under investigation. The change process will have to be executed gradually, resulting in intermediate solutions that do not fully comply with the desired carbon neutral energy supply. A gradual shift towards de-carbonation of fossil fuels by sequestration of solid carbon and the application of carbon neutral bio-based fuels like biodiesel (Chisti 2007; Ma and Hanna 1999) and hydrogen is often proposed. When biofuels are considered, the degree to which land surface area will be available is not certain, as it will have to compete with agriculture aimed at food production.

In many aspects, hydrogen gas is an ideal fuel. Not only as an alternative energy source, but also as a highly efficient energy carrier (Zajic et al. 1978). The hydrogen molecule has the highest energy content per unit of weight (120.7 $kJ \cdot g^{-1}$) in comparison to other energy sources, and its combustion yields only energy and water. Hydrogen gas is currently predominantly used as a bulk chemical in process industry, mainly in crude oil refining and the production of ammonia and methanol. It has been put forward by many scientists as the chemical energy storage form of the future, mainly in transportation and domestic applications (Armaroli and Balzani 2011; Balat 2009).

Roughly all hydrogen produced today is generated by steam reforming of hydrocarbons (mainly methane, but oil and coal are also used), followed by gas separation using zeolites and pressure swing absorption. This process is the most cost efficient and about a factor three more cost efficient when compared to the electrolysis of water (Lipman 2004).

The largest renewable energy source is the sun, exemplified by the fact that more energy impings on the earth in one hour then all energy consumed by man in one year (Lewis and Nocera 2006). In contrast, only about 0.25% of the global energy and about 0.5% of all applied fuels is generated by using renewable solar energy. The direct conversion of solar energy to electricity has recently made significant progress, with relatively simple thin layer silicon PV cells that do not contain any ‘rare earth’ metals reaching stable light to electricity conversion efficiencies of 8.54% (Chang et al. 2012). The downside of this direct

solar to electrical energy conversion for general energy supply is that it is intermittent. For that reason, energy generation and use are not synchronised, and a second energy conversion is required in order to store the harvested solar energy. Lewis and Nocera (Lewis and Nocera 2006) suggested that the efficient capture and storage of solar energy in the form of hydrogen or hydrocarbons has great potential for future energy supply. The efficiencies of these methods, however, need to be much higher than the ones reported to date for plant and algal photosynthesis.

Challenges related to the application of hydrogen as an energy carrier

Obviously, there are still some challenges that need to be solved. First, sufficient amounts of hydrogen need to be made available to cover a significant part of the global energy demand.

A second prerequisite is an infrastructure for the distribution of hydrogen to the end user. Such a separate distribution network will require significant investment costs. This becomes a serious restraint only when hydrogen supply really takes off, as during a transition phase the hydrogen produced for energy supply purposes can be suppleted to the natural gas supply without the need for an additional distribution network.

Another issue that requires attention is the storage of hydrogen gas. The energy density of hydrogen gas is very low. Its application as an energy carrier in for instance the transportation sector is only feasible if the resulting driving range is reasonable, for instance 500 km. As a result, an automotive hydrogen energy storage system needs to have a high energy density at low cost in order to be a suitable candidate for successful implementation. A hydrogen storage technology that meets these targets is currently not available (Chalk and Miller 2006; David 2005; Ross 2006). However, future developments might provide such technology.

The energetic efficiency of a proton exchange membrane fuel cell (or PEM fuel cell in short) ranges between 40 and 60%. This is far better than the energetic efficiency of an internal combustion engine, which is typically around 20%. As a result of their precious metal content (mostly platinum), PEM fuel cells are expensive. Their performance decrease over time and their price are fields in which improvement is required prior to large scale application in the automotive sector (Chalk and Miller 2006).

Hydrogen from biomass

There are several technologies available for the carbon neutral production of hydrogen from biomass feedstocks. Figure 1.2 gives an overview of these technologies, with a sub-division into biochemical and thermochemical routes.

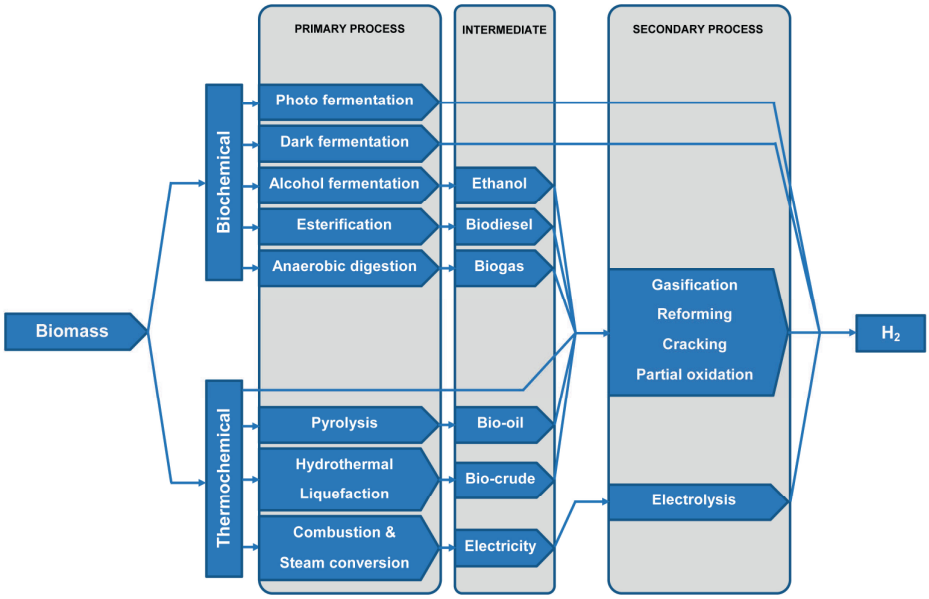

Figure 1.2 Overview of the technologies that are available for the conversion of biomass to hydrogen, adapted from Muradov and Veziroğlu (Muradov and Veziroğlu 2008).

Two stage hydrogen fermentation

The first two main technologies displayed in Figure 1.2 are biochemical fermentation technologies that result in direct hydrogen formation, without the formation of any intermediate energy carrier.

Hydrogen production by fermentative bacteria from sugars in dark fermentation proceeds according to stoichiometry Equation 1.1.

Equation 1.1 $C_6H_{12}O_6 + 4\ H_2O \rightarrow 2\ CH_3COO^- + 4\ H_2 + 2\ HCO_3^- + 4\ H^+ \quad \Delta G_0 = -206.1\ kJ{\cdot}mol^{-1}$

This process can be executed efficiently by extreme thermophilic micro-organisms like *Caldicellulosiruptor saccharolyitcus* and *Thermotoga elfii* and it has been studied extensively (van Niel et al. 2002). A further conversion of the formed acetate is not possible by most fermentative organisms, because the Gibbs free energy change (ΔG_0) of such a conversion has a positive value (see Equation 1.2), meaning that it is thermodynamically unfavourable.

Equation 1.2 $CH_3COO^- + 4\ H_2O \rightarrow 2\ HCO_3^- + 4\ H_2 + H^+ \quad \Delta G_0 = 104.6\ kJ{\cdot}mol^{-1}$

Equation 1.3 $C_6H_{12}O_6 + 12\ H_2O \rightarrow 12\ H_2 + 6\ HCO_3^- + 6\ H^+ \quad \Delta G_0 = 3.0\ kJ{\cdot}mol^{-1}$

In order to achieve complete conversion of glucose via acetate to hydrogen, according to Equation 1.3, two fermentative processes can be combined. In the first process step, glucose is fermented to hydrogen and acetate according to Equation 1.1, after which the acetate is converted to additional hydrogen in a second process step according to Equation 1.2.

This second process step can only proceed if additional energy is supplied to the system. This additionally required energy can be light energy, supplied to purple non-sulphur

bacteria (or PNS bacteria in short). This class of bacteria is capable of photoheterotrophic growth and hydrogen production on reduced organic substrates and light energy.

The combination of dark and photo fermentation creates the possibility of a complete conversion of residual carbohydrates, originating from for instance organic waste streams (Chen et al. 2008; Fascetti et al. 1998; Lee et al. 2002; Sasaki 1998) or especially grown energy crops. The process is depicted schematically in Figure 1.3. This process outline formed the basis for two projects, in which the chair group of Bio Process Engineering of Wageningen UR took part: The EU FP5 project Biohydrogen and the Dutch project EET Biological Hydrogen Production (2000-2003).

Most biomass sources contain significant amounts of lignocellulose, and as its structure causes it to be inaccessible to biological conversion, a pre-treatment is required (Claassen et al. 1999). The pre-treated biomass slurry is then fed to a bioreactor in which the microbial conversion according to Equation 1.1 takes place. Van Groenestijn proposed the application of thermophilic organisms in a trickling filter bioreactor for this conversion, as this concept allows a low H_2 partial pressure, which is a pre-requisite for the reaction in Equation 1.1 to take place (Van Groenestijn et al. 2002).

In a second bioreactor, the organic acids that were generated in the first are converted to additional hydrogen in a photoheterotrophic fermentation using PNS bacteria. We proposed a flat panel photobioreactor for this conversion, equipped with gas-recirculation for sufficient mixing in order to supply light energy to the entire photoheterotrophic bacterial culture (Hoekema et al. 2002).

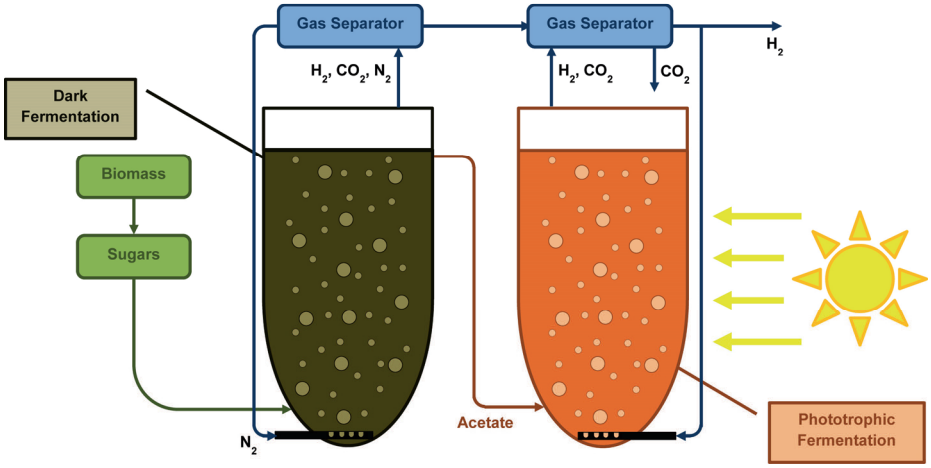

Figure 1.3 Graphical representation of the proposed two-stage bacterial fermentative process for the complete conversion of biomass to hydrogen.

Metabolism of the purple non-sulphur bacteria

PNS bacteria have a very versatile metabolism, resulting in their capability of growing under a wide variety of environmental conditions and their compatibility with a large number of substrates (Tabita 1995).

This class of bacteria is not capable of using sulphur compounds as reducing agent for growth. PNS bacteria are anoxygenic, as they perform photosynthesis without oxygen evolution. This is essential, as oxygen inhibits the activity of the enzymes that catalyse the production of hydrogen, as will be covered shortly.

Light harvesting and photosynthesis

All PNS bacteria belong to the α and β subdivisions of the phylum proteo-bacteria and are pigmented with bacteriochlorophyll (Bchl) and carotenoids, which give them colours ranging between purple, red, brown and orange (Bryant and Frigaard 2006). The complete

photosynthetic complex of PNS bacteria is located on chromatophores, which are small encapsulations in the bacterial cell membrane, as can be seen in Figure 1.4A, an electron microscopic picture of Rhodobacter *capsulatus* cells. A graphic representation of the main constituents of the cell membrane associated photosynthetic complex present in a chromatophore in is given in Figure 1.4B.

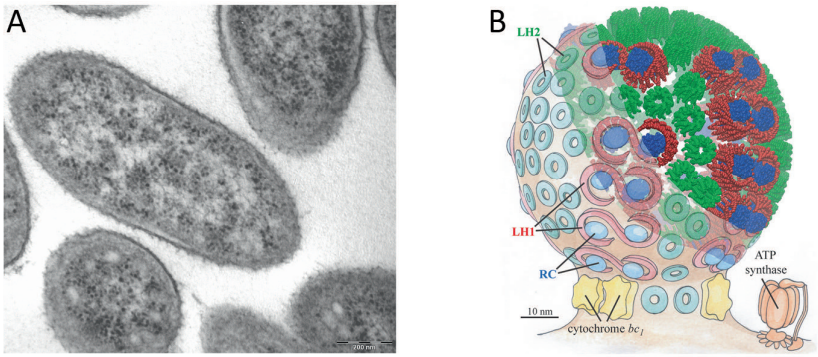

Figure 1.4 (A) An electron microscopic picture of *Rhodobacter capsulatus* cells, on which the individual chromatophores can be identified as black spherical bodies that form an integral part of the cell membrane (Borghese et al. 2004). (B) Graphic representation of the main constituents of the cell membrane associated photosynthetic complex of PNS bacteria inside a chromatophore. LH light harvesting complex; RC reaction center; ATP adenosine tri phosphate (Şener et al. 2007).

PNS bacteria have a distinct light absorption spectrum, resulting from the light absorbing properties of their light harvesting complex. Light harvesting complex 2 contains carotenoids that typically absorb photons in the 400-550 nm range, while light harvesting complex 1 contains bacteriochlorophylls, that have photon absorption maxima in the 750-950 nm range (see Figure 1.4B for the location of the light harvesting complexes

within a chromatophore). Figure 1.5A displays the wavelength dependent light absorbance characteristics of photo-heterotrophically grown *Rhodobacter capsulatus* NCIMB 11773 cells. Figure 1.5A also illustrates that the biomass specific absorption capacity increases at elevated biomass concentrations.

This is the result of a physiological response, triggered by a decrease in light availability within the culture, a phenomenon that will be investigated further in this thesis.

In Figure 1.5B, the spectral irradiance spectrum of two light sources is given. Phototrophic processes should finally be driven by the sun in order to be both energy-effective and for that reason also cost-effective. Tungsten-Halogen lamps, however, are used when conducting laboratory experiments with continuous cultures, because they are rich in far-red radiation as opposed to other artificial light sources.

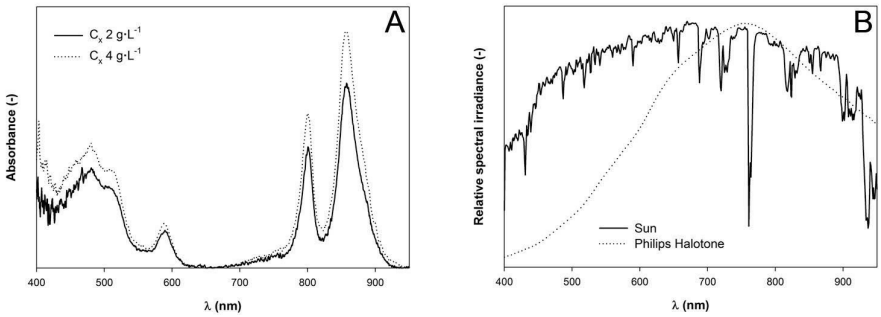

Figure 1.5 Biomass specific light absorption coefficient of photo-heterotrophically grown *Rhodobacter capsulatus* NCIMB 11773 cells at low (solid line) and high (dotted line) cell density (A). Spectral irradiance of two light sources: the sun (solid line, (ASTM 2005)) and a Philips Halotone halogen-tungsten lamp (dotted line) (B). λ wavelength; nm nanometers.

The photosynthetic complex of PNS bacteria contains one photosystem, which in turn contains a reaction center, referred to as P_{870} (as its light absorbance is maximal at 870 nm). The reaction center in fact is a special pair of Bchl-a molecules. Within the reaction

center, photon absorption leads to a singlet excited electronic state. This process is referred to as primary charge separation. After primary charge separation has taken place, the electron is transferred via a cascade of redox mediators, as displayed in Figure 1.6A. The corresponding free energy levels and time scales of the individual redox reactions are displayed in Figure 1.6B.

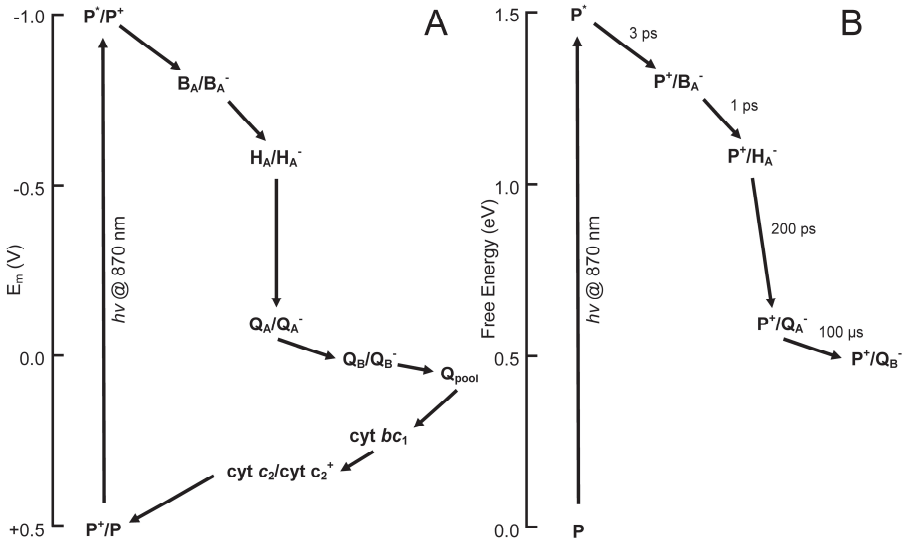

Figure 1.6 Electron transfer in the *Rhodobacter sphaeroides* photosystem. (A) redox potential of the electron transfer intermediates. (B) free energy and time scales of charge separation in the reaction center. Adapted from Fajer, Kirmaier and Holten and Tang et al. (Fajer et al. 1975; Kirmaier and Holten 1987; Tang et al. 1999). E_m redox midpoint potential; hv light flash; P primary electron donor P_{870}; B_A monomer bactereochlorophyll; H_A bactereopheophytin; Q ubiquinone; cyt cytochrome. Redox couples are denoted in reactant/product format.

Cyclic electron transfer

The electron that was initially excited in the reaction center can thus flow back to it to be excited again (Figure 1.6A), resulting in a continuous and cyclic electron transfer.

The light-induced electron transfer is coupled to proton transfer (Paddock et al. 2003), and results in a proton motive force. First, the electron transfer results in a reduced quinol molecule. The reduced quinol molecule transfers its protons and electrons to cytochrome bc_1. This complex transports them across the chromatophore membrane and transfers the protons to the outer side. It also transfers the electrons to cytochrome c_2, which in turn recycles the electrons to the reaction center.

In summary, Figure 1.7 provides a graphical representation of the complete process of light capture, cyclic electron transfer and ATP generation in PNS bacteria.

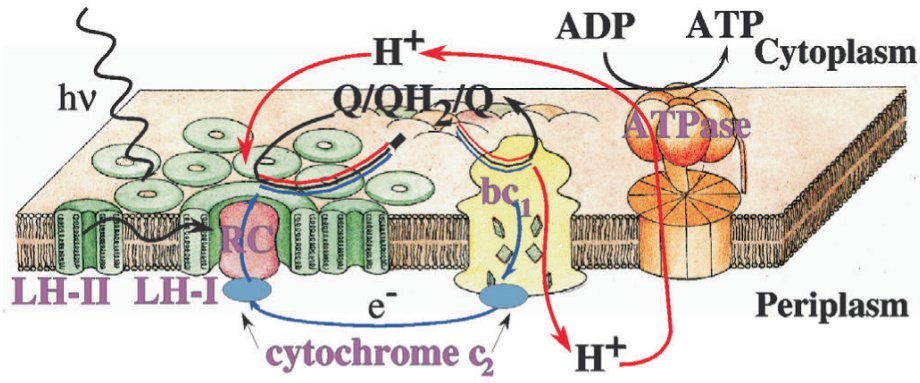

Figure 1.7 Graphical representation of light capture, cyclic electron transfer and ATP generation in PNS bacteria (Schulten 1999). hv light flash; Q ubiquinone; ADP adenosine diphosphate; ATP adenosine triphosphate; LH light harvesting complex.

Non-cyclic electron transfer

In case electrons are needed for assimilatory purposes, an electron donor is required. As the redox potential of P_{870} is +0.45 V (comparable to photosystem I in plant and algal photosynthesis, see Figure 1.6A), the bacterial photosystem is not able to split water and

use it as an electron donor, as it has a redox potential of 0.82 V. Instead, it requires a more reduced electron source, like acetate (redox potential -0.60 V). The electrons are taken up into the electron transport chain from the substrate by cytochrome c_2. Like cyclic electron transport, non-cyclic electron transfer also results in a proton motive force.

Efficiency of photosynthetic ATP generation by PNS bacteria

The quantum efficiency of primary charge separation of the purple non sulphur bacterial light harvesting complex has been reported to reach values in excess of 90% over a broad spectral range (Paddock et al. 2005; Trissl et al. 1990; Wraight and Clayton 1974). The subsequent electron transfer via the cell membrane spanning reaction centre associated cytochromes QA, QB, cytochromes bc_1 and c_2 (Nitschke and Dracheva 1995) all progress at near 100% efficiency (Paddock et al. 2005) and each pair of electrons transferred result in the export of 4 protons to the outer part of the chromatophore.

The exported protons migrate back into the cell via the cell membrane spanning enzyme ATPase (see Figure 1.7), which phosphorylates ADP to form ATP. Each ATP generated requires the migration of 4 protons through the ATPase enzyme (Allen 2003).

From the above we can summarize that PNS bacteria require 2 photons in order to photosynthetically generate 1 ATP. Some researchers have reported lower efficiencies, which might be explained by the lower accuracy of the analytical methods applied. In these cases light to biomass conversion (Göbel 1978) and light gradient fluorescence measurement, which has a lower accuracy at lower wavelengths (Trissl et al. 1990) were used.

An important pre-requisite for attaining this 2:1 conversion of absorbed photons to ATP is that the light supply is non-saturating for each individual reaction center. Light absorbed in excess of saturation will either not be absorbed by the photosystem at all or will not be processed due to the fact that the RC is not available for light absorption, as it has not yet changed back from its charge separated state (Trissl et al. 1990). The excess absorbed light will be dissipated to heat by non-photochemical quenching (Cleland et al. 1992;

Parson 1969; Wormit and Dreuw 2007). If the capacities of photochemistry and non-photochemical quenching together are not sufficient to process all absorbed light, photo-oxidative damage seems inevitable (Marshall et al. 2000; Müller et al. 2001).

Carbon metabolism in PNS bacteria

PNS bacteria exhibit a great diversity in their metabolism of simple carbon compounds. They are capable of breaking down and/or assimilate one, two, three and four carbon compounds and sugars. As a result, they are probably the most metabolically diverse organisms found in nature (Madigan and Gest 1979). As genetic manipulation of *Rhodobacter* and *Rhodospirillum* species is relatively easy, they form a group of organisms for which alternative routes for CO_2-assimilation to the Calvin cycle have been uncovered. Aside from anaerobic phototrophic metabolism, some carbon compounds also support aerobic chemotrophic metabolism, but PNS bacteria generally favour strictly anoxygenic growth conditions (Tabita 1995).

Virtually all PNS bacteria can grow on acetate (Thiele 1968). In the presence of acetate and active photosynthesis, acetate is metabolised via the glyoxylate cycle in most PNS bacteria (Blasco et al. 1991), although some data reported previously demonstrates that several PNS bacteria do not (Albers and Gottschalk 1976; Meister et al. 2005; Payne and Morris 1969). These observations might be caused by an adaptation to acetate assimilation, as described by Nielsen and Sojka (Nielsen and Sojka 1979), that is not always required.

PNS bacteria are also capable of accumulating poly-β-hydroxybutyrate (PHB in short) when metabolising substrates like acetate or butyrate, resulting in large intracellular PHB granules, like reported by Boatman for *Rhodospirillum rubrum* (Boatman 1964).

Metabolic control of carbon flow forms an integrated whole with the control of the cellular redox state of PNS bacteria. The metabolism of highly reduced electron donors like H_2, propionate or butyrate results in a stronger coupling of the two. As photoheterotrophic assimilation of carbon substrates in most PNS bacteria takes place via

the glyoxylate cycle, it generates CO_2, which in turn is reduced via reactions in the Calvin-Benson-Bassham pathway, again in order to maintain a balanced redox poise state (Tabita 1995).

Nitrogen metabolism in PNS bacteria

Many PNS bacteria are diazotrophs, meaning that they are capable of fixing molecular nitrogen using the nitrogenase enzyme (Madigan et al. 1984; Yoch 1978).

Bregoff and Kamen concluded from their experimental stoichiometry results that the electron supply required for the photo-evolution of H_2 could be accounted for by the dissimilation of organic acids (Bregoff and Kamen 1951). The relationship between N_2 fixation and H_2 evolution by PNS bacteria was postulated later by Ormerod and Gest (Ormerod and Gest 1962). The nitrogenase enzyme co-produces H_2 during N_2 fixation, as can be seen in Equation 1.4.

Equation 1.4 $N_2 + 8^+ + 8\ e^- + 16\ ATP \rightarrow 2\ NH_3 + H_2 + 16\ ADP + 16\ P_i$

$\Delta G_0 = -1086.7\ kJ \cdot mol^{-1}$

The electrons required for the nitrogenase activity according to Equation 1.4 are supplied by ferredoxin in *Rhodospirillum rubrum* (Yoch and Arnon 1975). In turn, the electrons required for the reduction of Fd_{ox} in PNS bacteria might well be supplied by the dissimilation of organic acids.

Alternatively, protons and electrons might be recycled from H_2 by a hydrogenase enzyme (explained in more detail later), as was proposed by Mortenson for *Clostridium pasteurianum* nitrogenase (Mortenson 1964).

Yoch demonstrated the high energy demand of nitrogen fixation by using either a N_2 atmosphere or NH_4^+ as nitrogen source, in combination with 5 mM of pyruvate as carbon source and electron acceptor during the growth of *Rhodopseudomonas palustris* cells.

NH_4^+ grown cells had a 30% higher growth yield on carbon compared to the N_2 grown cells, demonstrating an extra requirement for reductant in the latter case (Yoch 1978).

An overview of the general mechanism of the reactions that nitrogenase catalyses is given in Figure 1.8. Nitrogen fixation proceeds optimally under anaerobic conditions in the light (Paschinger 1974). During the process of nitrogen fixation, N_2 is reduced to NH_4^+ (see Equation 1.4). This N_2 reduction process depends strongly on the hydrogen partial pressure. Its stoichiometry is generally written as is in Equation 1.4, as the energetic cost of the transfer of 2 electrons by FeMo/Fe nitrogenase equals 4 ATP. As the N_2 partial pressure decreases, the ratio of N_2 reduced to H_2 evolved decreases drastically in Mo-Fe/Fe nitrogenase containing extracts of *A. vinelandii* (Hwang and Burris 1972).

As nitrogen fixation is a very energy demanding process (see Equation 1.4), both the synthesis of nitrogenase and its activity are tightly regulated in diazotrophs, in order to achieve an optimal metabolic efficiency.

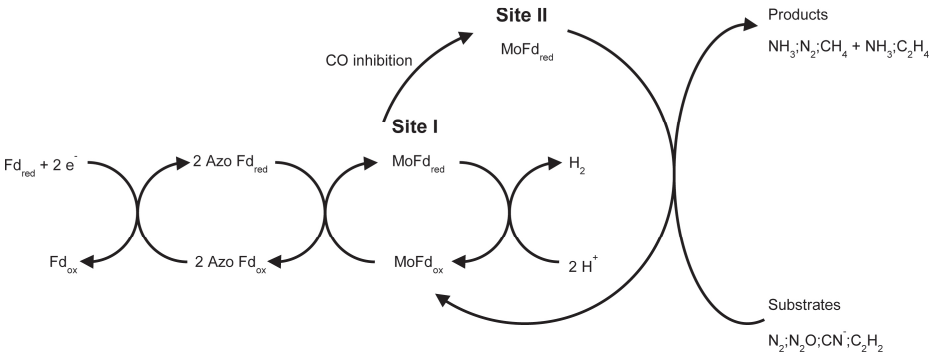

Figure 1.8 Schematic representation of the reductions catalysed by the nitrogenase enzyme. Adapted from Dalton and Mortenson (Dalton and Mortenson 1972) Fd ferredoxin; red reduced; ox oxidised; Mo molybdenum; CO carbon monoxide.

Short-term regulation of nitrogenase activity

Short-term post translational regulation of nitrogenase activity is triggered by the presence of O_2, NH_4^+, glutamine, asparagine and urea (Zumft and Castillo 1978).

Long-term regulation of nitrogenase activity

On a longer time scale, the nitrogenase activity in PNS bacteria is regulated transcriptionally. The most important factors that influence the transcriptional regulation of the nitrogenase activity of PNS bacteria are the applied nitrogen source (Alef et al. 1981; Arp and Zumft 1983; Jouanneau et al. 1985; Zumft and Castillo 1978), the NH_4^+ concentration (Jouanneau et al. 1984; Yakunin and Hallenbeck 1998), the rate of NH_4^+-uptake (Yakunin and Hallenbeck 1998), the severity of nitrogen limitation (Yakunin and Hallenbeck 1998), the adenylation state of the glutamine synthetase enzyme (Jouanneau et al. 1984; Yakunin and Hallenbeck 1998) and the local light intensity, which results in the local rate of photophosphorylation (Jouanneau et al. 1985).

NH_4^+-limitation yields cells that exhibit the highest nitrogenase activity, while cells that are grown under a N_2 atmosphere have a limited nitrogenase activity, as the freshly assimilated intracellular nitrogen in the form of NH_4^+ represses the synthesis of nitrogenase (Munson and Burris 1969).

Subsequent steps in the nitrogen assimilation pathway

After ammonia has been generated by the nitrogenase enzyme, it is subsequently incorporated by the glutamine synthetase / glutamine-2-oxaloglutarate aminotransferase (or GS/GOGAT) pathway, resulting in glutamate, which in turn is taken up into the cellular assimilative metabolism.

Hydrogen photo-production by PNS bacteria

Hydrogen can be used as an energy source by many bacteria, as many hydrogen consuming reactions of energy metabolism have a negative Gibbs free energy change

(Thauer et al. 1977). Depending on the redox potential at which bacteria are capable of oxidizing H_2 and the redox state of the cell, it is either oxidised (methanogens, fermentative bacteria, sulphate reducers, Fe^{3+}-reducers and denitrifiers are capable of consuming H_2) or excreted as a waste product (Vignais and Billoud 2007).

In case the growth conditions of PNS bacteria allows for the existence of active nitrogenase in combination with an excess of reduction equivalents, the nitrogenase enzyme can also catalyse hydrogen generation by combining protons and electrons according to Equation 1.5.

Equation 1.5 $2\,H^+ + 2\,e^- + 4\,ATP \rightarrow H_2 + 4\,ADP + 4\,P_i$ $\Delta G_0 = 199.7\ kJ{\cdot}mol^{-1}$

Accordingly, all parameters mentioned above that regulate the activity of nitrogenase also regulate hydrogen evolution by PNS bacteria. As the nitrogenase reaction is unidirectional, its activity will generate hydrogen according to Equation 1.5, irrespective of the hydrogen partial pressure (McKinlay and Harwood 2010). Hydrogen generation by nitrogenase is less energy consuming then nitrogen fixation, but still has a high metabolic energy demand.

Hydrogenases

A second class of enzymes related to hydrogen metabolism, the hydrogenases, is present in PNS bacteria. This class of enzymes catalyses the reduction of protons to form H_2, according to Equation 1.6. Hydrogenase based systems have the advantage of an order of magnitude higher catalytic rate (McKinlay and Harwood 2010), combined with a lower metabolic energy requirement when compared to nitrogenase based systems. For these reasons, hydrogenase based systems are very interesting candidates for photobiological hydrogen production.

Equation 1.6 $2\,H^+ + 2\,e^- \leftrightarrow H_2$ $\Delta G_0 = 79.7\ kJ{\cdot}mol^{-1}$

The net hydrogen producing catalytic activity of hydrogenase is sensitive to H_2 inhibition, as it is reversible (Vignais and Billoud 2007).

Outline of this thesis

In order to valorise bio-hydrogen and make it into a technology that can provide a contribution to renewable energy supply in the near future, fundamental knowledge of the underlying processes is required.
The main goal of this thesis is to investigate the process of photobiological hydrogen formation by photosynthetic bacteria, as part of the previously described two-stage process. Several sub-goals were identified, each of them leading to a chapter in this thesis:

1. What strategy is most suitable for the fast optimization of phototrophic bioprocesses in order to reach maximal productivity?
2. What photobioreactor design should be applied for anoxygenic hydrogen production from organic acids by PNS bacteria?
3. What are the kinetic parameters for growth of photo-heterotrophically grown PNS bacteria?
4. What light-to-hydrogen efficiency can be reached in theory versus in practise?
5. How do the current results compare to the active research field and what improvements are required in order to make photobiological hydrogen a serious renewable alternative to fossil fuels?

In order to optimize biomass and/or growth associated product formation in phototrophic cultures, various techniques can be applied.

Chapter 2, entitled 'Deceleration-stats save lots of time during phototrophic culture optimization', gives an overview of optimization techniques that can be applied in phototrophic fermentation. A comparison between the well-established series of chemostat experiments and the alternative, a single D-stat experiment, was made in terms of time expenditure. The time-gain that can be achieved by applying a D-stat as calculated based on model predictions turned out to be at least 80%.

Chapter 3, entitled 'A pneumatically agitated flat-panel photobioreactor with gas re-circulation: anaerobic photoheterotrophic cultivation of a purple non-sulphur bacterium', describes the various types of photo-bioreactors that are available to researchers and the development of an autoclavable flat panel photobioreactor with a very small (3 cm) optical path, in order to limit self-shading of the phototrophic culture. Also, this system has the possibility of re-circulating the gas stream, facilitating turbulent mixing combined with the production of a non-diluted hydrogen gas stream.
After defining the appropriate experimental technique and designing the appropriate photobioreactor, they were applied in order to find the kinetic parameters for growth by the PNS bacterium *Rhodobacter capsulatus* NCIMB 11773. Here, the cultures were kept in pseudo steady-state in order to facilitate an accurate measurement of yield and maintenance coefficients.

Chapter 4, entitled 'Controlling light-use by *Rhodobacter capsulatus* continuous cultures in a flat-panel photobioreactor' presents a light energy balance, in which the absorbed light energy is distributed amongst biomass formation, biomass maintenance, hydrogen formation and dissipation to heat.
The maintenance and yield parameters for biomass formation on light energy were determined and inserted into the light energy balance.
The light energy expenditure for biomass growth can be decreased, for instance by maintaining steady state at a low dilution rate. As a result, the fraction of the absorbed light energy that can be directed to hydrogen was estimated to have a maximum at 3.3%.

The light to hydrogen conversion efficiencies as predicted in Chapter 4 were measured during two stat experiments which are presented in Chapter 5, entitled 'Exploration of the hydrogen producing potential of *Rhodobacter capsulatus* chemostat cultures: The application of Deceleration-Stat and Gradient-Stat methodology'. The light to hydrogen conversion efficiency was determined in a continuously operated photo-bioreactor.
The hydrogen production capacity increased linearly with the biomass concentration. However, at biomass concentrations exceeding 1.5 $g \cdot L^{-1}$, light availability caused a decline in the specific hydrogen production capacity. As this decline was also present in the dedicated short-term batch experiments, light availability was not solely responsible for the decreased specific hydrogen production capacity. As a consequence, the light to hydrogen conversion efficiency that could be demonstrated was limited to 1.6%.

The potential of biological hydrogen production is discussed in **Chapter 6**, based on both literature results and the results generated in this thesis. Also, an overview is given of the potential directions of future research. It is discussed what further developments are needed in order to make photobiological hydrogen a serious renewable alternative for current fossil-based fuels.

Chapter 2

Deceleration-stats save much time during phototrophic culture optimization

The contents of this chapter have been published as

Hoekema S, Rinzema A, Tramper J, Wijffels RH, Janssen M. 2014. Deceleration-stats save much time during phototrophic culture optimization. Biotechnology and Bioengineering 111(4):792-802.

2. Deceleration-stats save much time during phototrophic culture optimization

Abstract

In case of phototrophic cultures, photobioreactor costs contribute significantly to the total operating costs. Therefore one of the most important parameters to be determined is the maximum biomass production rate, if biomass or a biomass associated product is the desired product. This is traditionally determined in time consuming series of chemostat cultivations.

The goal of this work is to assess the experimental time that can be saved by applying the D-stat (deceleration stat) technique to assess the maximum biomass production rate of a phototrophic cultivation system, instead of a series of chemostat cultures.

A mathematical model developed by Geider and co-workers was adapted in order to describe the rate of photosynthesis as a function of the local light intensity. This is essential for the accurate description of biomass productivity in phototrophic cultures.

The presented simulations demonstrate that D-stat experiments executed in the absence of pseudo steady-state (i.e. the arbitrary situation that the observed specific growth rate deviates less than 5% from the dilution rate) can still be used to accurately determine the maximum biomass productivity of the system. Moreover, this approach saves up to 94% of the time required to perform a series of chemostat experiments that has the same accuracy. In case more information on the properties of the system is required, the reduction in experimental time is reduced but still significant.

Introduction

Great potential has been attributed to phototrophic microorganisms as they can produce both high-value compounds and low-value bulk materials, such as second-generation biofuels (Chisti 2007; Rodolfi et al. 2009; Wijffels and Barbosa 2010; Wilhelm and Jakob 2011; Williams and Laurens 2010). However, high areal productivities can be reached only in optimized production systems (Janssen et al. 2001; Morweiser et al. 2010).

The reference approach for the determination of the properties of steady state continuous cultures is a series of chemostat cultivations (Yee and Blanch 1993). A sequence of step-wise changes in dilution rate, or medium composition, is applied. After each step the culture needs time to acclimate and reach a new steady-state. This approach is time consuming and a faster alternative would be beneficial to reduce the costs of process optimisation.

The acceleration stat (A-stat) cultivation technique is an alternative that yields more data in a limited period of time. The A-stat method was developed for the rapid investigation of growth kinetics of microorganisms (Müller et al. 1995; Paalme et al. 1995). This is achieved by applying a constant increase in dilution rate, referred to as the acceleration rate. If the dilution rate is decreased instead of increased, the cultivation is referred to as a deceleration stat (D-stat).

The advantage of the D-stat over the A-stat is two-fold: the dilution rate of the initial steady state is higher, and therefore it is reached faster and a D-stat can be terminated faster, provided that the maximum biomass production rate occurs at a high specific growth rate (see materials and methods section for a more detailed motivation).

The higher the change rate applied, the faster the procedure is finished. However, culture characteristics that approach true steady-state characteristics can only be maintained at infinitely low change rates.

If the change rate allows the microorganism to acclimate to its changing environment, the culture properties at a given time point in a D-stat are equal to those in a chemostat at

the same dilution rate (Paalme et al. 1995; van der Sluis et al. 2001a). The number of pseudo steady-states that can be measured in a given amount of time is then limited only by the rate of the required analyses.

A limited number of studies has been carried out using A-stat and D-stat techniques for both chemotrophic and phototrophic microorganisms. An overview of these studies, the applied microorganisms, the dilution change rates that safeguarded pseudo steady-state and the ones that did not, is given in Table 2.1. The estimation of steady-state characteristics was considered successful if the deviation between the set dilution rate and measured specific growth rate was less than 5%. So far it has remained unclear to what extent the acceleration or deceleration rate can be increased, while still providing reliable data for process optimization.

The goal of this work is to minimize the experimental time that is needed to provide a good estimation of the maximum biomass production rate in a microalgal cultivation system. This is done by model simulations of continuous microalga cultivation in photobioreactors (PBRs, see also the list of abbreviations).

Phototrophic organisms have evolved mechanisms for sensing and responding to changing light conditions, for instance as a result of diurnal or seasonal changes. They respond to a decrease in available light intensity by increasing the number of copies and size of their photosynthetic units, in order to maximize light harvesting and utilization efficiencies under low light, while preventing photo-oxidative damage under (too) high light (Dubinsky and Stambler 2009). As a result, photo-acclimation is one of the most important acclimation processes taking place during changes in cultivation conditions in phototrophic cultures. The kinetic model developed by Geider et al. (Geider et al. 1996) was used in this work. It provides a validated description of photosynthetic growth, as it corresponds well with experimentally acquired data on balanced growth and photo-acclimation of several diatom species, such as *Synechococcus, Chlorella, Skeletonema, Thalassiosira and Phaeodactylum* (Geider et al. 1996; MacIntyre et al. 2002). The signal that determines the rate of photo-acclimation is described mathematically as the ratio between the photosynthetic capacity and the rate of light absorption. This description is

in accordance with our current understanding of photo-acclimation (Li et al. 2009). Additionally, the Geider model requires only a limited number of kinetic and physiological properties of the applied phototrophic microorganism.

As it is widely recognized that the local light intensity governs the local rate of photosynthesis in PBRs (Takache et al. 2012), the Geider model was extended with a light balance, and an average rate of photosynthesis was calculated by averaging the local rates.

In this work, the extended Geider model was used to compare two different optimization approaches: The D-stat and the series of chemostats. Based on the work presented here, we conclude that data from D-stat cultures can be used to accurately determine the maximum biomass production capacity of the system, even if the deceleration rate exceeds the rate at which a pseudo steady-state is maintained. This means that the experimental time required to accurately assess the maximum biomass production rate of a phototrophic system can be reduced by up to 94% compared to the chemostat method.

Materials and Methods

Culture properties

In all simulations the properties of the microalga *Thalassiosira pseudonana* published by Geider et al. (Geider et al. 1996) were used (see Table 2.2). These properties are the functional cross section of the light harvesting complex (σ, $m^2 \cdot mol^{-1}$ photons PAR), the maximum rate of photosynthesis (P^E_m, d^{-1}). Table 2.2 also gives the constant proportion of assimilated carbon dioxide (3-carbon sugars) which is directed towards the biosynthetic machinery, κ_E, and the decay coefficient (r_m, d^{-1}). The maximum specific growth rate (μ_{max}, d^{-1}) can be recalculated from the model parameters (Geider et al., 1996).

Table 2.1 Applied change rates in dilution rate reported in literature. The estimation of steady state characteristics was considered successful in case the deviation between dilution rate and resulting specific growth rate was less than 5%.

Microorganism	Applied acceleration rate (% of $\mu_{max} \cdot d^{-1}$)	
	Success	Failure
D. tertiolecta[1]	6.3	43
Z. rouxii[2]	13.3	133
L. plantarum[3]	-	72
E. coli K12[4]	-	49.3
S. cerevisiae[5]	-	54.6
R. capsulatus[6]	1.32	-

PBR properties

In principle simulations can be executed using any PBR for which light distribution can be described mathematically. In the simulations presented here, the properties of a PBR that were described previously (Hoekema et al. 2006) were used: a flat panel PBR illuminated from one side with a depth of 3 cm.

[1] (Barbosa et al. 2003)
[2] (van der Sluis et al. 2001a)
[3] (Kask et al. 1999)
[4] (Paalme et al. 1995)
[5] (Paalme et al. 1997)
[6] (Hoekema et al. 2006)

Light intensity

The light intensity on the surface of the PBR is given as the photon flux density (I), in mol photons·m^{-2}·d^{-1} in the PAR range (photosynthetically active radiation: 400-700 nm). Simulations were performed using an incident light intensity of 8.65 (low) or 86.5 (high) mol photons·m^{-2}·d^{-1}, corresponding to 100 and 1000 µmol photons PAR·m^{-2}·d^{-1}.

A one-dimensional light-path perpendicular to the light-exposed reactor surface was assumed with a uniform light distribution. Lambert-Beer's law (Equation 1 in Figure 2.1) was used to calculate the local light intensity. Even though Lambert-Beer's law is only valid for one-dimensional light propagation, it was found previously to describe the irradiance distribution inside a PBR sufficiently accurate (Evers 1991; Luo and Al-Dahhan 2012; Wu and Merchuk 2001).

Table 2.2 Modeling parameter values for *T. pseudonana* (Geider et al. 1996). An overview of the parameter-values that were used in all simulations using the model described in Figure 2.1. The parameters are defined in the list of abbreviations.

Parameter	Value	Units
σ	2.0	m^2·mol photons^{-1}
Chl: C	0.2	g·g^{-1}·L^{-1}
A^*_{Chl}	10	m^2·g Chl a^{-1}
$\kappa_E (= \rho_E)$	0.6	-
P_E^m	5.55	d^{-1}
r_m	0.05 (0.15[1])	d^{-1}
μ_{max}	3.28	d^{-1}

Mathematical model

For this study the model of Geider et al. (Geider et al. 1996) was adapted (see Figure 2.1) to describe local light intensities and photosynthesis rates. Based on the local rates, the average rate of photosynthesis over the photobioreactor volume can be calculated, resulting in the average biomass productivity. Next, a program based on the model was constructed in order to simulate cultures grown in batch, chemostat, and D-stat mode. All simulations were done with Mathcad 14.0. Differential equations were solved numerically with the Radau ODE solver.

A schematic representation of the applied model is presented in Figure 2.1. The light intensity profile along the light path in the PBR, which is illuminated from one side, is calculated with Equation 1, the light balance.

1 Light balance

$$I = I_0 \cdot e^{-a^*_{Chl} \cdot Chl : L \cdot L \cdot z}$$

2 Local specific rate of photosynthesis

$$P^E = P^E{}_m \cdot \left(1 - e^{\frac{-\sigma \cdot I \cdot L}{P^E{}_m \cdot E}} \right)$$

3-5 Local fractions of photosynthate allocated to E, L and R

$$\rho_E = \kappa_E$$

$$\rho_L = (1 - \kappa_E) \cdot \left(\frac{P^E \cdot E}{\sigma \cdot I \cdot L} \right)$$

$$\rho_R = (1 - \kappa_E) \cdot \left(1 - \frac{P^E \cdot E}{\sigma \cdot I \cdot L} \right)$$

6-8 Component Balances

$$\frac{d}{dt} E(t) = \left(\rho_E \cdot \frac{1}{Z} \cdot \int_0^Z P^E \cdot dz \right) \cdot E(t) - r_m \cdot E(t) - D(t) \cdot E(t)$$

$$\frac{d}{dt} L(t) = \left(\frac{1}{Z} \cdot \int_0^Z \rho_L(t,z) \cdot P^E \cdot dz \right) \cdot E(t) - r_m \cdot L(t) - D(t) \cdot L(t)$$

$$\frac{d}{dt} R(t) = \left(\frac{1}{Z} \cdot \int_0^Z \rho_R(t,z) \cdot P^E \cdot dz \right) \cdot E(t) - r_m \cdot R(t) - D(t) \cdot R(t)$$

9 Biomass concentration

$$X(t) = E(t) + L(t) + R(t)$$

10 Biomass production rate

$$r_X(t) = \left(\frac{1}{Z} \cdot \int_0^Z P^E \cdot dz \right) \cdot E(t) - r_m \cdot X(t)$$

11 Specific growth rate

$$\mu(t) = \frac{r_X(t)}{X(t)}$$

Figure 2.1 Outline of the mathematical model that was applied to generate all presented simulations.

Photo-saturation in photosynthesis can be accurately described as an exponential function referred to as the photosynthesis irradiance curve (or PI curve in short), as Webb et al. demonstrated first (Webb et al. 1974). Accordingly, Equation 2 describes the local specific rate of photosynthesis based on the local light intensity.

Photo-acclimation is governed by the ratio of photosynthetic rate ($P^E \cdot E$) over light absorption ($\sigma \cdot I \cdot L$) (Geider et al. 1996). This can be seen in Equations 3-5, in which the local fractions of new photosynthate that is directed towards the biosynthetic machinery E, the light harvesting complex L, and storage material R are calculated. The sum of these three fractions is 1.

With the local distribution of assimilated carbon known, the global changes in concentrations of L, E and R can be calculated from the component balances; the integrals give the average specific rates over the depth of the PBR (Equations 6-8). The light gradient across the PBR results in a similar variation in the local rate of photosynthesis and distribution of assimilated carbon. These terms are averaged over the entire PBR after their local values have been determined for each time step. Summation of the concentrations of the three biomass fractions gives the biomass concentration (Equation 9) and Equations 10 and 11 give the biomass production rate and the specific growth rate, respectively.

Starting values of model simulations

The starting point for each simulation was a chemostat culture in steady state. The dilution rate was either decreased gradually (D-stat) or step-wise (series of chemostats).

First, a batch culture was simulated. The batch time was chosen such that a biomass concentration was reached that matches the predicted steady state biomass concentration for the initial chemostat culture. Subsequently, this chemostat was simulated. The time required to reach steady state following a step change in dilution rate was assessed from the simulation results. Steady state was assumed when a residual difference between μ and D of 1% or less was observed.

Simulation of chemostat experiments using trisection

The biomass production rate is the product of the dilution rate and the biomass concentration. The mathematical relation between the production rate and dilution rate has a maximum (Goldman 1979). This maximum is characterized by the location on the curve where the slope is zero. Due to the need for numerical integration of the differential equations (see Figure 2.1), the maximum cannot be found analytically. It has been approximated by using a trisection method.

First, an estimate of the maximum specific growth rate of the alga under investigation is required. This information might be retrieved from literature or assessed by means of a wash-out experiment. Accordingly, one value at 85% of the highest supported dilution rate is arbitrarily chosen, as well as one value close to zero. Then two intermediate dilution rates are chosen, such that the total range in dilution rate is sub-divided into three equally distributed intervals.

Chemostat simulations are run at these dilution rates and the corresponding biomass production rates are calculated. The slope of the biomass production rate as a function of the dilution rate ($\Delta_{r_x}/\Delta D$) is calculated for each interval resulting in three values. The maximum biomass production rate is reached at a dilution rate that lies within one of two intervals adjacent to the point where the slope changes sign.

The remaining interval can be discarded during a subsequent repetition of the procedure, which requires two additional steady states. The procedure was halted when the maximal observed difference within the three remaining biomass production rates was less than 5%, as this level of accuracy can also be achieved experimentally (based on for instance biomass dry weight analysis). By summation of the time-intervals required for each steady state, the time required for the assessment of the specific growth rate that results in the maximum biomass production rate is determined.

Simulation of D-stat experiments

In a D-stat, the initial hydraulic residence time is shorter, resulting in a faster arrival at the initial steady state, provided that the initial dilution rate does not exceed $0.9 \cdot \mu_{max}$, as beyond this value, a system will typically take a long time to reach steady state (Perram 1973). For this reason, a D-stat is more advantageous than an A-stat, assuming that a fixed number of hydraulic residence times is required to reach initial steady state. A further reduction in experimental time can be achieved if an experiment is terminated once the maximum biomass production rate has been reached. This optimum is mostly found at elevated specific growth rates in light limited phototrophic cultures (Barbosa et al. 2005; Cuaresma et al. 2009; Goldman 1979; Molina Grima et al. 1997; Pruvost et al. 2011; Zijffers et al. 2010), thus a D-stat experiment can be terminated faster. For these reasons, we have chosen to exclusively simulate D-stat experiments as a second process optimization option.

Results and Discussion

Chemostat simulations

Before simulating an optimization study based on either D-stats or chemostats, the productivity of the system was assessed as a function of the specific growth rate. This was done by simulating a large number of chemostats at different dilution rates. The simulations were done for the diatoms *Thalassiosira pseudonana and Phaeodactylum tricornutum* (see Appendix I). The applied model parameters were taken from literature (Geider et al. 1996) and are presented in Table 2.2. Simulations were executed at low and high light intensity, corresponding to 8.65 and 86.5 mol photons PAR $m^{-2} \cdot d^{-1}$ respectively. The results of these simulations are presented in Figure 2.2A for low light intensity and Figure 2.2B for high light intensity.

A tenfold increase in light intensity results in a mere 4.5-fold increase in biomass production rate. This can be ascribed to photo-saturation in the photic zone of the PBR. Here, the rate of light absorption is considerably higher than the maximum rate at which it can be used to drive photosynthesis, resulting in dissipation of the excess absorbed light. Figure 2.2 shows that at low light intensity the maximum in the biomass production rate is much more pronounced than at high light intensity. To the left of the maximum, at low specific growth rate and high biomass concentration, the larger contribution of the decay coefficient results in a decrease in biomass production rate. To the right, an elevated growth rate can only be supported if the average light intensity increases, which requires a lower biomass concentration. Photons that have not been absorbed then pass the reactor, resulting in an increasing fraction of incident light that is not absorbed by the culture. The remaining information displayed in Figure 2.2 will be discussed later in this chapter.

Maximization of the biomass production rate by a series of chemostats

The time required to find the chemostat settings that result in the maximum biomass production rate was minimized by using the trisection method (see Materials and Methods section). The method aims at re-constructing part of Figure 2.2 in order to find the maximum biomass production rate in the smallest amount of time.

Table 2.3 summarizes the simulation results. It demonstrates that at low light intensity 64 days of experimental time are needed in order to find the maximum biomass production rate at the required 5% accuracy and at high light intensity 36 days.

As the procedure is executed, the biomass production rate soon stabilises at both applied light intensities, due to the broad optima shown in Figure 2.2. The maximum biomass production rate was determined within a 5% deviation margin after 3 and 2 iterations for low and high light intensity, respectively.

As will be discussed later, such broad optima are not always present in experimental data. When a more distinct optimum is present, a larger number of iterations would be required in order to find it.

Figure 2.2 Simulation results of *T. pseudonana* chemostat cultures in steady state at low (A) and high (B) light intensity. Biomass productivity (r_x, black solid line) and the fraction of the incident light that is not absorbed (I_{out}/I_{in}, grey line) using the standard parameter values. Biomass productivity (r_x, black dashed line) and the fraction of the incident light that is not absorbed (I_{out}/I_{in}, grey dashed line), using a three-fold increased decay coefficient. The dotted vertical lines represent the compensation point, at which the rate of photosynthesis equals the decay rate in the back of the PBR, resulting in the maximally attainable biomass production rate. Low and high light intensities correspond with 100 and 1000 µmol photons $m^{-2} \cdot s^{-1}$ of PAR.

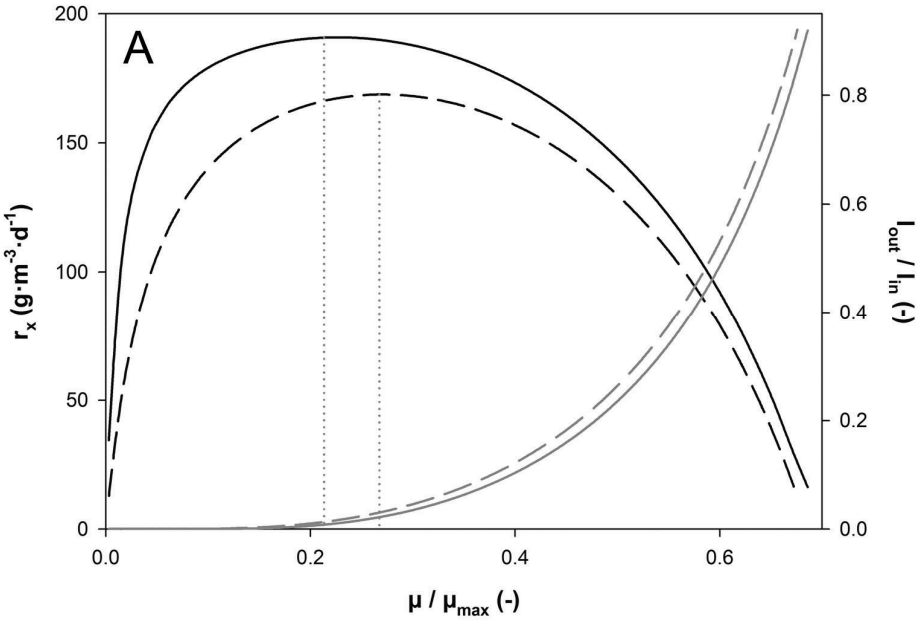
A
200
150
100
50
0
0.0
0.2
0.4
0.6
0.8
0.6
0.4
0.2
0.0
r_x (g·m^{-3}·d^{-1})
I_{out} / I_{in} (-)
μ / $μ_{max}$ (-)

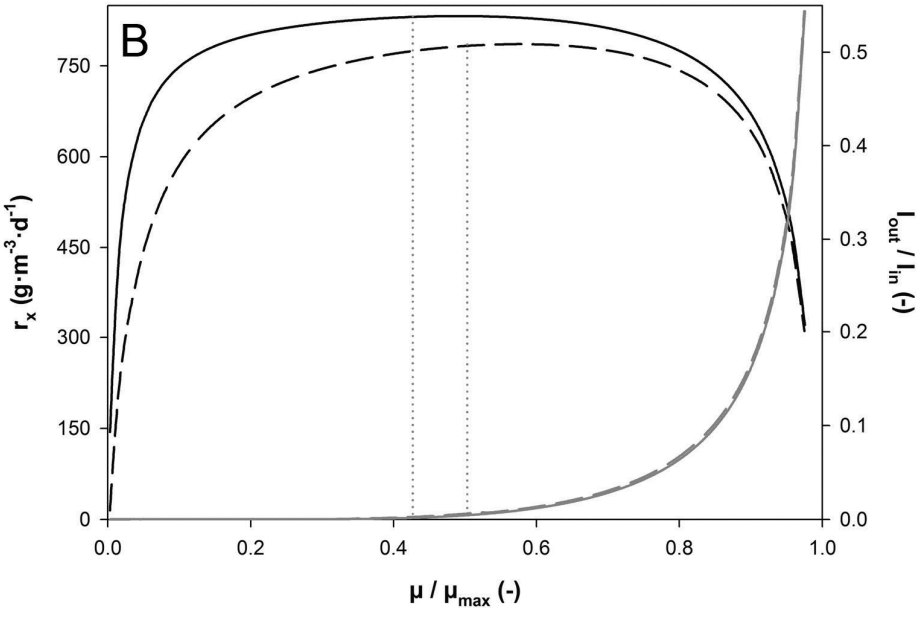
B
750
600
450
300
150
0
0.0
0.2
0.4
0.6
0.8
1.0
0.5
0.4
0.3
0.2
0.1
0.0
r_x (g·m^{-3}·d^{-1})
I_{out} / I_{in} (-)
μ / $μ_{max}$ (-)

Maximization of the biomass production rate in a D-stat experiment

Low deceleration rates (typically below 10% of μ_{max} per day for phototrophic cultures, see Table 2.1) provide a more accurate approximation of steady state, but take more time. The results of a D-stat simulation at low light intensity and a deceleration rate of 10% of μ_{max} per day are presented in Figure 2.3A. The figure demonstrates that already at this moderate deceleration rate, the culture does not remain in pseudo steady state, as the specific growth rate deviates more than 5% from the applied dilution rate. If the dilution rate decreases fast enough, the availability of light exceeds the availability at the corresponding steady state in a chemostat, resulting in a specific growth rate that is higher than the applied dilution rate.

Figure 2.3B illustrates the specifics of photo-acclimation during the simulation, which results in a change in biomass composition. A decrease in dilution rate leads to accumulation of biomass and causes a decrease in light available per cell. This results in up-regulation of the fraction of assimilated carbon directed to the light harvesting complex since the ratio of photosynthetic rate ($P_E \cdot E$ over light absorption ($\sigma \cdot I \cdot L$) approaches unity (Equations 3-5, Figure 2.1).

Figure 2.3 D-stat simulation for the microalga *T. pseudonana* grown at low light intensity with a deceleration rate of $0.1 \cdot \mu_{max}$. (A) Dilution rate (D, black line), specific growth rate (μ, dashed black line), the volumetric biomass production rate (r_x, grey line). (B) Fraction of new photosynthate allocated to the synthesis of light harvesting complex (ρ_L, solid line) and reserve compounds (ρ_R, dotted line). The fraction of the incident light energy that is not absorbed (I_{out}/I_{in}, grey line) is also shown. Low light intensity corresponds with 100 µmol photons $m^{-2} \cdot s^{-1}$ of PAR.

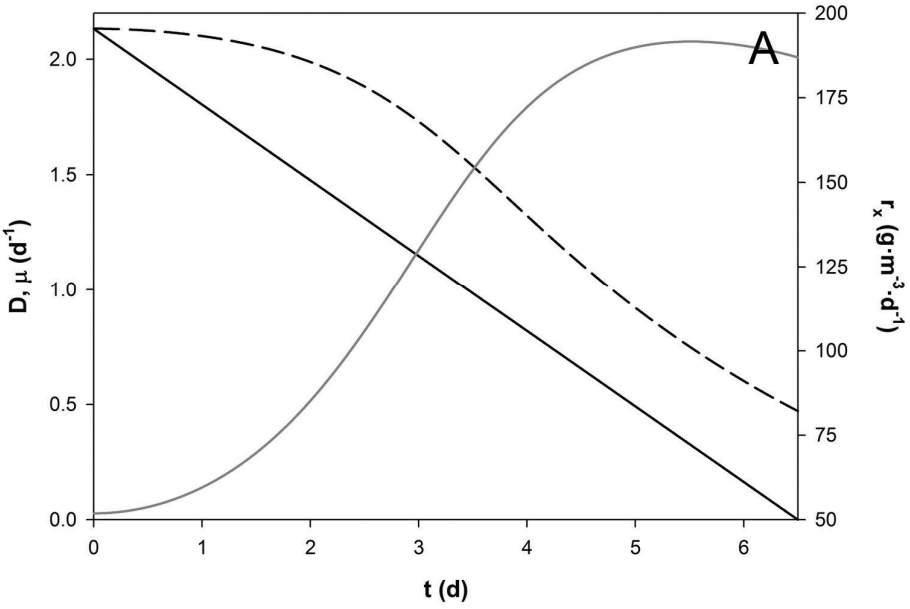
A
D, μ (d-1)
rx (g·m-3·d-1)
t (d)
0.0
0.5
1.0
1.5
2.0
50
75
100
125
150
175
200
0
1
2
3
4
5
6

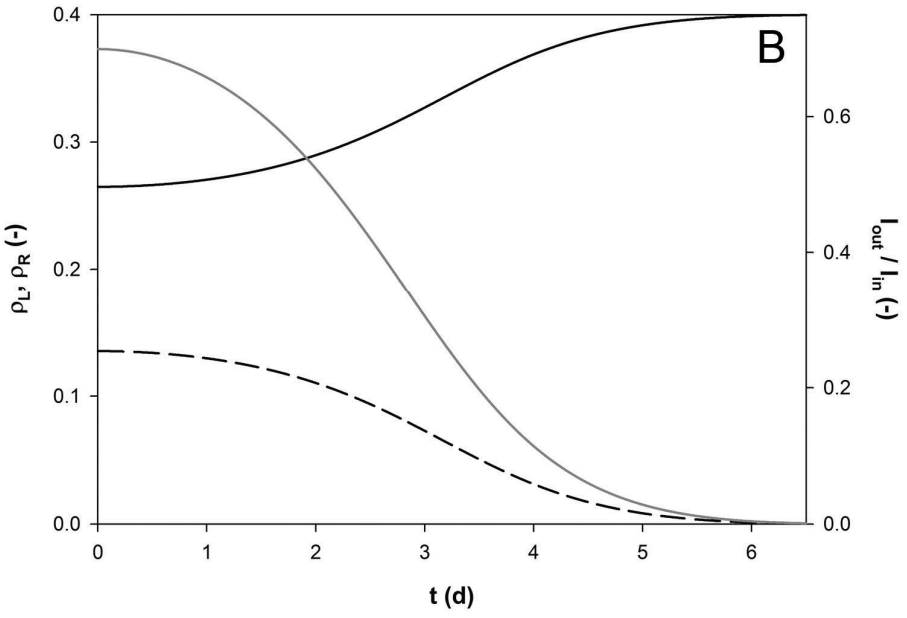
B
ρL, ρR (-)
Iout / Iin (-)
t (d)
0.0
0.1
0.2
0.3
0.4
0.0
0.2
0.4
0.6
0
1
2
3
4
5
6

The fraction of carbon directed to the light harvesting complex increases from 0.26 to 0.40 at the expense of the fraction directed to reserve compounds. Moreover, the increased size of the light harvesting complex results in a more rapid attenuation of light along the reactor depth. This in turn results in a faster change of the local light intensity when the biomass density increases which has a direct effect on the local rates of photosynthesis.

As the deceleration rate is increased, the deviation between the specific growth rate and the imposed dilution rate increases further (results not shown). Also, at high light intensity the maximum biomass productivity is higher for the simulations carried out with higher deceleration rates (Figure 2.4B). In this situation photo-acclimation lags behind, resulting in cells with a smaller light harvesting complex in comparison to the real steady state situation. This in turn results in a reduced biomass specific light absorption coefficient and thus less over-saturation at the light exposed surface and a higher yield of biomass on absorbed light.

At low light intensity (Figure 2.4A), deceleration rates exceeding $0.25 \cdot \mu_{max}$ per day result in a situation where the maximum productivity is not reached, as at the end of the experiment, the biomass concentration that is present in the PBR is still too low to absorb the majority of the incident light, resulting in a restriction on the maximum deceleration rate that can be applied.

Figure 2.4 D-stat simulations for the microalga *T. pseudonana* grown at low (A) and high (B) light intensity with deceleration rates of 0.001 (solid line), 0.01 (long dash), 0.1 (medium dash), 0.25 (short dash) and 0.5 (dot)$\cdot\mu_{max}$. Low and high light intensities correspond with 100 and 1000 µmol photons$\cdot m^{-2} \cdot s^{-1}$ of PAR.

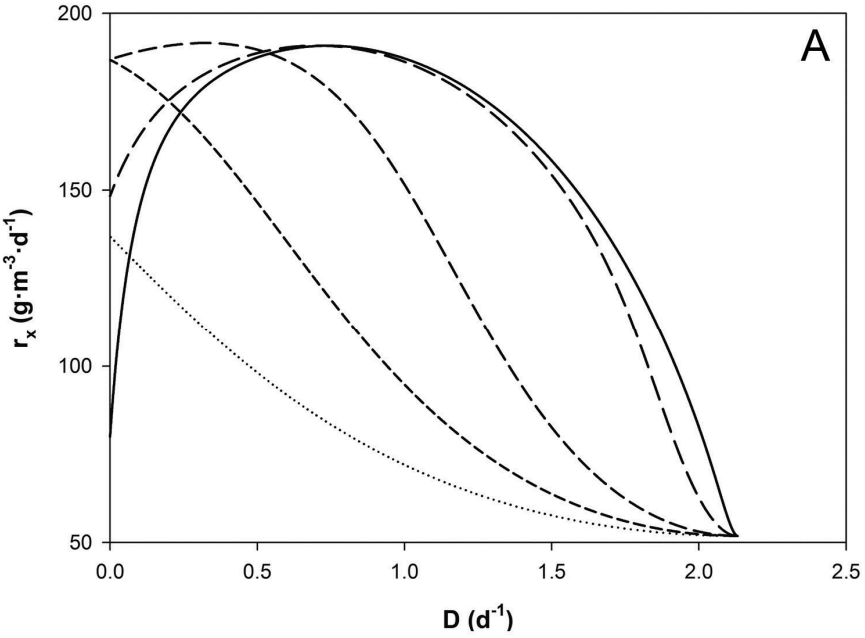
A
200
150
100
50
0.0
0.5
1.0
1.5
2.0
2.5
r_x (g·m^{-3}·d^{-1})
D (d^{-1})

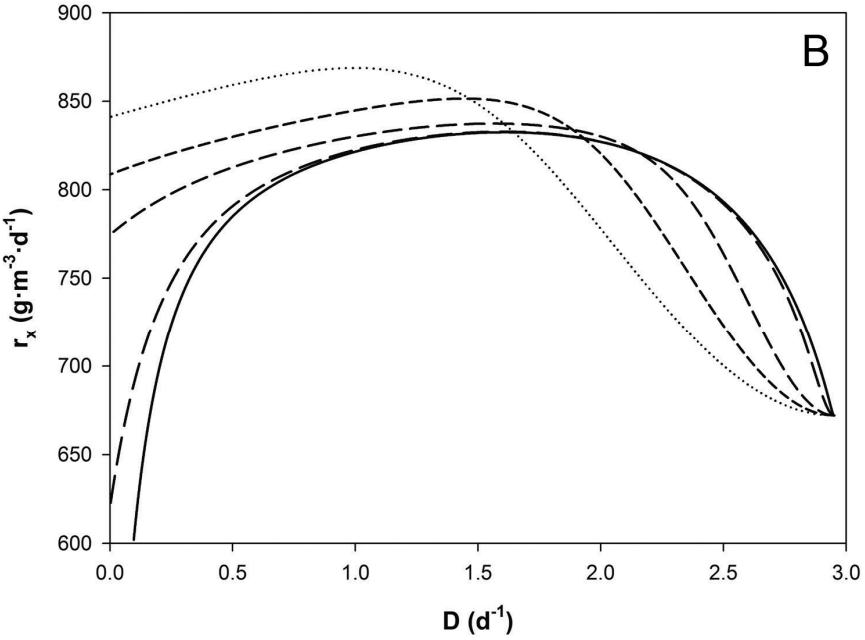
B
900
850
800
750
700
650
600
0.0
0.5
1.0
1.5
2.0
2.5
3.0
r_x (g·m^{-3}·d^{-1})
D (d^{-1})

Table 2.3 Simulation of PBR optimization for *T. Pseudonana* cultures at low (A) and high (B) light intensity.

A↓ Iteration	μ [d^{-1}]	r_x [$g \cdot m^{-3} \cdot d^{-1}$]	$\Delta r_x/\Delta\mu$ [$g \cdot m^{-3}$]	t [d]
0	2.13 1.48 0.82 0.16	51.8 160.9 190.5 158.2	-166.2 -45.1 49.3	2[1] 7 6 22
1	1.48 1.04 0.60 0.16	160.9 186.2 189.7 158.2	-57.9 -7.9 72.0	- 7 7 -
2	1.04 0.75 0.46 0.16	186.2 (-2.4%) 190.8 185.8 (-2.6%) 158.2	-158 17.1 94.8	- 5 8 -
Total time required for the execution of the series of chemostats				**64**
D-stat, 28% of $\mu_{max} \cdot d^{-1}$	1.16	181.9	-	**10**
Time saved in case of D-stat, in comparison with this series of chemostats				**54** **86%**

B↓ Iteration	μ [d^{-1}]	r_x [$g \cdot m^{-3} \cdot d^{-1}$]	$\Delta r_x/\Delta\mu$ [$g \cdot m^{-3}$]	t [d]
0	2.79 1.91 1.04 0.16	737.8 829.3 822.8 661.0	-104.6 7.5 184.9	2[1] 2 4 22
1	2.79 2.20 1.62 1.04	737.8 818.4 (-1.7%) 832.4 822.8 (-1.2%)	-138.2 -24.0 16.5	- 4 2 -
2	-	-	-	-
Total time required for the execution of the series of chemostats				**36**
D-stat, 60% of $\mu_{max} \cdot d^{-1}$			-	**6**
Time saved in case of D-stat, in comparison with this series of chemostats				**31** **85%**

The experimental time required for both optimization strategies (D-stat and series of chemostats) is calculated, as well as a comparison in required experimental time. The comparisons made are best-case scenarios, as the fastest D-stat experiments that still give accurate steady state values for the maximum biomass production rate (Figure 2.5) were selected. See the materials and methods section for a description of the trisection method used during the chemostat optimization strategy.

[1] Total time required, including batch pre-growth and initial steady state.

Error analysis at elevated deceleration rate

In order to assess which deceleration rates still provide a good estimate of the maximum biomass production rate, a sequence of simulations was performed at various deceleration rates. The maximum biomass production rate and the associated specific growth rate from D-stats were compared with those from steady state chemostat cultures (Figure 2.2). The maximum error that is accepted between the two is ± 5% of the value determined in chemostat simulations. Figure 2.5A shows the error for low light intensity, and Figure 2.5B for high light intensity, both as a function of the applied deceleration rate.

As can be seen in Figure 2.5, the errors made in the determination of the maximum biomass productivity remain acceptable up to a deceleration rate of 28% of μ_{max} per day at low light intensity and 60% of μ_{max} per day at high light intensity. This observation confirms the notion that even though the dilution rate is too high for pseudo-steady state to be maintained (Figure 2.3), the maximum biomass production rate can still be predicted with an accuracy of ± 5% compared to chemostat cultures. Probably, most literature data shown in the column entitled 'Failure' in Table 2.1, can be used to accurately assess the maximum biomass production rate, even though the cultures did not remain in pseudo steady-state. The error in the determination of the specific growth rate that corresponds to the maximum biomass production rate that is also presented in Figure 2.5 is discussed below in the 'practical relevance of the simulation results' section.

As the time that is required for a series of chemostat experiments and D-stat experiments executed at varying deceleration rate has now been determined, the experimental time that can be saved by applying the D-stat technique can be quantified.

Reduction of experimental time by using the D-stat approach

The simulated experimental time that is required for the successful execution of the two biomass production maximization strategies presented in this work is compared in Table 2.3. It shows that the assessment of the maximum biomass production rate by a D-stat experiment saves over 80% of the experimental time needed for a series of chemostat experiments using the kinetic parameters of *T. pseudonana*, both at low and high light intensity.

In order to demonstrate general applicability of this approach, simulations were repeated using the kinetic parameters of *P. tricornutum*. This is a diatom species with both a maximum specific growth rate that is less than half that of *T. pseudonana* and different light absorption characteristics. These simulation results are presented in Appendix I and show similar characteristics, resulting in an even stronger reduction in experimental time obtained with the D-stat approach.

Figure 2.5 Errors in the D-stat estimation of the steady state parameters at which the maximum biomass production rate occurs in comparison to the true chemostat optimum, as a function of the deceleration rate for *T. pseudonana* cultures. Errors in the simulated determination of r_x (black line) and the associated specific growth rate μ (dashed line), expressed as a percentage of the values that resulted in the maximum biomass production rate in chemostat. Cultures of the microalga *T. pseudonana* were simulated at low (a) and high (b) light intensity. The dotted grey lines represent the accepted ± 5% error margin. Also shown is the reduction in required experimental time in case the D-stat technique is applied (grey line), expressed in a percentage of the time needed for a series of chemostat experiments. Low and high light intensities correspond with 100 and 1000 µmol photons $m^{-2} \cdot s^{-1}$ of PAR.

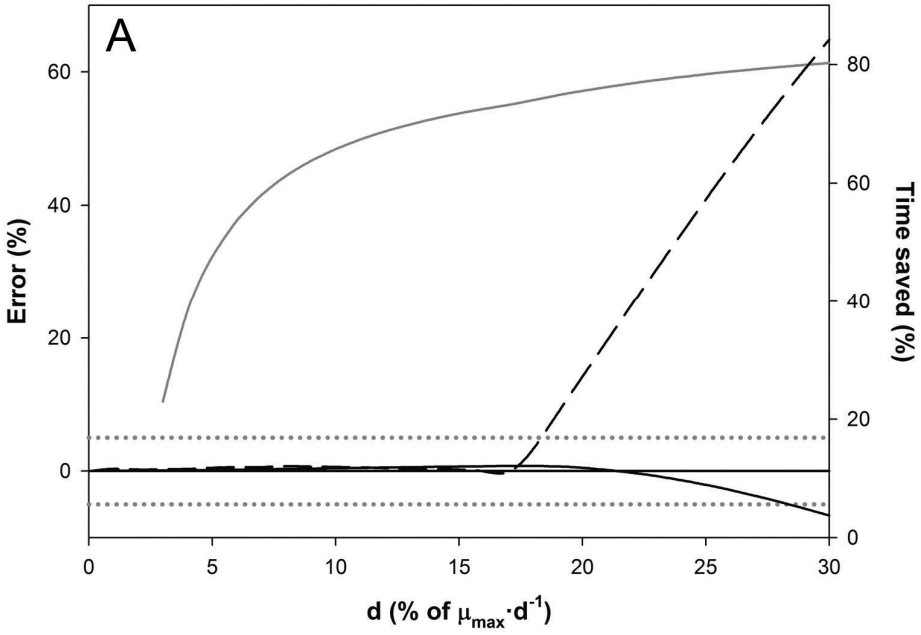
A
Error (%)
Time saved (%)
d (% of μ_{max}·d^{-1})
0
20
40
60
0
20
40
60
80
0
5
10
15
20
25
30

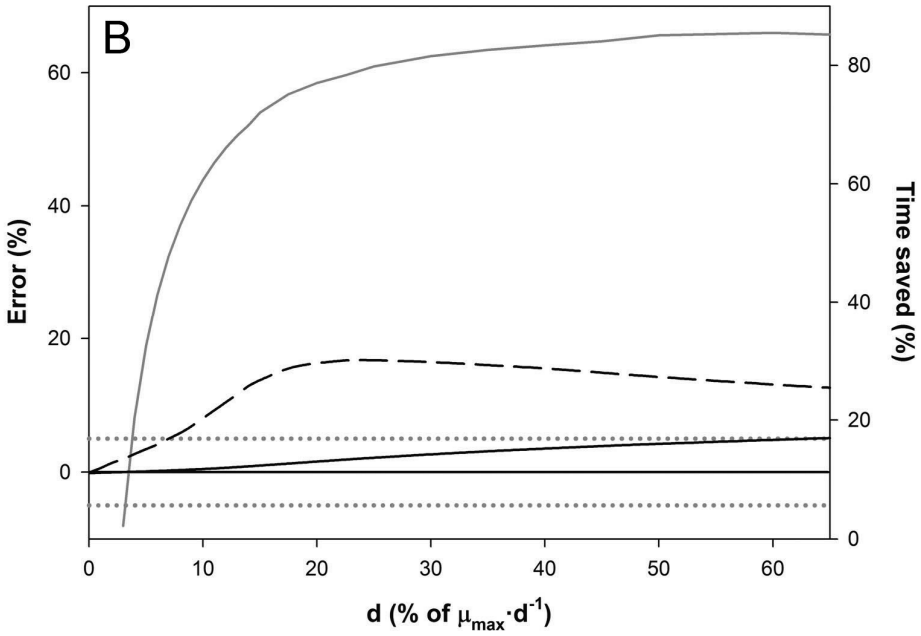
B
Error (%)
Time saved (%)
d (% of μ_{max}·d^{-1})
0
20
40
60
0
20
40
60
80
0
10
20
30
40
50
60

The influence of the decay coefficient on the simulation results

The chemostat simulation results displayed in Figure 2.2 show a broad optimum. This trend can be observed in data presented previously (Barbosa et al. 2005; Molina Grima et al. 1997; Zijffers et al. 2010). In several cases however, published experimental data has shown more distinct maximum biomass productivities (Cuaresma et al. 2009; Pruvost et al. 2011). The decay coefficient has a large effect on the 'sharpness' of the optimum. The decay coefficient of microalgal cultures has been reported to have values of up to 5% of μ_{max} (Kliphuis et al. 2011). The relatively low value of 1.5% of μ_{max} used in this study contributed to the observed broad optimum in biomass production rate; this is illustrated by additional chemostat simulations with an increased decay coefficient of 4.5% of μ_{max} (Figure 2.2).

An increase in r_m results in an overall lower biomass production rate and in a more distinct optimum at a higher specific growth rate. This shift is caused by the higher decrease in biomass productivity at lower dilution rates. It results in a sharper optimum and the need for more iterations during the chemostat optimization, shifting the comparison even more in favour of the D-stat approach.

Practical relevance of the simulation results

In practise, researchers will be interested in identifying the specific growth rate (which equals the dilution rate in a continuous culture) that results in the maximum biomass production rate. The accurate determination of this optimum specific growth rate requires a lower deceleration rate in D-stat cultures than accurate determination of the highest possible production rate, as can be seen in Figure 2.5. At the same time however, more iterations are required in the chemostat (see Table 2.3). The experimental time that can be saved by using the D-stat method for finding both the maximum biomass production rate and the specific growth rate at which it occurs therefore remains significant.

The observed deviations in maximum biomass production rate remain much smaller than the deviation in the optimal specific growth rate, because errors in the specific growth

rate and errors in the biomass concentration partially compensate each other in a D-stat (data not shown). A further increase in deceleration rate would result in a deviation between the D-stat and chemostat estimated values that exceed the accepted ± 5% error criterion. This is due to the fact that photo-acclimation cannot keep up, as described earlier.

Conclusions

In this work, continuous cultures of the microalgae *Thalassiosira pseudonana* and *Phaeodactylum tricornutum* were simulated using a model that describes phototrophic growth and photo-adaptation based on the local rate of photosynthesis.

The model was used to simulate two optimization methods in order to compare their experimental time expenditures. The first optimization method is the traditional series of chemostats, combined with a trisection optimization routine. The second optimization method is a D-stat experiment. During a D-stat experiment, the dilution rate is decreased at a constant speed.

The presented simulations demonstrate that D-stat experiments executed in the absence of pseudo steady-state – *i.e.* $|\mu - D| > 0.05D$ – can still be used to accurately determine the maximum biomass productivity of the system. Moreover, the application of this approach saves up to 94% of the time required to perform a series of chemostat experiments with the same accuracy.

The D-stat optimization method is thus an attractive alternative to a series of chemostats during the optimisation of the biomass production rate in phototrophic reactors.

Nomenclature

A^*_{Chl}	Chl a specific light absorption coefficient	[$m^2 \cdot g\ Chl\ a^{-1}$]
Chl: L	Carbon fraction of chlorophyll a in L	[g Chl a· $g\ L^{-1}$]
C_x	Biomass concentration	[g C·m^{-3}]
d	Deceleration rate	[d^{-2}]
D	Dilution rate	[d^{-1}]
E	Biomass of the biosynthetic machinery	[g C·m^{-3}]
I	Light intensity	[mol photons·m^{-2}·d^{-1}]
I_0	Incident light intensity	[mol photons·$m^{-2}d^{-1}$]
L	Biomass of the photosynthetic apparatus	[g C·m^{-3}]
PAR	Photosynthetically Active Radiation (400- 700 nm)	[-]
PBR	photobioreactor	[-]
P^E	E-specific rate of photosynthesis	[d^{-1}]
P^E_m	Maximum E-specific rate of photosynthesis	[d^{-1}]
r_m	Decay coefficient	[d^{-1}]
r_x	Biomass production rate	[g·m^{-3}·d^{-1}]
R	Biomass of the storage pool	[g C·m^{-3}]
z	Location inside the PBR along light path	[m]
Z	Optical depth of photobioreactor	[m]
κ_E	Proportion of biosynthate allocated to synthesis of E	[-]
μ	Specific growth rate	[d^{-1}]
ρ_L	Proportion of photosynthate allocated to L synthesis	[-]
ρ_E	Proportion of photosynthate allocated to E synthesis	[-]
ρ_R	Proportion of photosynthate allocated to R synthesis	[-]
σ	Functional cross section of L	[m^2·mol $photons^{-1}$]

Appendix 1 Simulation results for *P. tricornutum* cultures.

In order to demonstrate general validity of the presented results, additional simulations were done for the significantly slower growing diatom *Phaeodactylum tricornutum*. The model parameters presented in Table 2.4 were taken from literature (Geider et al. 1996) and the model presented in Figure 2.1 was used.

Table 2.4 Modeling parameter values for *P. tricornutum* (Geider et al. 1996).

Parameter	Value	Units
σ	1.0	$m^2 \cdot mol\ photons^{-1}$
$Chl:C$	0.1	$g \cdot g^{-1} \cdot L^{-1}$
A^*_{Chl}	10	$m^2 \cdot g^{-1}$ Chl a
$\kappa_E (= \rho_E)$	0.6	-
P_E^m	2.40	d^{-1}
r_m	0.05	d^{-1}
μ_{max}	1.39	d^{-1}

Figure 2.6A shows the errors made in both the maximum biomass production rate and the associated growth rate at low light intensity, and Figure 2.6B for high light intensity, both as a function of the applied deceleration rate. Table 2.5 summarizes the *P. tricornutum* simulation results. It shows that the D-stat experiment results in a similar reduction of required experimental time compared to a series of chemostat experiments, as was found for *T. pseudonana* (Table 2.3).

The advantage of applying D-stat methodology is even more pronounced in this case, as *P. tricornutum* has a maximum specific growth rate that is less than half that of *T. pseudonana*. Thus it takes more time to achieve steady state in chemostat cultures, as can be seen in Table 2.5.

Figure 2.6 Errors in the D-stat estimation of the steady state parameters at which the maximum biomass production rate occurs in comparison to the true chemostat optimum, as a function of the deceleration rate. Errors in the simulated determination of r_x (black line) and the associated specific growth rate μ (dashed line), expressed as a percentage of the values that resulted in the maximum biomass production rate in chemostat. Cultures of the microalga *P. tricornutum* were simulated at low (a) and high (b) light intensity. The dotted grey lines represent the accepted ± 5% error margin. Also shown is the reduction in required experimental time in case the D-stat technique is applied (grey line), expressed in a percentage of the time needed for a series of chemostat experiments. Low and high light intensities correspond with 100 and 1000 µmol photons $m^{-2} \cdot s^{-1}$ of PAR.

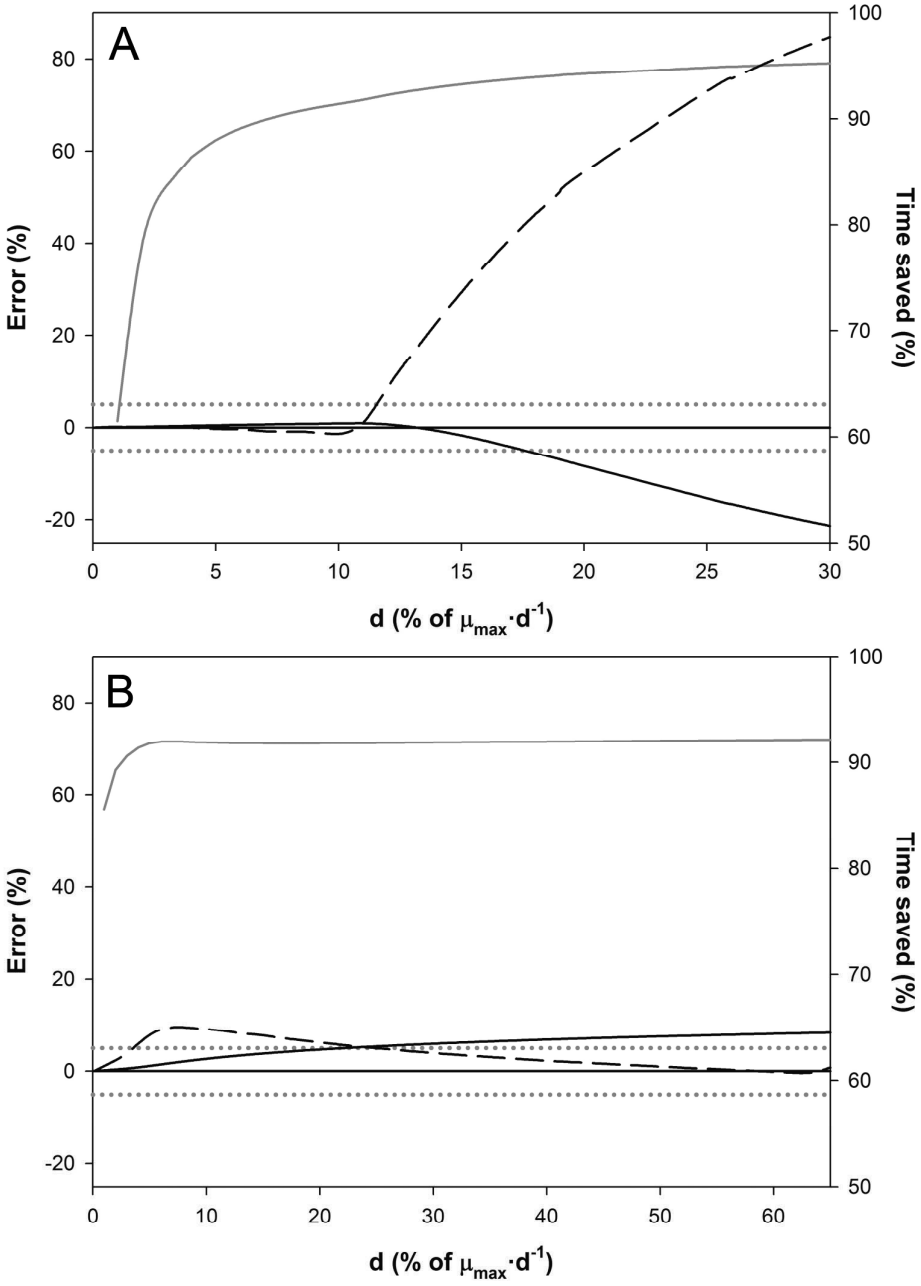
A
B
Error (%)
Time saved (%)
d (% of μ_{max}·d^{-1})
d (% of μ_{max}·d^{-1})

Table 2.5 Simulation of PBR optimization for *P. tricornutum* cultures at low (A) and high (B) light intensity.

A ↓ Iteration	μ [d^{-1}]	r_x [$g \cdot m^{-3} \cdot d^{-1}$]	$\Delta r_x/\Delta\mu$ [$g \cdot m^{-3}$]	t [d]
0	0.63 0.3 5	72.3 154.2 170.9 115.8	-294.7 -60 197.9	4[1] 12 12 41
1	0.4 4 0.2 5	154.2 170.4 165.7 115.8	-87.6 25.3 269.2	- 14 14 -
2	0.3 2 0.1 9	170.4 169.8 158.0 115.8	4.7 95.6 341.5	- 9 16 -
3	0.3 6 0.2 8	170.4 (-0.4%) 171.1 167.4 (-2.1%) 158.0	-7.9 44.1 114.2	-
Total time required for the execution of the series of chemostats				145
D-stat, 17% of $\mu_{max} \cdot d^{-1}$	0.55	164.1	-	9
Time saved in case of D-stat, in comparison with this series of chemostats				**136 94%**

B ↓ Iteration	μ [d^{-1}]	r_x [$g \cdot m^{-3} \cdot d^{-1}$]	$\Delta r_x/\Delta\mu$ [$g \cdot m^{-3}$]	t [d]
0	1.18 0.81 0.44 0.07	684.4 745.7 718.7 465.6	-165.2 72.7 682.9	6[1] 4 8 41
1	0.81 0.56 0.32 0.07	745.7 734.4 691.4 465.6	45.6 174.1 913.6	- 10 11 -
2	0.81 0.65 0.48 0.32	745.7 740.8 (2.2%) 724.9 691.4 (-4.6%)	29.5 96.5 203.6	- 7 7 -
-	-	-	-	-
Total time required for the execution of the series of chemostats				94
D-stat, 20% of $\mu_{max} \cdot d^{-1}$	0.85	780.5	-	8
Time saved in case of D-stat, in comparison with this series of chemostats				**86 92%**

The experimental time required for both optimization strategies (D-stat and series of chemostats) is calculated, as well as a comparison in required experimental time. The comparisons made are best-case scenarios, as the fastest D-stat experiments that still give accurate steady state values for the maximum biomass production rate (Figure **2.6***) were selected. See the materials and methods section for a description of the trisection method used during the chemostat optimization strategy.*

[1] Total time required, including batch pre-growth and initial steady state.

Chapter 3

A pneumatically agitated flat-panel photobioreactor with gas re-circulation: anaerobic photoheterotrophic cultivation of a purple non-sulfur bacterium

The contents of this chapter have been published as

Hoekema S, Bijmans M, Janssen M, Tramper J, Wijffels RH. 2002. A pneumatically agitated flat-panel photobioreactor with gas re-circulation: anaerobic photoheterotrophic cultivation of a purple non-sulfur bacterium. International Journal of Hydrogen Energy 27:1331-1338.

3. A pneumatically agitated flat-panel photobioreactor with gas re-circulation: anaerobic photoheterotrophic cultivation of a purple non-sulfur bacterium

Abstract

The application of hydrogen as a notable energy carrier in the near future becomes more and more evident. Within the process of photobiological hydrogen production, purple non-sulfur bacteria are an interesting subject of study because of their high hydrogen producing capacity. In the research presented, a *Rhodopseudomonas* species was used, which had proven to be an efficient hydrogen producer from acetic acid and light energy.

A combination of a short light path, combined with turbulent mixing, can counter-act the effect of self-shading in a photobioreactor. Therefore we constructed a pneumatically agitated flat-panel photobioreactor with a light path of only 3 cm. The gas used for agitation was re-circulated in the closed, anaerobic system.

Batch experiments and a chemostat experiment were performed to demonstrate the proper functioning of the new reactor. Evidence is provided that gas re-circulation might even be a prerequisite for growth in a pneumatically agitated system in order to retain a sufficient concentration of dissolved carbon dioxide in the culture liquid.

Introduction

The worldwide energy requirement is growing exponentially, the reserves of fossil fuels are decreasing rapidly and the combustion of fossil fuels has serious negative effects on the environment. For this reason, much research is aimed at the exploration of new and sustainable energy production systems that could substitute energy production based on fossil fuels.

Hydrogen is a clean and efficient fuel and is definitely a potential substitute. Most hydrogen used today is produced in physical-chemical processes (steam reforming of natural gas) or electrochemical processes (electrolysis of water). These processes are energy intensive and they are not sustainable because there is only a limited reserve of fossil fuels.

Biomass can also be used as the raw material to produce hydrogen. This can be done either by physical/chemical treatment, for instance gasification, or by conversion in a biological system. A drawback of gasification is the large amount of energy needed to evaporate the water present in the biomass. Wet substrates are favorable to biological systems for hydrogen production. Biological hydrogen production could play an important role in developing a renewable hydrogen industry (Benemann 1996).

Anoxygenic photosynthetic bacteria (purple non-sulfur bacteria) can produce hydrogen from simple organic molecules like organic acids or alcoholic compounds. Light energy (sunlight) is used to provide the energy needed for this thermodynamically unfavorable conversion. The combination of these bacteria and other bacteria (Facultative anaerobes, obligate anaerobes or even thermophiles and aerobes) in a two-step system could provide a system that can efficiently produce hydrogen from carbohydrates present in (waste) biomass. In the first step of such a process bacteria convert the carbohydrates to organic acids like acetate. In the second photoheterotrophic step the organic acids are converted to hydrogen (Barbosa et al. 2001; Claassen et al. 1999).

Examples of full-scale application of biological systems for the production of hydrogen are not presented in literature, but research on lab scale is well documented (Asada and Miyake 1999; Zürrer and Bachofen 1979). For the successful scale-up of the second photoheterotrophic step, the efficiency at which light energy is directed to biomass growth and hydrogen production is the most important optimization parameter.

Also in algal biotechnology research has been focused on the efficient utilization of solar irradiance. The light utilization efficiency was found to be close to the theoretical maximum in short light-path photobioreactors operated at high biomass densities and intense aeration (Qiang et al. 1996; Richmond 2000). This was demonstrated under outdoor solar irradiation for the cultivation of the phototrophic cyanobacterium *Spirulina platensis* (Qiang et al. 1998a).

For this reason we developed a lab-scale flat-panel photobioreactor for the anaerobic cultivation of purple non-sulfur bacteria and concomitant hydrogen production from organic acids. Richmond and co-workers (Richmond 2000) were able to use air as the gas facilitating turbulent mixing. For the process of photoheterotrophic hydrogen production, argon needs to be used because oxygen (air) and nitrogen gas lower nitrogenase-based hydrogen production. The continuous throughput of fresh argon gas is expensive and the hydrogen produced will be diluted strongly. These effects are undesirable and applying a closed gas-re-circulation system could provide a solution for this problem.

In this study a lab scale flat-panel photobioreactor design is described. It was tested for its applicability for the cultivation of the purple non-sulfur bacterium *Rhodopseudomonas* sp. The experiments were done using continuous re-circulation of argon gas. It was demonstrated that the system works well and that a steady state could be attained. In addition, it will be shown that gas re-circulation might even be essential to maintain optimal growth conditions.

Materials and Methods

Bacterial strain and medium composition

A *Rhodopseudomonas* sp. HCC 2037 culture was kindly provided by JoAnn Radway of the University of Hawaii. The culture was maintained in so-called 'SyA' medium under a nitrogen headspace. The composition of the SyA medium is given in Table 3.1. The cultures were illuminated with 90 µmol $m^{-2} \cdot s^{-1}$ of PAR (Photosynthetic Active Radiation, 400 – 700 nm) in a day/night cycle of 16 h/8 h at 25˚C.

During the batch experiments so-called 'AA-b' medium was used. During the chemostat experiment the culture was diluted with so-called 'AA-c' medium. The composition of the media is given in Table 3.1. The media were prepared from concentrated stock solutions and autoclaved prior to use. Calcium chloride and magnesium sulfate were autoclaved together, but separated from the other components to prevent calcium- and magnesium phosphate depositions. The concentrated vitamin solution used was filter sterilized first.

Initially AA-b1 medium was used, which is similar to the SyA medium except for the concentrations of the carbon- and nitrogen source. After some experiments it was found that the gas spargers clogged. This was probably due to calcium- and magnesium phosphate precipitations. In further experiments, the concentrations of phosphate buffer and macronutrients (calcium chloride and magnesium sulfate) were reduced to the levels indicated under AA-b2 medium in Table 3.1.

The concentrations of elements needed to yield a certain biomass concentration (C_x) were calculated according to the elemental composition of our bacterium (measurements not published). This composition was $CH_{1.76}O_{0.38}N_{0.14}$. The phosphorous content was taken to be 1.61% as reported by Tsygankov and Laurinavichene (Tsygankov and Laurinavichene 1996b) for *Rhodobacter capsulatus*. The sulfur content of the bacteria was assumed to be 0.0045 mol·mol C^{-1}. Taking this into account, the elemental composition of the biomass yielded $CH_{1.76}O_{0.38}N_{0.14}P_{0.01}S_{0.0045}$.

Table 3.1 Composition of the different media used.

Component class	Component	Concentration [mg·L^{-1}]			
		SyA medium	**AA-b1 medium**	**AA-b2 medium**	**AA-c medium**
Vitamins	biotin	1	-	-	1
	thiamin	1	-	-	1
	p-amino benzoic acid	1	-	-	1
	vitamin b_{12}	1	-	-	1
	nicotinamide	1	-	-	1
Phosphate buffer	KH_2PO_4	1732	1732	108.3	433
	K_2HPO_4	1466	1466	91.6	366
Macro nutrients	$MgSO_4.7H_2O$	200	200	12.5	50
	$CaCl_2.2H_2O$	99	99	6.2	25
	$Na_2EDTA.H_2O$	20	20	20	20
	$FeSO_4.7H_2O$	11.8	11.8	11.8	11.8
	H_3BO_3	2.8	2.8	2.8	2.8
	$MnSO_4.H_2O$	2.77	2.77	2.77	2.77
	$Na_2SO_4.7H_2O$	0.75	0.75	0.75	0.75
	$ZnSO_4.7H_2O$	0.24	0.24	0.24	0.24
	$Cu(NO_3)_2.3H_2O$	0.04	0.04	0.04	0.04
C and N sources	Na-succinate	8100	-	-	-
	Yeast extract	1000	-	-	100
	Na-acetate [mM]	20	40	40	105
	NH_4Cl [mM]	-	9.3	9.3	24.3
	$(NH_4)_2SO_4$ [mM]	-	-	0.39	1.11

On the basis of this elemental composition, the AA-b2 medium was designed to support a C_x of 1.7 $g \cdot L^{-1}$. The concentrations of magnesium and calcium were assumed to be sufficient to support this biomass density although no references were found in literature to support this. The composition of the 'AA-c' medium that was used for chemostat cultivation is also shown in Table 3.1. It was designed to support a C_x of 4 $g \cdot L^{-1}$.

Acetic acid determination

The acetic acid concentration in the culture medium was determined by gas chromatography. Samples were centrifuged and the supernatant was diluted 1:1 with 3% (v/v) formic acid and stored at -80 °C. The samples were analyzed on a HP 5890 gas chromatograph equipped with a glass packed column (length 2 m, internal diameter 2 mm, 10% Fluorad 431 on Supelco-port, 100 – 120 mesh) and a FID (flame ionization detector). The column and the FID were kept at 130 and 280 °C, respectively. Nitrogen saturated with formic acid was used as the carrier gas at a flow rate of 40 $mL \cdot min^{-1}$.

Ammonium determination

Samples for ammonium determinations were centrifuged and the supernatant was stored at -80°C. The concentration of ammonium in the samples was determined using Nessler's reagent. Nessler's reagent (HgI_4^{2-}) together with NH_4^+ forms the yellow complex NH_4HgI_4; potassium sodium tartrate was added to keep the salts dissolved that might interfere with the determination. The absorbance was read at 440 nm on a Spectronic 20 Genesys spectrophotometer and compared to the absorbance of standard solutions.

Hydrogen determination

The volume fraction of hydrogen in the gas produced was determined using a gas chromatograph: Chrompack CP9000 series equipped with a packed column (length 1.8 m, internal diameter 0.25 inch, molsieve 13X, 60-80 mesh) and a TCD (thermal conductivity

detector). The column and the TCD were kept at 100 and 120˚C, respectively. The carrier gas was argon at a flow rate of 20 mL·min^{-1}.

Light intensity

The PAR light intensity was measured using a LI SA-190 quantum sensor combined with a LI-250 read-out unit (Li-Cor, USA).

Other determinations

Bacterial growth was monitored measuring the optical density of the cultures at 660 nm (OD_{660}) using a Spectronic 20 Genesys spectrophotometer. The cell dry weight was determined by centrifuging 50 ml of cell suspension (7000 g for 10 min), washing the pellet with deionized water and drying at 103˚C until constant weight. One OD_{660}-unit was found to be equal to a C_x of 0.7 g·L^{-1}.

Chemicals

All chemicals used were reagent grade and produced by Merck, Darmstadt, Germany.

Flat-panel photobioreactor

The new design of the flat-panel photobioreactor (PRB) is depicted in Figure 3.1. It was autoclaved completely prior to all runs. It consists of a stainless steel frame and polycarbonate panels. A membrane gas pump circulates the gas through the spargers (hypodermic needles) at the bottom of the reactor. The produced gas is collected in a gasbag. Two 1-liter pressure vessels prevent pressure fluctuations in the gas re-circulation system. A pressure valve maintains a constant input pressure to the mass flow controller. A condenser prevents water vapor from entering the gas re-circulation system. A pH electrode and a redox electrode were fitted into the reactor for pH-control and monitoring purposes, respectively. The medium was autoclaved separately and fed to the reactor after autoclaving.

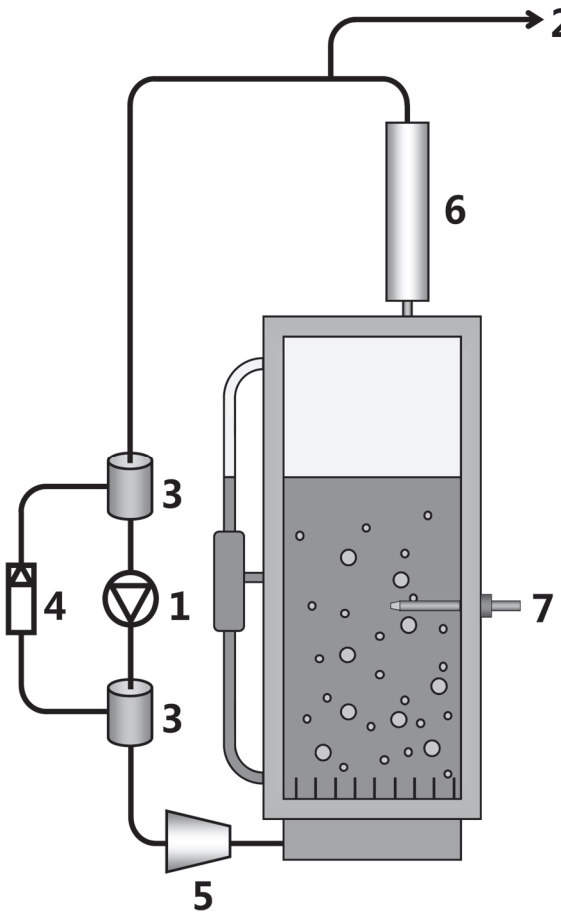

Figure 3.1 Schematical drawing of the bioreactor setup. Membrane gas pump (1); gasbag for collection of produced gas (2); two 1-liter pressure vessels (3); pressure valve (4); mass flow controller (5); condenser (6); pH/redox electrode (7).

The reactor is composed of two compartments located behind each other. The front compartment contains the bacterial culture (3 cm deep). The culture volume is 2.4 liters. Through the other compartment (2 cm deep) water was circulated via a temperature controlled water bath in order to maintain the temperature at 30˚C.

Two 500 W tungsten-halogen lamps (Philips Halotone R7s fitted in Philips QVF 415n reflectors) are placed on one side of the reactor. The lamps are mounted above each other in a frame and placed on 75 cm distance from the reactor. The average light intensity at the reactor surface was 325 μmol PAR·m^{-2}·s^{-1}.

Bacterial growth was monitored on-line. On the left-hand side of the reactor a small tube was attached to the reactor Figure 3.1). The bacterial suspension flowed through this tube as a result of an airlift effect. A red light emitting diode (LED) peaking at 665 nm was used as a light source on one side of the tube. On the other side an in-house constructed PAR light sensor registered the remaining PAR light intensity as a mV signal. This signal was translated to a value similar to the absorbance measured in a spectrophotometer according to Equation 3.1.

Equation 3.1 $$\mathrm{ABS} = -\log\frac{\mathrm{I}}{\mathrm{I_o}}$$

Where ABS = absorbance [-]

I = light-induced signal after passage through the tube [mV]

I_0 = reference light-induced signal with only medium without bacteria in the tube [mV]

The liquid level was controlled using another similar homemade light sensor as described previously. The sensor is placed behind the reactor at the desired level and the effluent pump was controlled on the basis of this signal. The set-up was computer controlled and most signals were recorded using a data logger. The pH was controlled at 6.8 – 7.0 in all experiments using 0.5 M HCl dosing.

Serum flask experiments

In one experiment to assess the influence of the ammonium concentration 8 closed 100 mL serum flasks were used. These were filled with 50 mL of medium and autoclaved. The flasks were inoculated under an argon headspace. The flasks were stirred continuously using a magnetic stirrer and illuminated with 90 μmol PAR·m^{-2}·s^{-1} in a day/night cycle of 16 h/8 h at 25˚C.

Bubble column experiments

Other experiments were done in small 300 mL glass bubble columns to investigate the effect of shear on *Rhodopseudomonas* sp. The reactors were equipped with a water jacket for the re-circulation of cooling water via a temperature controlled water bath. The temperature was controlled at 30˚C. The reactors were autoclaved empty and filled with medium afterwards. Two 300 W tungsten-halogen lamps (Philips Halotone R7s fitted in Philips QVF 415n reflectors) were placed on one side of the reactor. The lamps were mounted above each other and placed on 30 cm distance from the reactor in order to yield an average light intensity of 250 μmol PAR·m^{-2}·s^{-1} at the reactor surface.

Results and Discussion

Operation of flat-panel photobioreactor with continuous gassing of argon

During this first experiment using the flat-panel bioreactor AA-b2 medium was used, containing 40 mM acetate and 9.3 mM ammonium. The reactor was gassed continuously with argon at a flow rate of 0.83 L·L^{-1}·min^{-1}. Argon was used as the agitation gas because oxygen and nitrogen negatively affect the hydrogen evolving capacity of the bacterial nitrogenase enzyme.

The recorded on-line absorbance of the bacterial suspension is shown in Figure 3.2. This absorbance was measured in a small tube attached to the reactor in which the culture

flowed. It can be seen clearly that the absorbance of the culture does not change and apparently no growth occurred.

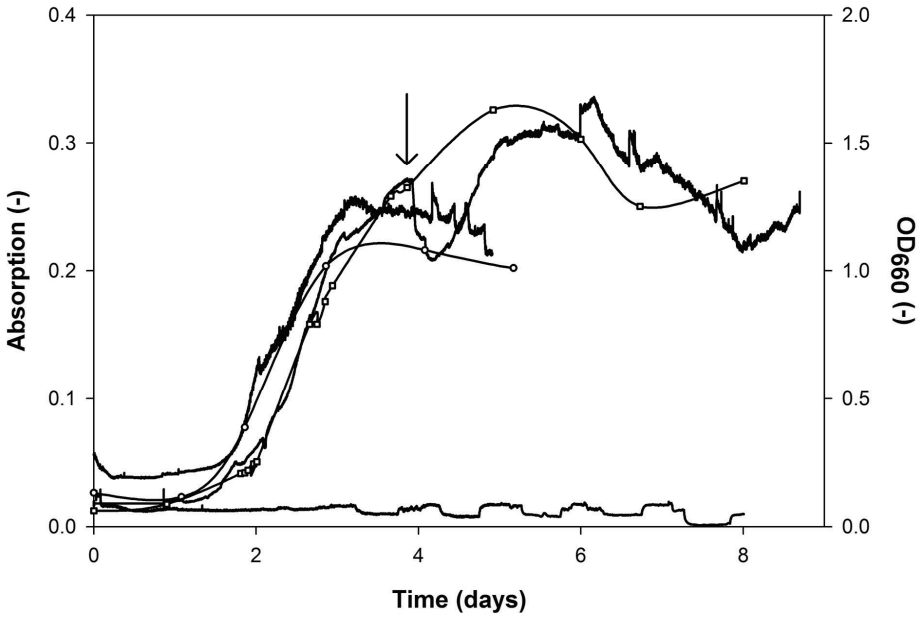

Figure 3.2 Light absorbance and OD_{660}-values during all experiments in the flat-panel photobioreactor. On-line light absorbance measurement during the batch experiment with continuous argon sparging (1). On-line light absorbance measurement and off-line OD_{660} measurements (○) during the batch experiment with gas re-circulation (2). On-line light absorbance measurement and the off-line OD_{660} measurements (□) during the chemostat experiment (3). The arrow indicates the point where the batch pre-culture ended and chemostat operation was started.

It was unclear what the reason for the absence of growth was. Possibly ammonium-inhibition played a role. No data was available on possible growth inhibition of ammonium on *Rhodopseudomonas* sp. Therefore, a set of serum flask experiments was performed to assess the effect of ammonium on the growth and hydrogen evolution of our species.

The results are presented in Figure 3.3. Batch incubations were performed using AA-b1 medium with 30 mM acetate and 0, 1, 2, 5, 10, 15 and 20 mM of ammonium respectively. At the end of the growth phase the OD_{660} and the volume fraction of H_2 in the headspace were determined. Using the volume fraction the total amount of hydrogen gas produced was calculated. It can be seen clearly that the final OD_{660} value increases with the increasing initial concentration of ammonium up to 20 mM. A concentration of 9.3 mM of ammonium is therefore much too low to cause full inhibition of growth. From Figure 3.3 it is also clear that ammonium represses hydrogen production significantly above a concentration of 5 mM. It is a well-known fact from literature that ammonium inhibits the nitrogenase enzyme at milli-molar concentrations (Fedorov et al. 1999; Yagi et al. 1994; Yakunin and Hallenbeck 1998).

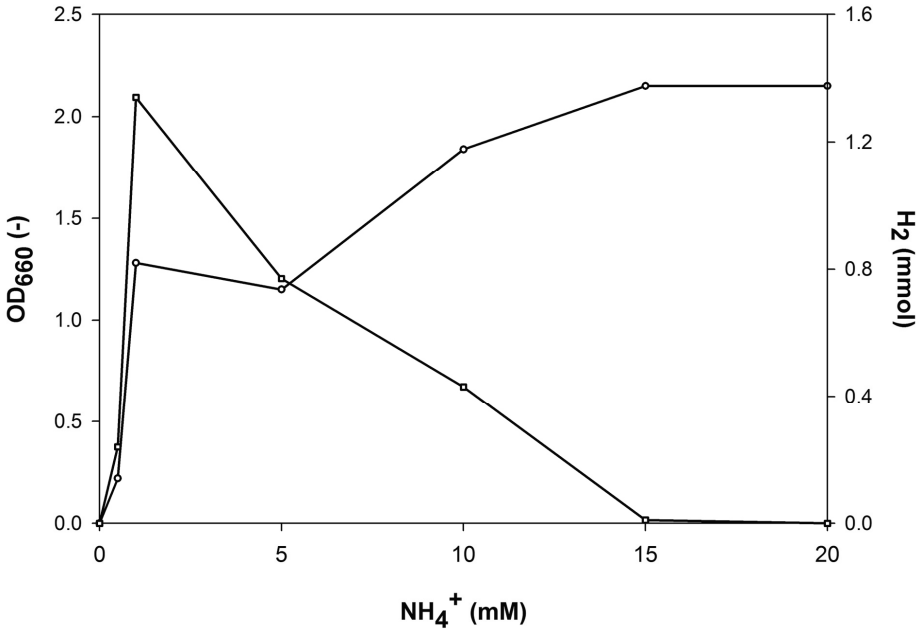

Figure 3.3 The influence of the initial ammonium concentration on the final OD_{660} value (○) and the total amount of hydrogen gas evolved (□) in closed 100 ml serum flasks.

Another explanation for the lack of growth in the flat-panel photobioreactor continuously gassed with argon could be shear stress caused by gas bubbling. In order to investigate this further, five experiments were performed in 300 ml glass bubble columns, using nitrogen or argon at various flow rates. AA-b1 medium with 40 mM of acetate and 9.3 mM of ammonium was used. Five experiments were done: one experiment without any agitation, another experiment applying 2 $L \cdot min^{-1}$ nitrogen, and three more experiments applying argon at 0.33, 1.66 and 6.66 $L \cdot L^{-1} \cdot min^{-1}$ respectively. Figure 3.4 shows the optical density (OD_{660}) in time for all experiments. Only in the experiment in which no agitation was applied an OD_{660}-increase was observed. The optical density reached a value of 2.4; this is equal to a C_x of 1.7 $g \cdot L^{-1}$, which was the biomass concentration the medium was

designed for. The remaining incubations did not show any increase in OD_{660} in time, indicating that no growth had occurred. From these results it is clear that pneumatic agitation with nitrogen or argon inhibited bacterial growth at 6.66 $L \cdot L^{-1} \cdot min^{-1}$ and at any flow rate ranging from 0.33 to 6.66 $L \cdot L^{-1} \cdot min^{-1}$ respectively.

The extremely low flow rate of 0.33 $L \cdot L^{-1} \cdot min^{-1}$ already prevented the culture from growing, which made shear stress improbable. Moreover, all bacteria from the Rhodospirillaceae family are contained by a cell wall (Weckesser et al. 1995) that offers extra protection against shear stress.

The absence of growth could also have something to do with stripping of carbon dioxide from the culture medium by the continuous gas flow. The carbon dioxide dependent growth of members of the Rhodospirillaceae family on acetate as the only organic substrate can be explained in two ways. Firstly, when phototrophic bacteria grow on highly reduced substrates they must have a means for disposing of excess reducing equivalents, in order to retain the redox balance between the substrates consumed and their metabolic products (Ferguson et al. 1987). These reduction equivalents can be consumed by the Calvin cycle enzymes during carbon dioxide fixation (Lascelles 1960). Dependent on the discrepancy between the degree of reduction of the biomass and the organic substrate carbon dioxide can be either produced or consumed (Sojka 1978). The incorporation of $^{14}CO_2$ into cell material during growth of *Rhodospirillum rubrum* on a range of reduced carbon substrates including acetate was observed. There was only net uptake of carbon dioxide during growth on propionate and butyrate (Ormerod 1956). Moreover it was shown that the activity of ribulose bisphosphate carboxylase (the enzyme responsible for carbon dioxide fixation in the Calvin cycle) of *Rhodobacter sphaeroides* was strongly de-repressed during growth on highly reduced substrates (Gibson and Tabita 1976). Although the operation of the Calvin cycle may be needed to a certain extent, it is energetically expensive and assimilation of a broad spectrum of reduced substrates is apparently favored over wholesale carbon dioxide fixation (Ferguson et al. 1987).

Secondly, a large group of phototrophic bacteria from the Rhodospirillacae family lack the enzyme isocitrate lyase. This enzyme is part of the glyoxylate cycle that replenishes the pool of citric acid cycle intermediates. A large group of these bacteria are able to grow on acetate as the sole organic substrate and therefore need another route for the replenishment of the used citric acid cycle intermediates. Ivanovskii et al (Ivanovskii et al. 1997) proposed an anaplerotic cycle of acetate assimilation in which citramalate is an intermediate during glyoxylate formation. In this citramalate cycle carbon dioxide is used and formed again and no net consumption takes place. However, since propionyl-CoA carboxylase (the enzyme that couples carbon dioxide to propionate) has a low affinity for carbon dioxide a certain carbon dioxide concentration is needed to maintain a high rate of growth and acetate assimilation (Ivanovskii et al. 1997).

Possibly most of the carbon dioxide produced was removed in our pneumatically agitated systems quite efficiently due to the continuous stripping with argon gas. This might have caused the absence of growth in this first experiment with the flat-panel photobioreactor. It gave an extra incentive to start with experiments using the gas re-circulation system. In this mode of operation all the carbon dioxide produced is retained in the system.

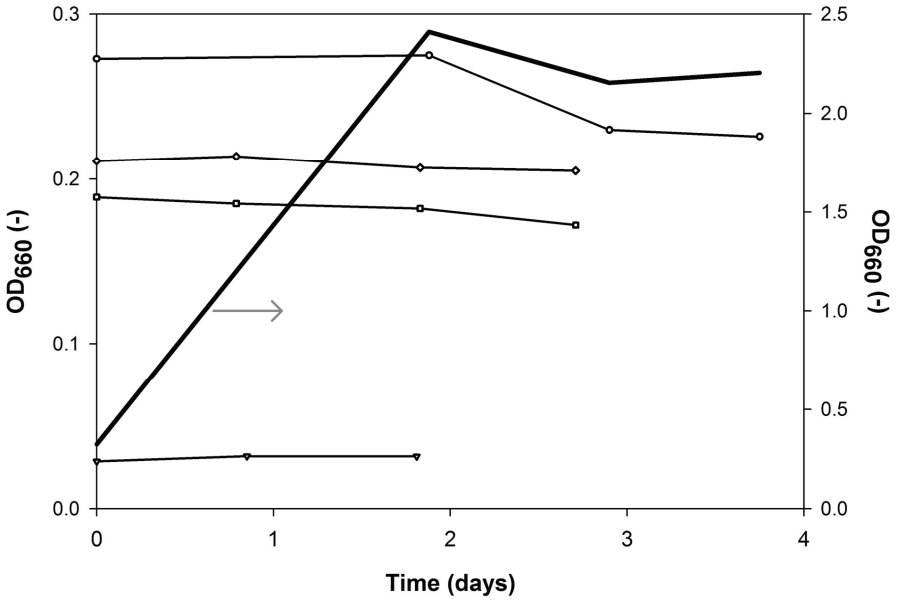

Figure 3.4 The influence of the type of gas agitation and its flow rate on bacterial growth, measured as OD_{660} in 300 mL bubble columns. No gas agitation (bold line); Nitrogen 6.66 $L{\cdot}L^{-1}{\cdot}min^{-1}$ (○); Argon 6.66 $L{\cdot}L^{-1}{\cdot}min^{-1}$ (□); Argon 1.66 $L{\cdot}L^{-1}{\cdot}min^{-1}$ (◊); Argon 0.33 $L{\cdot}L^{-1}{\cdot}min^{-1}$ (▽).

Operation of the flat-panel photobioreactor with gas re-circulation

A batch experiment in the flat-panel photobioreactor system was performed using gas re-circulation. After inoculation the complete system was flushed with argon to create anaerobic conditions and the gas re-circulation was switched on at 0.83 $L{\cdot}L^{-1}{\cdot}min^{-1}$. AA-b2 medium was used, containing 40 mM acetate and 9.3 mM ammonium. In Figure 3.2 the development of both the recorded on-line culture absorbance, and the OD_{660} measured off-line are shown. During the course of the experiment the absorbance of the bacterial suspension increased significantly from 0.01 to 0.25. The off-line OD_{660} measurements, also shown in Figure 3.2, show the same trend and increased from 0.15 to 1.2. It is clear

that growth occurred now and apparently our assumption of carbon dioxide depletion in the previous experiment was correct because during this new experiment with gas re-circulation growth was supported. The medium was designed to support 1.7 $g \cdot L^{-1}$ of dry weight biomass and as can be seen from Figure 3.2 an OD_{660} of 1.2 was reached. This value equals 0.85 $g \cdot L^{-1}$ of biomass. It is not clear why the biomass concentration remained lower than anticipated, while acetate and ammonium were still present in the medium.

After growth was demonstrated in batch culture, an experiment was performed to cultivate *Rhodopseudomonas* sp. in chemostat. During this experiment the redox potential of the culture was monitored to check for anaerobicity. First, a batch pre-culture was grown similar to the one described above. This time, AA-b2 medium was used; a small amount of yeast extract and vitamins was added to stimulate growth at concentrations indicated under AA-c medium (Table 3.1). After the batch pre-culture, the culture was switched to a chemostat at a dilution rate of 0.035 h^{-1}. This rate equals 50% of the maximum growth rate of our *Rhodopseudomonas* sp. of 0.07 h^{-1} measured in batch experiments previously (data not published).

During chemostat mode the AA-c medium (Table 3.1) was used. The elemental composition of this medium supports a C_x of 4 $g \cdot L^{-1}$. Figure 3.2 shows the development of both the culture absorbance recorded on-line and the OD_{660} measured off-line. As can be seen from Figure 3.2, the OD_{660} was 1.2 at the end of the batch pre-culture, which equals a C_x of 0.84 $g \cdot L^{-1}$. This is identical to the previous experiment. Apparently the vitamins and yeast extract added did not contribute to a higher biomass concentration at the end of the batch culture.

After switching to a chemostat on day 4, a slight temporal decrease in absorbance can be observed (Figure 3.2). Possibly the culture needed some adaptation time. After this the C_x rose again and became more stable at an OD_{660} of 1.63, which equals 1.14 g of biomass$\cdot L^{-1}$. It is not clear what is the reason why the C_x was lower than anticipated.

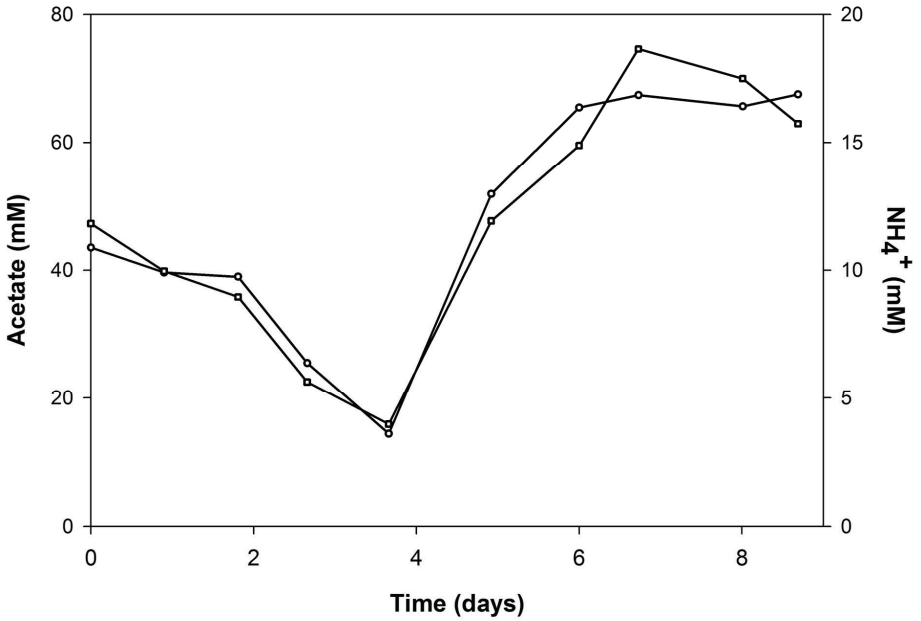

Figure 3.5 Concentrations of acetate (○) and ammonium (□) during the chemostat experiment in the flat panel photobioreactor (line 3 in Figure 3.2).

Possibly it was caused by a limitation in the concentrations of calcium chloride, magnesium sulfate or phosphate in the medium. During preliminary experiments in the flat-panel photobioreactor we observed clogging of the gas spargers due to salt precipitates. Probably these precipitates were calcium- and magnesium phosphates. Therefore we decided to lower the concentrations of calcium chloride, magnesium sulfate and phosphate buffer, which resulted in the AA-b2 medium as given in Table 3.1. Another possibility is that the light intensity on the reactor surface, 325 µmol $m^{-2} \cdot s^{-1}$ on average, did not support a high concentration of biomass in our chemostat.

Figure 3.5 shows the concentrations of acetate and ammonium during the entire experiment. It can be seen that the concentrations decrease fast during the batch period. After day 4, at the start of continuous chemostat dilution, the concentrations of both

acetate and ammonium increase again due to the fact that more of the substrates is introduced than can be consumed by the culture. During the entire experiment the ammonium concentration remains higher than 4 mM. This is too high to facilitate hydrogen production, as can be seen in Figure 3.3. In Figure 3.5 we can also see that the consumption of the two substrates follows the biomass composition perfectly. The C/N ratio in the consumption of substrates equals 8.3 throughout the experiment. This corresponds perfectly with the elemental balance shown in Equation 3.2, from which a C/N ratio of 8 can be calculated. The biomass composition was determined in previous experiments (data not published).

Equation 3.2 $3.96\ CH_3COOH + NH_4+ \rightarrow 7.143\ CH_{1.76}O_{0.38}N_{0.14} + 0.79\ CO_2 + 3.64\ H_2O$

The redox potential remained around –50 mV during the entire experiment, indicating anaerobic conditions.

Conclusions

It was demonstrated that the newly developed photobioreactor with gas re-circulation functions properly. It was possible to attain a chemostat culture of a photoheterotrophic bacterium under anaerobic conditions.

The observed absence of growth of *Rhodopseudomonas* sp. during experiments with continuous gassing with argon was probably caused by the need for carbon dioxide. When gas re-circulation was applied, growth was observed. Apparently carbon dioxide is needed when photosynthetic bacteria grow on reduced carbon substrates. Indications in this direction were also found in literature.

This new design of a flat-panel photobioreactor with pneumatic agitation opens up a future in which possibly light energy can be directed to hydrogen gas production at high efficiency.

Chapter 4

Controlling light-use by *Rhodobacter capsulatus* continuous cultures in a flat-panel photobioreactor

The contents of this chapter have been published as

Hoekema S, Douma, RD, Janssen M, Tramper J, Wijffels RH. 2006. Controlling light-use by *Rhodobacter capsulatus* continuous cultures in a flat-panel photobioreactor. Biotechnology and Bioengineering 95(4):613-626.

4. Controlling light-use by *Rhodobacter capsulatus* continuous cultures in a flat-panel photobioreactor

Abstract

The main bottleneck in scale-up of phototrophic fermentation is the low efficiency of light energy conversion to the desired product, which is caused by an excessive dissipation of light energy to heat. The photoheterotrophic formation of hydrogen from acetate and light energy by the microorganism *Rhodobacter capsulatus* NCIMB 11773 was chosen as a case study in this work. A light energy balance was set up, in which the total bacterial light energy absorption is split up and attributed to its destinations. These are biomass growth and maintenance, generation of hydrogen and photosynthetic heat dissipation.

The constants defined in the light energy balance were determined experimentally using a flat-panel photobioreactor with a three centimeter optical path. An experimental method called D-stat was applied. Continuous cultures were kept in a so-called pseudo steady-state, while the dilution rate was reduced slowly and smoothly. The biomass yield and maintenance coefficients of *Rhodobacter capsulatus* biomass on light energy were determined at 8.4 $W \cdot m^{-2}$ ($400 - 950$ nm) and amounted to $3.8 \pm 0.03 \cdot 10^{-8}$ $kg \cdot J^{-1}$ and 71.6 ± 11.3 $W \cdot kg^{-1}$, respectively.

The fraction of the absorbed light energy that was dissipated to heat at 410 $W \cdot m^{-2}$ depended on the biomass concentration in the reactor and varied between 0.85 and 0.90, as the biomass concentration was increased from 2.0 to 8.0 $kg \cdot m^{-3}$. The process conditions were estimated at which a 3.3% conversion efficiency of absorbed light energy to produced hydrogen energy should be attainable at 410 $W \cdot m^{-2}$.

Introduction

Phototrophic microorganisms are of commercial interest due to the fact that they produce a wide variety of valuable compounds that are used in industry today. Their protein and pigment content makes them suitable for whole cell application in food- and feed industry. Extracts containing compounds such as colouring agents, biopolymers, anti-oxidants and vitamins can be used in functional foods, personal care products and pharmaceuticals (Apt and Behrens 1999; Pulz et al. 2001). Purple non-sulphur bacteria in specific are interesting because of their ability to generate the energy carrier hydrogen from simple organic molecules, under photoheterotrophic conditions (Sasikala et al. 1993).

Industrial application of phototrophic fermentation is generally restricted by the limited efficiency of light energy conversion. This photosynthetic efficiency is defined as the fraction of the absorbed light energy that is converted into the energy content (enthalpy of combustion) of the desired product. This product can be either the generated biomass itself or a certain product 'p' either contained in the biomass or excreted by it.

The development of strategies on how to improve the photosynthetic efficiency of the direct conversion of light energy to specific metabolites has not been looked into in great detail. For example in case the product of interest is not part of the biomass produced, but an extra-cellular metabolite. As a case study, we investigated the conversion of acetate and light energy to hydrogen energy by the purple non-sulphur bacterium *Rhodobacter capsulatus* NCIMB 11773. Values reported in literature on the photosynthetic efficiency of photoheterotrophic hydrogen formation can be as high as 9.6 – 35% (Miyake and Kawamura 1987; Nagamine et al. 1996; Yamada et al. 1998). However, these efficiencies were measured in small scale batch experiments at low light intensities, applying illumination by xenon lamps. The photosynthetic efficiency of photoheterotrophic hydrogen formation that can be calculated from literature data when solar or tungsten halogen illumination is used are in the 0.5 – 6% range. It declines as the

volume to surface ratio and/or the light intensity is increased (Otsuki et al. 1998; Sasaki 1998; Steinborn and Oelze 1989; Zürrer and Bachofen 1982). Evidently, larger scale processes and real daylight conditions need to be considered when investigating the efficient use of sunlight. The global solar irradiance on a day in June in Seville (south of Spain) for example varies from 100 $W \cdot m^{-2}$ in the morning to 1100 $W \cdot m^{-2}$ from 2 – 3 p.m. Similar light intensities should be taken as a reference point to investigate the possibilities of the commercial application of the direct conversion of light energy to hydrogen energy using a photobiological process.

In order to do so, a systematic approach was chosen towards studying the growth and hydrogen producing capacity of continuous *Rhodobacter capsulatus* cultures. All continuous experiments in this work were performed in a 3.6 L flat-panel photobioreactor with a working volume of 2.4 L and an optical path (OP) of 3 cm, as described previously (Hoekema et al. 2002). A light energy balance, in which the energetic expenses related to light absorption for biomass formation, biomass maintenance, photosynthetic heat dissipation and hydrogen production are included is presented. Also, a strategy on calculating the maximally achievable volumetric rate of hydrogen production is given.

Equation 4.1 $$r_{le}^{u} = [I_{in} - I_{out}(C_x)] \cdot A$$

Where r_{le}^{u} = Volumetric light energy absorption in $W \cdot m^{-3}$ (400 – 950 nm)

I = Light intensity in $W \cdot m^{-2}$ (400 – 950 nm)

in = Entering

out = Exiting

C_x = Biomass concentration in $kg \cdot m^{-3}$

A = Specific surface area in $m^2 \cdot m^{-3}$

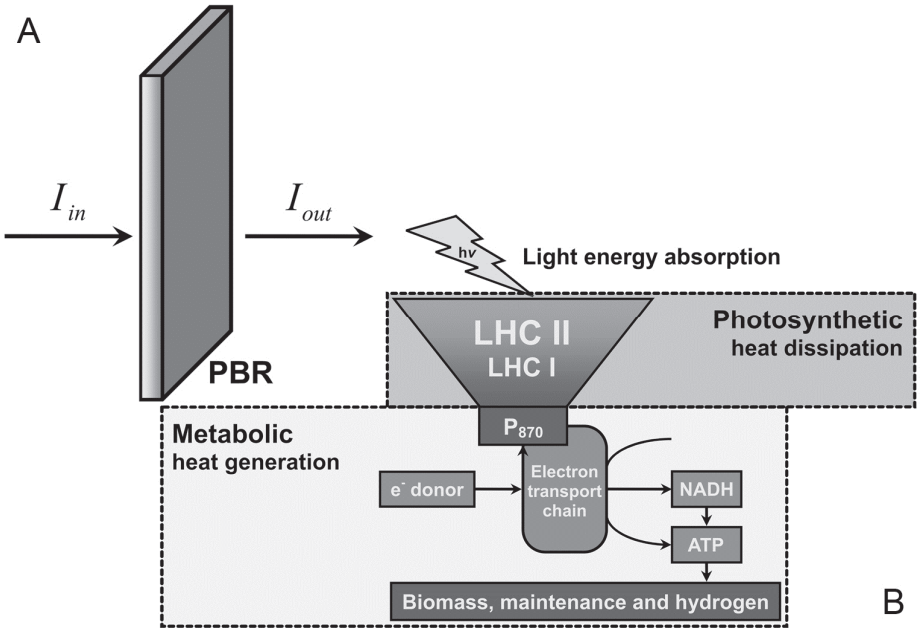

Figure 4.1 Schematic representation of light energy absorption by a phototrophic microorganism. Overall light energy absorption on reactor scale according to Equation 4.1 (A). Metabolic heat is released during the entire metabolism. Photosynthetic heat dissipation is defined as the overflow mechanism of the light harvesting antenna system in Equation 4.2 (B). Abbreviations: LHC light harvesting complex; P_{870} photosystem reaction center; NADH protonated nicotinamide adenine di-nucleotide; ATP adenosine tri-phosphate.

Theory

The light energy balance

The overall light energy absorption inside a photobioreactor (PBR) can be described using Equation 4.1.

Figure **4.1** A is a schematic representation of this process.

The light energy that is absorbed has several destinations. In case of purple non-sulphur bacteria producing hydrogen photoheterotrophically, these are: (1) biomass growth, (2) biomass maintenance, (3) hydrogen generation and (4) photosynthetic heat dissipation. When the primary electron donor P_{870} in the photosystem of purple non sulphur bacteria is saturated by photons, additional photons that are absorbed by that photosystem do not result in additional primary charge separation (Sundström and van Grondelle 1995). This phenomenon occurs at high light intensities. All additional light energy that is absorbed on top of saturation is therefore dissipated as heat (Koyama 1991). This dissipation of light energy within a photosynthetic unit is illustrated in

Figure 4.1B and is considered to be a separate heat flow next to the metabolic heat generated during overall metabolism.

The total volumetric light energy absorption can be assigned to its 4 destinations according to Equation 4.2, when steady-state is assumed.

Equation 4.2 $$\mathrm{r_{le}^{u}} = \frac{\mathrm{r_{x}^{u}}}{\mathrm{Y_{x,le}}} + \mathrm{m_{le}} \cdot \mathrm{C_x} + \frac{\mathrm{r_{H_2}^{u}}}{\mathrm{Y_{H_2,le}}} + \mathrm{f_{heat}(C_x)} \cdot \mathrm{r_{le}^{u}}$$

Where
- r_x^u = $C_x \cdot \mu$, giving the volumetric biomass production rate in kg·m^{-3}·s^{-1}
- $Y_{x,le}$ = yield coefficient of biomass on light energy in kg·J^{-1}
- m_{le} = biomass maintenance coefficient on light energy in W·kg^{-1}
- $r_{H_2}^u$ = $C_x \cdot q_{H_2}$, giving the volumetric hydrogen production rate in mol m^{-3}·s^{-1}
- $Y_{H_2,le}$ = yield coefficient of hydrogen energy on absorbed light energy in mol·J^{-1}
- f_{heat} = fraction of the absorbed light energy that is dissipated to heat within the photosystem.

The relationship between the stoichiometry of substrate to biomass conversion, light energy absorption and heat generation in the photosystem and that resulting from overall metabolism of a photoheterotrophic culture will be demonstrated a by means of an enthalpy balance.

Equation 4.2 was extended with a restriction that limits the specific hydrogen production rate q_{H_2} to the experimentally determined maximal specific hydrogen production rate ($q_{H_2,max}$, mol·kg^{-1}·s^{-1}). This restrictive addition to Equation 4.2 can be expressed according to Equation 4.3.

Equation 4.3 $r^u_{H_2} \leq C_x \cdot q_{H_2,max}$

The use of Equation 4.2 to model and predict the $r^u_{H_2}$ that can maximally be achieved requires the experimental determination of $Y_{x,le}$, m_{le}, $Y_{H_2,le}$ and $q_{H_2,max}$, as well as a relation for the dependency of f_{heat} on C_x.

Yield, maintenance and photosynthetic heat dissipation coefficients

The yield coefficient of biomass on light energy $Y_{x,le}$ and the biomass maintenance coefficient on light energy m_{le} can be determined experimentally. The specific light absorption characteristics of the culture (r^u_{le}/C_x, W·kg^{-1}) can be plotted against the specific growth rate for a number of steady-state combinations at different dilution rates, while applying a constant light intensity. This results in a straight line with slope $1/Y_{x,le}$ and offset m_{le}. The photosynthetic heat dissipation and hydrogen production terms in Equation 4.2 are required to remain zero in this case.

The extent of photosynthetic heat dissipation can be minimized by applying low light intensities. The specific growth rate (μ, s^{-1}) of a continuous *Rhodobacter capsulatus* culture was reported to increase linearly with the incident light intensity up to 30 W·m^{-2} (Tsygankov and Laurinavichene 1996b). This indicates that by applying an incident light

intensity below a certain value, the photosynthetic dissipation of light energy to heat can be reduced to an insignificant level. Since the applied photobioreactor differs in various aspects from the one used by Tsygankov and Laurinavichene (Tsygankov and Laurinavichene 1996b), the assumption that photosynthetic heat dissipation does not occur below a light intensity of 30 $W \cdot m^{-2}$ requires experimental validation.

Hydrogen production can be prevented by the presence of ammonium in the culture medium. The process of photobiological hydrogen production by purple non-sulfur bacteria like *Rhodopseudomonas capsulatus* is catalyzed by the nitrogenase enzyme-complex. Hydrogen production by *Rhodobacter capsulatus* can be prevented by inactivating the nitrogenase enzyme-complex using ammonium ions. The nitrogenase activity of a *Rhodobacter capsulatus* culture is completely repressed when ammonium is present in the culture medium at a concentration of at least 1 mM (Jouanneau et al. 1984).

Knowing $Y_{x,le}$ and $\mathrm{m_{le}}$, the dependency of the fraction of the absorbed light energy that is dissipated to heat on the applied biomass concentration $\mathrm{f_{heat}(C_x)}$ can be quantified experimentally at high incident light intensity by applying Equation 4.2 and the parameters $Y_{x,le}$ and $\mathrm{m_{le}}$. Prevention of hydrogen production by means of ammonium addition is still required.

Estimation of the yield of hydrogen energy on light energy

On average, the photosystem of purple non sulfur bacteria can convert one mole of quanta from tungsten halogen light to 0.51 moles of ATP (Göbel 1978) and own estimation). Miyake and Zaborsky estimated that nitrogenase-mediated photoproduction of one mole of hydrogen requires 6 moles of ATP and additionally 2 moles of quanta for the liberation of the required electrons (Miyake and Zaborsky 1998). In total, 12.9 moles of quanta are then needed for the photo production of 1 mole of hydrogen. The average energy content of a mole of quanta emitted by the applied tungsten halogen lamps in the 400 – 950 nm range equals 167.3 kJ and the enthalpy of combustion of hydrogen is

285 kJ·mol^{-1}. Using these data, the yield coefficient of hydrogen energy on light energy $Y_{H_2,le}$ can be estimated to be 8.86·10^{-7} mol·J^{-1}. This corresponds to a light energy conversion yield to hydrogen energy of 25.3% in case tungsten halogen light is applied. In case of sunlight, the value of $Y_{H_2,le}$ becomes 10.6%, since a considerably smaller fraction of the energy in the solar spectrum is located around 860 nm, the absorption maximum of the photosystem of purple non-sulphur bacteria.

Materials and methods

Bacterial strain and medium composition

The purple non-sulphur bacterium *Rhodobacter capsulatus* NCIMB 11773 was used in all experiments described in this work. It was selected based on its wide substrate range and high C-substrate to hydrogen conversion efficiency (Segers and Verstraete 1983). An exponentially growing culture was stored at -80°C in aliquots of 1 mL containing 15% glycerol. Prior to starting an experiment, a cryo-vial was thawed and its contents transferred aseptically to a 500 mL flask containing 250 mL of SYA-medium under a nitrogen headspace. This medium is based on previously reported aSy-medium (Miyake et al. 1984). The culture flasks were incubated at 30°C, stirred and continuously illuminated at about 90 μmol m^{-2}·s^{-1} of photosynthetically active radiation (PAR, μmol photons m^{-2}·s^{-1}, 400 – 700 nm).

All D-stat experiments were performed with modified aSy-medium, designated 'AA'- medium ('Acetate Ammonium' medium). During the D-stat experiment under high light intensity (410 W·m^{-2}), halfway the experiment all macro- and micro nutrient concentrations in the medium were doubled, to prevent them from becoming limiting for biomass growth. This medium was designated AA^{+}-medium. All media used in the D-stat experiments had a carbon to nitrogen ratio (C/N-ratio) of 8.2. This value is equal to the C/N-ratio of the dried culture biomass.

The maximal hydrogen production rate $q_{H_2,max}$ of the *Rhodobacter capsulatus* NCIMB 11773 cultures was assessed in $q_{H_2,max}$-medium. It contained no ammonium and had a higher buffer capacity.

The composition of all media described above is displayed in Table 4.1. The media were prepared from concentrated stock solutions, set to pH 7.0 and autoclaved prior to use. Only the calcium chloride and magnesium sulphate stock solution was autoclaved separately. The concentrated vitamin stock solution used was filter sterilized (0.2 μm) before aseptic addition to the medium.

D-stat experiments

The determination of the described parameters in Equation 4.2 requires the quantification of multiple steady-states at different combinations of volumetric light energy absorption r_{le}^{u}, biomass concentration C_x and specific growth rate μ. Acquiring such a data set is time consuming.

A faster experimental technique is the acceleration (A)-stat. During this experimental procedure, the dilution rate (D, d^{-1}) of a steady-state culture is increased slowly and smoothly towards a higher value using a certain acceleration rate (a, d^{-2}). Since the culture remains in equilibrium with the increasing dilution rate, we refer to this dynamic equilibrium as 'pseudo steady-state' (Barbosa et al. 2003; Paalme et al. 1995). The concept was demonstrated before for continuous cultures of the bacterium *E.* coli (Paalme et al. 1995), the yeast *Z. rouxii* (van der Sluis et al. 2001b) and the marine micro-alga *D. tertiolectra* (Barbosa et al. 2005).

To allow for a further reduction in experimental time, all described experiments were started at the highest dilution rate in the desired range. After steady-state was demonstrated, the dilution rate was decelerated at a certain deceleration rate (d, d^{-2}) and therefore we refer to these experiments as deceleration (D)-stat experiments.

A- and D-stat experiments will give reliable predictions, provided that the metabolic adaptation time is smaller than the applied change in dilution rate (van der Sluis et al.

2001b). When the observed specific growth rate deviated less than 25% from the set dilution rate, pseudo steady-state was assumed to be maintained.

We chose a deceleration rate of maximally -0.17 d^{-2}. The pseudo steady-state criterion $\mu = D$ was validated during all experiments. Each D-stat experiment was started at the initial dilution rate D_0 (, d^{-1}), equal to 40% of the maximal specific growth rate at the applied light intensity. The dependency of the specific growth rate of *Rhodobacter capsulatus* on the incident light intensity was estimated from literature data (Tsygankov and Laurinavichene 1996b). After steady-state was demonstrated at D_0, the decrease in the dilution rate was started until the final dilution rate, which was equal to zero, was reached. Halfway the experiment, the deceleration was halted to verify comparability between the pseudo steady-state situation and steady-state situation. In all cases these two situations were comparable.

D-stat calculations

Equation 4.1 and Equation 4.2 were re-written to give Equation 4.4, which describes the light energy absorption and utilization during a D-stat experiment in time, as C_x increases.

Equation 4.4 $$r_{le}^{u}(t) = [I_{in} - I_{out}(C_x)] \cdot A = \frac{r_x^u(t)}{Y_{x,le}} + m_{le} \cdot C_x(t) + \frac{r_{H_2}^u(t)}{Y_{H_2,le}} + f_{heat}(C_x) \cdot r_{le}^{u}(t)$$

Biomass yield and maintenance under low light intensity

By applying a light intensity below 30 $W \cdot m^{-2}$ and maintaining the ammonium concentration above 1 mM, both photosynthetic heat dissipation and hydrogen production are probably negligible, as motivated in the Theory section. Their corresponding terms can therefore be deleted from Equation 4.4, which then reduces to Equation 4.5.

Equation 4.5 $$r_{le}^{u}(t) = \frac{1}{Y_{x,le}} \cdot r_{x}^{u}(t) + m_{le} \cdot C_x(t)$$

Equation 4.5 can be re-written to Equation 4.6:

Equation 4.6 $$\frac{r_{le}^{u}(t)}{C_x(t)} = \frac{\mu(t)}{Y_{x,le}} + m_{le}$$

The specific light energy absorption $r_{le}^{u}(t)/C_x(t)$ can be plotted against the specific growth rate $\mu(t)$ for a dataset containing a number of pseudo steady-state combinations of $r_{le}^{u}(t)$ and $C_x(t)$ at constant (low) incident light intensity I. This results in a straight line with slope $1/Y_{x,le}$ and offset m_{le}, as described in the Theory section.

Determination of the specific growth rate

The rate of biomass production during a D-stat experiment can be described according to Equation 4.7.

Equation 4.7 $$r_{x}^{u}(t) = \mu(t) \cdot C_x(t) = \frac{dC_x(t)}{dt} + D(t) \cdot C_x(t)$$

From Equation 4.7, $\mu(t)$ can be isolated according to Equation 4.8:

Equation 4.8 $$\mu(t) = \frac{\frac{dC_x(t)}{dt}}{C_x(t)} + D(t)$$

The biomass concentration was measured discontinuously. Therefore, an approximation of dC_x/dt is used in Equation 4.9:

Equation 4.9 $$\mu(t) = \frac{\left(\frac{[C_x(t+1) - C_x(t)]}{[t(t+1) - t(t)] \cdot C_x(t)} + D(t)\right) + \left(\frac{[C_x(t) - C_x(t-1)]}{[t(t) - t(t-1)] \cdot C_x(t)} + D(t)\right)}{2}$$

Photosynthetic heat dissipation at high light intensity

Knowing $Y_{x,le}$ and m_{le}, the dependency of the photosynthetic heat dissipation term on the biomass concentration $f_{heat}(C_x)$ at high incident light intensity can be quantified. A D-stat experiment executed at high incident light intensity, while still preventing the hydrogen production by ammonium, provides the required data to fit f_{heat} to an arbitrary function of C_x. When the photosynthetic heat dissipation term is included in Equation 4.5, it can be re-written to give Equation 4.10:

Equation 4.10 $$r_{le}^{u}(t) = \frac{r_x^u(t)}{Y_{x,le}} + m_{le} \cdot C_x(t) + f_{heat}(C_x) \cdot r_{le}^{u}(t)$$

The volumetric hydrogen production capacity

With the other parameters within Equation 4.4 known, the volumetric hydrogen production capacity $r_{H_2}^{u}$ and its dependency on D and C_x can now be estimated. Equation 4.4 can be re-written to Equation 4.11, from which the volumetric hydrogen production capacity $r_{H_2}^{u}$ can be calculated for each chemostat situation at constant D and C_x.

Equation 4.11 $$r_{H_2}^{u} = \left([1 - f_{heat}(C_x)] \cdot r_{le}^{u} - \frac{r_x^u}{Y_{x,le}} - m_{le} \cdot C_x \right) \cdot Y_{H_2 le}$$

Carbon substrate feeding

A prerequisite for a successful light limited D-stat experiment is that no other substrate limitation- or toxicity effects occur. However, as the dilution rate is decreased in time and the biomass density increases, substrates administered through the influent will be depleted at some point during the experiment. During biomass formation, acetate consumption and hydroxide formation are equimolar, according to Equation 4.12.

Equation 4.12

$$xCH_3COO^- + yNH_4^+ + zH_2O \xrightarrow{hv} CH_aO_bN_c + kCO_2 + (m+y)H_2O + (x-y)OH^-$$

An acetate supply through pH control with acetic acid provides acetate to the reactor on the basis of the culture's demand. As a result of this demand based feeding strategy, not only the pH but also the acetate concentration is maintained constant in time, irrespective of the dilution rate. The C/N-ratio of the pH-regulation solution should be 8.2, similar to that of the medium used, by adding ammonium to the solution.

But, due to the acidic action of the ammonium ion, adding only acetic acid and ammonium to the pH-regulation solution causes the total amount of carbon added to be smaller than the total amount of carbon consumed. This discrepancy in feed rate and consumption rate of acetate can be prevented by adding Ac^- to the solution in an equimolar concentration to NH_4^+. With a total carbon concentration of 4.0 M and a C/N ratio of 8.2, the composition of the pH-regulation solution becomes 1511 mM HAc, 489 mM Ac^- and 489 mM NH_4^+. The composition of the pH-regulation solution was kept unaltered in all D-stat experiments and is displayed in Table 4.1.

Experimental configurations

D-stat experiments

All D-stat experiments were performed in a flat-panel PBR described before (Hoekema et al., 2002) that was computer controlled using LabVIEW© 5.1 software (National Instruments, Austin, TX) via an ADAM-5000 data acquisition and control module (Advantech, Milpitas, CA). It was autoclaved completely prior to all experiments. Mixing was facilitated by a gas mixture of 2 $nL \cdot min^{-1}$ N_2 containing 0.5% v/v CO_2 that was sparged into the culture chamber through 25 hypodermic needles (0.5 mm int. diam., 16 mm in length).

The reactor consisted of two compartments, the first one being oriented to the light. Water was circulated through it via a cryostat water bath to remove excessive thermal radiation emitted by the lamps and to maintain the temperature in the culture compartment at 30˚C. The culture compartment had an optical path of 3 cm and a

working volume of 2.4 L (total volume 3.6 L). The pH was controlled at 7.0 by dosing acetic acid enriched with acetate and ammonium to the reactor (see Table 4.1 for the composition).

The reactor was illuminated using two 500 W tungsten halogen lamps that were placed on one side of the reactor. The lamps were mounted in a frame, on top of each other. The desired incident light intensity was reached by placing white paper sheets between the lamps and the reactor. It was fine-tuned by altering the distance between the reactor and the lamp-frame. When paper sheets were used, their influence on the spectral composition of the incident light was measured and corrected for.

The medium and outflow vessels were autoclaved separately and connected to the reactor after autoclaving. The medium was fed to the reactor using a peristaltic pump. The culture was pumped out of the reactor via an L-shaped glass tube with its opening placed at the desired liquid level. The weight of the effluent vessel was logged in order to calculate the actual dilution rate of the system. A diluted (40 times) Antifoam B Silicone emulsion (J. T. Baker, Deventer, the Netherlands) was automatically dosed into the culture as foam was detected in the headspace by means of a conductivity sensor.

$q_{H_2,max}$ determination experiments

Three glass batch reaction vessels with an internal volume of about 120 mL were used for the experimental quantification of the maximal specific hydrogen production rate of the culture ($q_{H_2,max}$, mol·kg^{-1}·s^{-1}). Stirring was facilitated using magnetic stirrer bars at a rate of 300 rpm. The temperature of the double-jacketed vessels were controlled at 30˚C. On top of the vessels light diffusing plates and 50 W tungsten halogen spots were fitted.

The vessels were flushed with argon and 10 mL cell suspension with known cell concentration (washed and/or concentrated if required) was added. Two screw-caps with septa in the vessels' walls facilitated argon flushing and headspace sampling. The increase in the hydrogen concentration was measured as well as the final pressure in the vessels using a Cerabar M PMP41 0 – 4 bar*a* pressure sensor (Endress + Hauser, Germany). The

value of $q_{H_2,max}$ was calculated from the region with linear kinetics (see Results). The pH of the applied medium was set to 7.0 initially and checked after the experiment was ended. It increased between 0.7 to 2.0 units.

Analyses

Small samples (up to 20 mL) were withdrawn from the flat-panel PBR using a sampling port connected to the outflow. Larger samples for dry weight determination were collected overnight on ice from the regular outflow of the reactor.
The volume fraction of hydrogen in the off-gas and the acetate and biomass concentrations (dry weight and optical density) were determined as described previously (Hoekema et al., 2002).

Ammonium
Samples for determination of the ammonium concentration were centrifuged and the supernatant was stored at -80˚C. The ammonium concentration was determined at a later time using a spectrophotometer test kit issued by Dr. Lange (Dr. Lange GmbH, Germany).

Absorptive properties of the biomass
During the time-course of the D-stat experiments described in this work, the specific absorption surface (a^*_{dw}, $m^2 \cdot kg^{-1}$) of the biomass was quantified daily. This was done in the 350 - 1000 nm range using a Beckman DU 640 UV/VIS spectrophotometer (Beckman Coulter, Inc., Fullerton, CA) equipped with a Labsphere RSA-BE-65 integrating sphere (Labsphere, North Sutton, NH). This integrating sphere collects forward scattered light, in addition to non-absorbed and non-scattered light, and reflects it towards the detector. Samples were standardized to a biomass concentration of 0.33 $kg \cdot m^{-3}$ using reactor medium without acetate and ammonium.

Table 4.1 Composition of all media and stock solutions used to prepare the media.

	Stock Solutions, C/N sources	Medium → Stock g·L^{-1}↓	SYA (μM)	AA (μM)	AA^{+} (μM)	$q_{H_2,max}$ (μM)	pH-regulation solution
			20 mL·L^{-1}↓	**6 mL·L^{-1}↓**	**12 mL·L^{-1}↓**	**40 mL·L^{-1}↓**	
Buffer	KH_2PO_4	86.6	12726	3818	7636	25452	-
	K_2HPO_4	73.3	8416	2525	5050	16832	
			40 mL·L^{-1}↓	**40 mL·L^{-1}↓**	**80 mL·L^{-1}↓**	**40 mL·L^{-1}↓**	
Macro nutrients	$MgSO_4.7H_2O$	5.00	812	812	1624	812	-
	$CaCl_2.2H_2O$	2.48	674	674	1348	674	
			10 mL·L^{-1}↓	**10 mL·L^{-1}↓**	**20 mL·L^{-1}↓**	**10 mL·L^{-1}↓**	
Micro nutrients	$Na_2EDTA.2H_2O$	2.00	53.7	53.7	107.5	53.7	-
	$FeSO_4.7H_2O$	1.18	42.5	42.5	84.9	42.5	
	H_3BO_3	0.280	45.3	45.3	90.6	45.3	
	$MnSO_4.2H_2O$	0.277	16.4	16.4	32.8	16.4	
	$Na_2MoO_4.2H_2O$	0.0750	3.10	3.10	6.20	3.10	
	$ZnSO_4.7H_2O$	0.0240	0.835	0.835	1.67	0.835	
	$Cu(NO_3)_2.3H_2O$	0.0040	0.166	0.166	0.331	0.166	
			10 mL·L^{-1}↓	**10 mL·L^{-1}↓**	**20 mL·L^{-1}↓**	**10 mL·L^{-1}↓**	
Vitamins	Biotin	0.1	1 mg·L^{-1}	1 mg·L^{-1}	2 mg·L^{-1}	1 mg·L^{-1}	-
	Thiamin	0.1	1 mg·L^{-1}	1 mg·L^{-1}	2 mg·L^{-1}	1 mg·L^{-1}	
	p-aminobenzoic acid	0.1	1 mg·L^{-1}	1 mg·L^{-1}	2 mg·L^{-1}	1 mg·L^{-1}	
	vitamin B_{12}	0.1	1 mg·L^{-1}	1 mg·L^{-1}	2 mg·L^{-1}	1 mg·L^{-1}	
	nicotinamide	0.1	1 mg·L^{-1}	1 mg·L^{-1}	2 mg·L^{-1}	1 mg·L^{-1}	
			50 mL·L^{-1}↓				
	Na_2 succinate	81	25 mM				
SYA	Yeast extract	10	500 mg·L^{-1}	-	-	-	-
	Na acetate	16.4	10 mM				
Carbon source	HAc	-	-	-	-	-	1511 mM
	NaAc	-	-	25 mM	25 mM	30 mM	489 mM
Nitrogen source	NH_4Cl	-	-	6.11 mM	6.11 mM	-	489 mM
	Headspace	-	nitrogen	nitrogen	nitrogen	argon	-

Light composition and intensity

The spectral distribution of the light emitted by the tungsten halogen lamps was acquired using an IRRAD 2000 fiber-optic spectroradiometer (TOP sensor systems, Eerbeek, the Netherlands). The spectral limits of the spectroradiometer are 340 and 999 nm.

The light intensity on the reactor surfaces, on the other hand, was measured as the photon flux density (PFD, µmol·m^{-2}·s^{-1}) in the PAR range (photosynthetic active radiation, 400 – 700 nm). A 2π LI-190SA quantum sensor (Li-Cor, Lincoln, NE) was used for this.

The PAR photon flux density entering the PBR was measured prior to fermentation at 38 locations distributed uniformly over the illuminated culture compartment surface in the empty PBR using a grid, with the cooling water compartment present in front of it. The light intensities at the bottom of the vessels used for the $q_{H_2,max}$ determinations were measured in an open version of the vessel, constructed especially for this purpose.

The average PAR photon flux density (PFD$_{in}$, µmol·m^{-2}·s^{-1}) value was re-calculated to the light energy flux density or light intensity I (W·m^{-2}, 400 – 950 nm), by multiplying the PAR-value with a conversion-factor, for which the spectral distribution of the light emitted by the tungsten halogen lamps was used. An identical procedure was employed for the quantification of the light intensity entering the vessels used for the $q_{H_2,max}$ determinations. All light intensities reported are I -values, unless stated otherwise.

The PFD exiting the photobioreactor (PFD$_{out}$, µmol·m^{-2}·s^{-1} from 400 – 700 nm) was quantified daily, using the same grid. This PAR value was converted to a light intensity using the spectral distribution of the light emitted by the lamps, corrected for the wavelength dependent absorption by the culture, analogous to a method described previously by Dubinsky et al. (Dubinsky et al. 1986).

Viability of the biomass

Cell viability was determined using a FACSCalibur flow cytometer (Becton Dickenson Immunocytometry Systems, Franklin Lakes, NJ). The viability assessment was performed using a Propidium Iodine (PI) staining procedure. PI penetrates bacteria with damaged cell

membranes and complexes with cellular DNA. This complex has a higher fluorescence at 670 nm (Bunthof et al. 2001) on the basis of which these cells can be identified. Green fluorescent latex beads (488 nm) with a diameter of 6 μm at a final concentration of $3 \cdot 10^6$ beads·mL^{-1} were added to the samples as an internal standard. Each analysis was performed in triplicates of 20.000 counts. The collected data were analyzed using the CellQuest program (version 4.02, Becton Dickenson Immunocytometry Systems, USA). As a positive control, heat-killed cells (20 minutes at 70˚C) were analysed. Fluorescent beads were added after the heat treatment.

Biomass elemental composition

At regular time intervals, the elemental composition of the washed and dried biomass was determined using a Fisons EA 1108 CHN-O element analyzer (Fisons, Beverly, MA). Atropine (elemental composition 71.11% C, 4.86% N, 8.06% H) was used as a reference compound. The remainder, minus the ash-residue, was assumed to be oxygen, as the other constituents of the biomass are present in traces only.

Results & Discussion

Deceleration-stat experiments

Four D-stat experiments were performed. Their experimental settings and results are summarized in Table 4.2. Figure 4.2 displays the values of the dilution rate, the growth rate (calculated according to Equation 4.9) and the biomass dry weight values obtained during the D-stat executed at 21.9 W·m^{-2}. All other D-stats followed a similar pattern (data not shown).

During all complete D-stat experiments, the observed value of μ was structurally slightly larger than the value of D. This was caused by its continuous adaptation to the imposed decreasing D. When *D. tertiolectra* was cultured in *A*-stat, μ also lagged behind D,

resulting in a value of μ that was structurally slightly smaller than the imposed increasing D (Barbosa et al., 2005). The average deviation between μ and D was about 8%. Only those data-points were used for which μ and D had a non-structural deviation of less than 25%. Pseudo steady-state was assumed to be maintained in this case. Every steady-state situation was only used once in the calculations. If more data was available on a single steady-state situation, an average was taken.

In all D-stat experiments, the application of the demand based feeding strategy resulted in stable acetate and ammonium concentrations in the PBR. The acetate and ammonium concentrations remained between 10 - 25 mM and 5 - 10 mM respectively during pseudo steady-state. This prevented both substrate limitation and -inhibition of growth for these substrates during all D-stat experiments (data not shown). Simultaneously, the applied ammonium concentration prevented the occurrence of active nitrogenase and with that the production of hydrogen.

Effect of the light intensity and dilution rate on culture characteristics

It can be seen from Figure 4.2 that the pseudo steady-state criterion $\mu = D$ was maintained during the larger part of the experiment, even though the applied deceleration rates of the dilution rate were up to 6 times faster compared to the maximal acceleration rate that could be applied on *D. tertiolectra* continuous cultures (Barbosa et al. 2005), without compromising the pseudo steady-state criterion.

From Figure 4.2 it can also be seen that the increase in the biomass dry weight value was steeper as the value of the dilution rate was lower. The deceleration rate was decreased from -0.17 d^{-2} to -0.072 d^{-2} at a D of 0.65 d^{-1} (Table 4.2) to allow the biomass more time to adapt to the more rapid change in light regime.

Table 4.2 Settings and results for the four D-stat experiments performed and resulting values for the yield coefficient of biomass on light energy ($Y_{x,le}$) and biomass maintenance energy requirement of the biomass (m_{le}). Abbreviations: I light intensity; $\mu_{max}(I)$ maximal specific growth rate at light intensity I; a acceleration rate; D dilution rate; $Y_{x,le}$ yield coefficient of biomass on light energy; m_{le} biomass maintenance coefficient on light energy; s.e. standard error; n degrees of freedom; r^2 correlation coefficient; r^u_{le}/C_x specific light energy absorption ($W \cdot kg^{-1}$); μ specific growth rate (d^{-1}).

		D-stat			
		1	**2**	**3**	**4**
Settings					
I	$W \cdot m^{-2}$	8.4	11.9	21.9	410
$\mu_{max}(I)$	d^{-1}	1.85	2.56	3.81	7.56
D_{start}; 40% of $\mu_{max}(I)$	d^{-1}	0.65	1.01	2.00	3.02
Deceleration I					
a	d^{-2}	-	-0.17	-0.17	-0.17
D_{end}	d^{-1}	0.65	0.65	0.65	0.65
Deceleration II					
a	d^{-2}	-0.018	-0.072	-0.072	-0.072
D_{end}	d^{-1}	0	0	0	0
Calculations					
OD_{860}/OD_{660} ± s.e.	-	1.41 ± 0.03	1.10 ± 0.01	1.56 ± 0.01	1.70 ± 0.02
$Y_{x,le}$ ± s.e.	$kg \cdot J^{-1}$	$3.8 \pm 0.3 \cdot 10^{-8}$	$2.5 \pm 0.3 \cdot 10^{-8}$	$2.3 \pm 0.3 \cdot 10^{-8}$	-
m_{le} ± s.e.	$J\ kg^{-1} \cdot s^{-1}$	71.6 ± 11.3	92.0 ± 22.2	197.4 ± 48.4	-
n	-	23	6	13	-
r^2 [r^u_{le}/C_x vs μ]	-	0.90	0.97	0.93	-

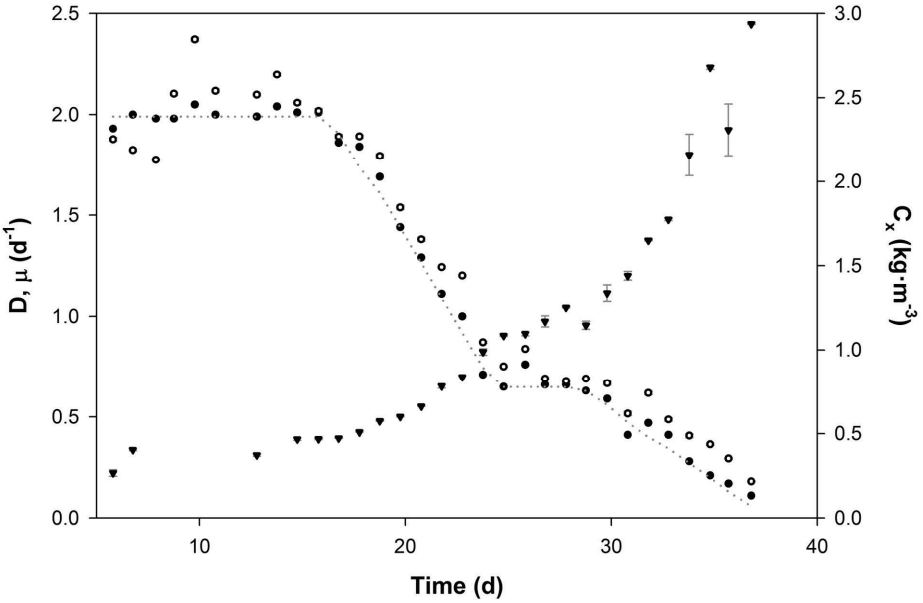

Figure 4.2 Effect of the dilution rate (D, ●) on the specific growth rate (μ, ○) and the biomass concentration (C_x, ▼) during the D-stat experiment performed in the flat panel PBR at a light intensity of 21.9 $W \cdot m^{-2}$. The dotted line represents the set dilution rate. The error bars represent standard errors.

In general, purple non-sulphur bacteria respond to a decrease in the average light intensity they are exposed to (I_{av}, $W \cdot m^{-2}$), resulting from an increase in biomass concentration at constant incident light intensity, by increasing their cellular chlorophyll content (Göbel 1978). Notably, the OD_{860}/OD_{660}-ratio of the cultures (Table 4.2), which is an indication for the cellular BChl *a* content, remained constant during each complete individual D-stat. Photoautotrophs also respond to an increase in mutual shading by increasing their cellular chlorophyll content (Tredici and Zittelli 1998; Zou and Richmond 2000). However, no increase in cellular chlorophyll concentration could be observed as the biomass concentration of continuous cultures of the micro-alga *Dunaliella tertiolectra*

grown in A-stat increased (Barbosa et al. 2005). Within our and Barbosa's experiments, the increase in biomass concentration during each individual experiment was only about a factor four, which might not have been sufficient to realize a noticeable change in the (bacterio-)chlorophyll content of the cultures.

Amongst the individual experiments, the differences in the OD_{860}/OD_{660}-ratio are more noticeable. In general, this ratio increased slightly with the applied light intensity, as can be seen in Table 4.2.

At 8.4 $W \cdot m^{-2}$, the culture required larger adaptation times. A lower deceleration rate of -0.018 d^{-2} during the entire run resolved this and resulted in a culture for which the pseudo steady-state criterion $\mu = D$ was valid for the larger part of the D-stat (data not shown). Possibly, the lower than anticipated OD_{860}/OD_{660}-ratio of 1.10 observed at 11.9 $W \cdot m^{-2}$ (Table 4.2) was also caused by a requirement for larger adaptation times.

An attempt was made to run a D-stat at 4.1 $W \cdot m^{-2}$. It was possible to achieve a steady-state situation at a dilution rate of 0.38 d^{-1} (40% of $\mu_{max}(I)$). As the dilution rate was decreased, the growth rate was about 30% higher than the set dilution rate structurally (data not shown). During this experiment, the OD_{860}/OD_{660}-ratio was stable at 1.07. Possibly, at these very low light intensities, the culture was so energy limited that it was not capable of synthesizing a normal amount of light harvesting complexes, disqualifying such very low light intensities for the determination of parameters related to light energy expenditures for biomass growth and maintenance by phototrophs.

A low dilution rate might compromise the viability of a cell suspension. The cultures grown at 8.4 and 410 $W \cdot m^{-2}$ were therefore checked for viability towards the end of the experiments. In both cases, more than 94% of the cells were demonstrated to be viable (data not shown). Dilution rates in the range of 0.05 d^{-1} do not seem to have a noticeable influence on the viability of the bacterial cells, even at biomass concentrations as high as 8.0 $kg \cdot m^{-3}$.

Biomass yield on light energy and light energy maintenance requirements

The collected data were used to calculate $r_{le}^{u}(t)$ and $\mu(t)$, according to Equation 4.1 and Equation 4.9, respectively. The data from the D-stat experiments that were performed at 8.4, 11.9 and 21.8 W·m^{-2} (Table 4.2) were used to find the yield coefficient of biomass on light energy, $Y_{x,le}$, and the biomass maintenance coefficient on light energy, m_{le}. The specific light energy absorption (r_{le}^{u}/C_x, W·kg^{-1}) was plotted against μ in Figure 4.3 for these three experiments. Linear fits were made through the data points, resulting in correlation coefficients of around 0.90, as can be seen from Table 4.2. The offsets of these fits represent m_{le}, while the slopes represent the reciprocal of $Y_{x,le}$. The values of $Y_{x,le}$ and m_{le}, together with their standard errors are displayed in Table 4.2 for all three experiments.

The values of $Y_{x,le}$ and m_{le} as determined from Figure 4.3 are displayed as a function of the applied incident light intensity in Figure 4.4. It demonstrates that $Y_{x,le}$ decreases and m_{le} increases at increasing incident light intensity. Probably, part of the absorbed light energy is dissipated as heat already at the applied low light intensities. We anticipated photosynthetic heat dissipation to occur above a light intensity of 30 W·m^{-2}, based on data presented previously by Tsygankov and Laurinavichene (Tsygankov and Laurinavichene 1996b) on *Rhodobacter capsulatus* continuous cultures. However, the PBR used in this work has an optical path of 3 cm, which is about twice that of the cylindrical system used by Tsygankov and Laurinavichene. Therefore it is probable that light saturation occurs already at lower incident light intensities, resulting in an increase in the - *apparent* - m_{le} and a decrease in the - *apparent* - $Y_{x,le}$ at increasing light intensity, even below 30 W·m^{-2}.

The values for $Y_{x,le}$ and m_{le} that were determined at 8.4 W·m^{-2}, the lowest applied light intensity that resulted in a pseudo steady-state during the larger part of the D-stat, are therefore probably the most accurate. The value for $Y_{x,le}$ equalled $3.76 \pm 0.03 \cdot 10^{-8}$ kg·J^{-1} and the value of m_{le} was 71.6 ± 11.3 W·kg^{-1} within this experiment (see Table 4.2).

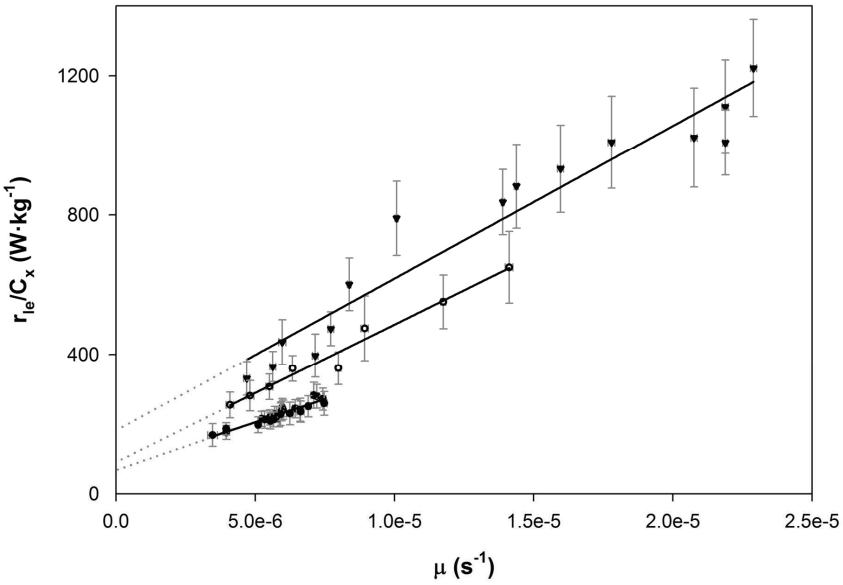

Figure 4.3 Total specific light absorption r_{le}^{u}/C_x as a function of the specific growth rate μ for the three D-stat experiments performed in the flat panel PBR at light intensities of 8.4 (●), 11.9 (○) and 21.9 (▼) W·m^{-2}. The error bars represent standard errors.

The value of $Y_{x,le}$ is comparable to the upper value of 2.15·10^{-8} kg·J^{-1} reported previously (Tsygankov and Laurinavichene 1996b) for a *Rhodobacter capsulatus* continuous culture growing on lactate and tungsten halogen light at 6.7 W·m^{-2}. Photo-autotrophically grown *Rhodobacter capsulatus* cultures exhibited a lower $Y_{x,le}$ of 0.59·10^{-8} kg J^{-1} and a higher m_{le} of 527 W·kg^{-1} on tungsten halogen illumination (Minkevich et al. 2004). The enthalpy balance for biomass growth of a *Rhodobacter capsulatus* continuous culture illuminated at 8.4 W·m^{-2} is illustrated in Figure 4.9A in Appendix I.

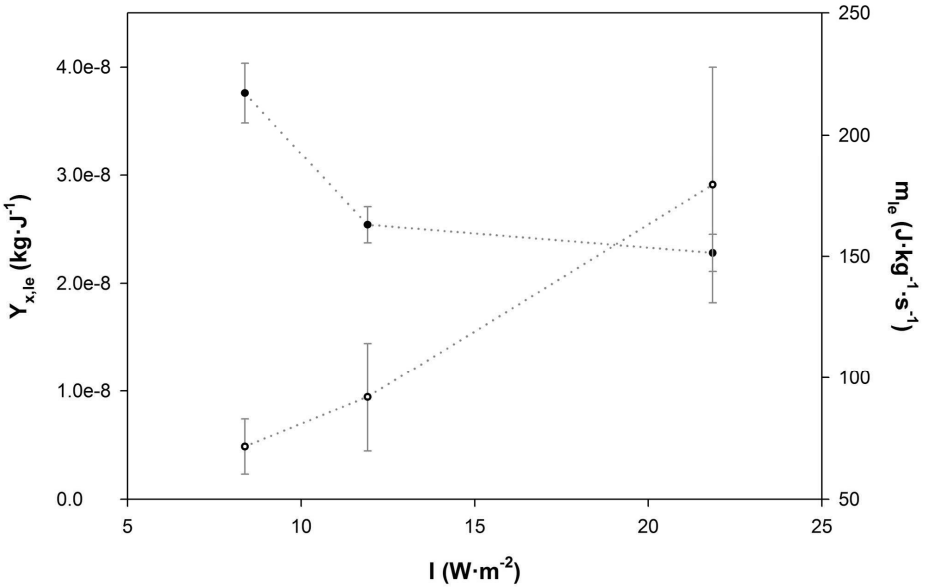

Figure 4.4 Yield coefficient of biomass on light energy ($Y_{x,le}$,●) and biomass maintenance light energy requirement of the biomass (m_{le},○) in the flat panel PBR as a function of the applied light intensity. The error bars represent standard errors.

Photosynthetic heat dissipation at high light intensity

With $Y_{x,le}$ and m_{le} known, the fraction of the total absorbed light energy that is dissipated to heat $f_{heat}(C_x)$ can be quantified in a D-stat experiment performed at high light intensity (410 W·m^{-2} in this case). The light energy that was absorbed by the culture and that was not used to generate or maintain biomass must have been dissipated as heat, as can be seen from Equation 4.10.

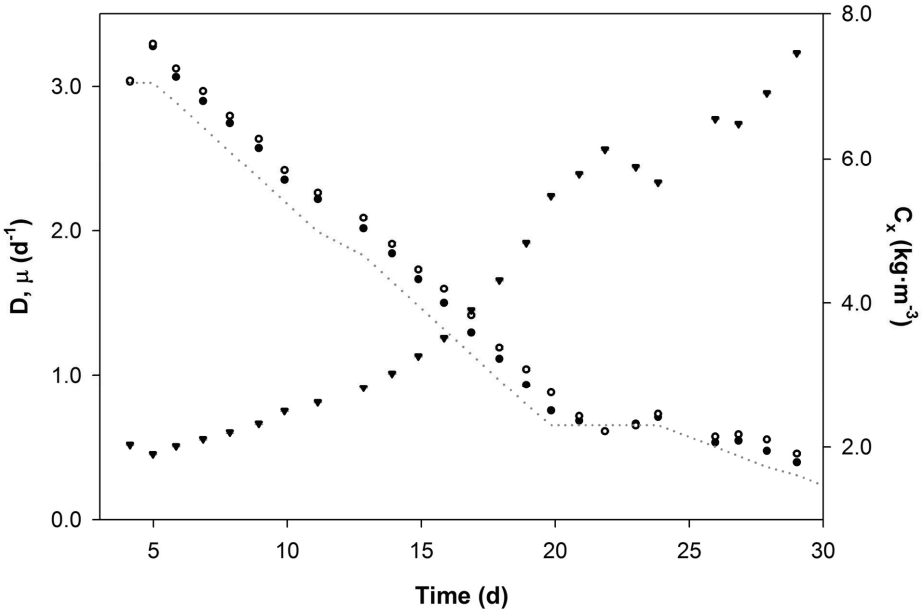

Figure 4.5 Effect of the dilution rate (D, ●) on the specific growth rate (μ, ○) and the biomass concentration (C_x, ▼) during the D-stat experiment performed in the flat panel PBR at a light intensity of 410 W·m^{-2}. The dotted line represents the set dilution rate. The error bars represent standard errors.

Figure 4.5 displays the values of the dilution rate D, the growth rate μ (calculated according to Equation 4.9) and the biomass dry weight values obtained during the D-stat experiment executed at 410 W·m^{-2}. Again, D and μ have similar values during the larger part of the experiment and the value of μ is structurally a bit larger than the value of D. From these data, the fractions of the total light energy absorption attributed to biomass growth, biomass maintenance and photosynthetic heat dissipation could be calculated for the complete pseudo steady-state part of this experiment (Equation 4.2). The results are plotted in Figure 4.6. In the biomass concentration range of 2.0 – 8.0 kg·m^{-3}, the fraction of the total absorbed light energy that is used for biomass synthesis f_{bm} decreased from

0.18 to 0.08, while the fraction that is used for biomass maintenance f_m increased from 0.013 to 0.052.

As can be seen from Figure 4.6, $f_{heat}(C_x)$ ranges from 0.80 at 2.0 kg·m^{-3} to 0.87 at 8.0 kg·m^{-3}. This extent of light energy dissipation to heat is rather similar to values reported previously for photoautotrophic micro-algal cultivations of 0.80 to 0.90 (Goldman 1979; Hallenbeck and Benemann 2002). It depends on the applied optical path, light intensity, biomass concentration and mixing intensity (Qiang et al. 1998b). Therefore, this variable is system specific and the reported values only hold for the applied combination of photobioreactor and operational settings. As a consequence, the reported values for $f_{heat}(C_x)$ could possibly be reduced significantly upon optimization of the applied mixing rate.

From these results we can find that the determination of the maximally achievable rate of product formation in phototrophic culture at high incident light intensity is always a trade-off between the extent of photosynthetic heat dissipation and the volumetric production capacity of the culture. A higher biomass concentration causes a larger production capacity of the system. At the same time however, the fraction of absorbed light energy that is dissipated as heat increases at a higher biomass concentration, unless the rate of mixing is increased accordingly (Qiang et al. 1998b).

The enthalpy balance for biomass growth of a *Rhodobacter capsulatus* continuous culture illuminated at 410 W·m^{-2} is illustrated in Figure 4.9B in Appendix I.

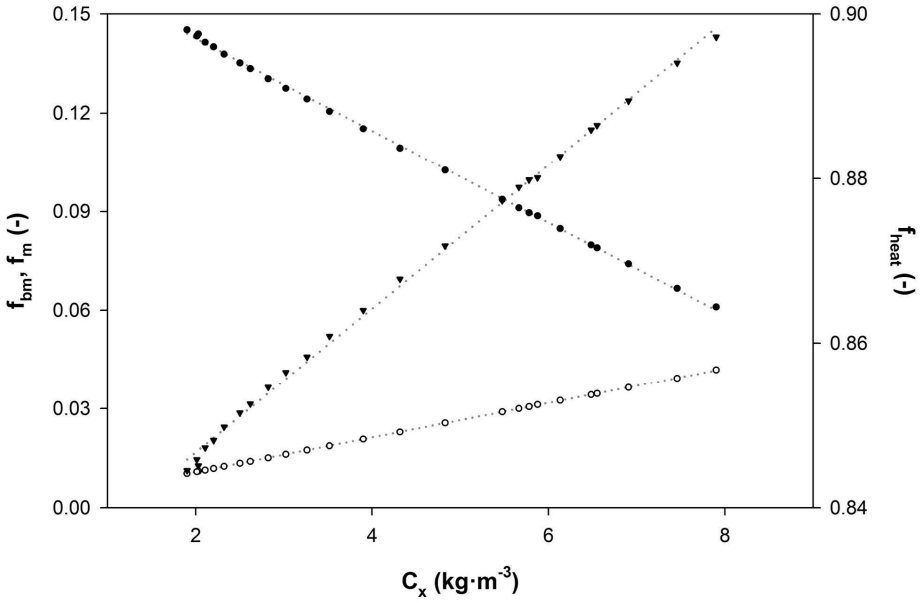

Figure 4.6 Fraction of the absorbed light energy used for biomass growth ($f_{bm} = (r_x^u/r_{le}^u) \cdot (1/Y_{x,le})$, ●), biomass maintenance ($f_m = (m_{le} \cdot C_x)/r_{le}^u$, ○) and photosynthetic heat dissipation (f_{heat},▼) as a function of the biomass concentration C_x for the D-stat experiment performed in the flat panel PBR at a light intensity of 410 W·m^{-2}.

The maximal specific hydrogen producing capacity of the culture

The maximal specific hydrogen producing rate $q_{H_2,max}$ of the *Rhodobacter capsulatus* culture used was determined by directly applying samples of a culture that was grown in the same flat-panel PBR set-up, but under argon sparged (2 L·min^{-1}), ammonium limited conditions, at 410 W·m^{-2} tungsten halogen illumination, a biomass concentration of 0.7 - 1.5 kg·m^{-3} at a dilution rate of 0.4 d^{-1}. The results of one set of three parallel repeated $q_{H_2,max}$ determinations acquired at a C_x of 1.5 kg·m^{-3} are displayed in Figure 4.7. From these data, a $q_{H_2,max}$ value of 0.52 ± 0.02 mmol·kg^{-1}·s^{-1} was calculated.

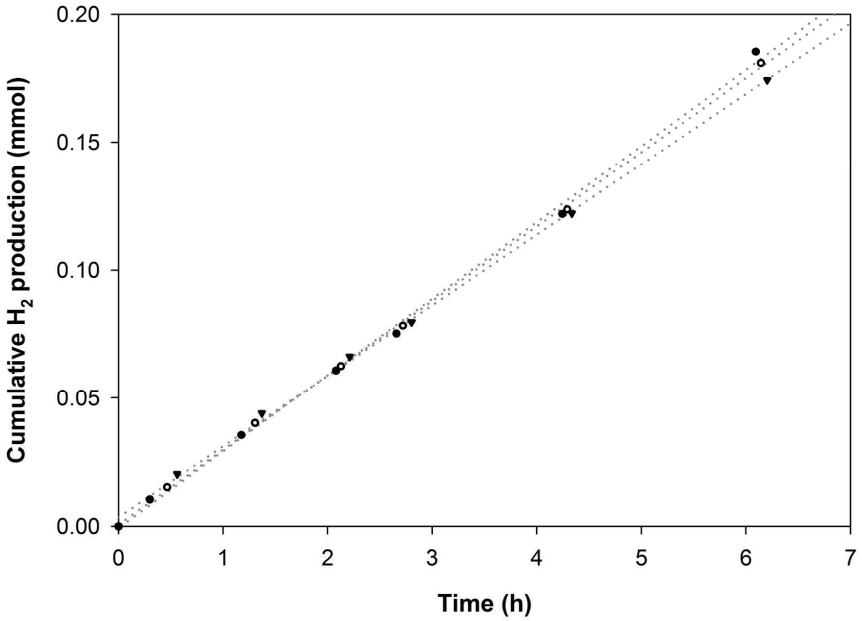

Figure 4.7 Maximal cumulative hydrogen production as determined in three (●,○,▼) 120 mL reaction vessels containing 10 mL of bacterial suspension sampled from an ammonium limited, hydrogen producing flat-panel PBR culture at a C_x of 1.5 kg m^{-3}.

The influence of the applied biomass concentration and agitation rate on the observed value of $q_{H_2,max}$ was investigated. There was no clear influence on the observed $q_{H_2,max}$ upon varying the biomass concentration between the applied extremes, 2.27 and 14.31 kg·m^{-3} and upon varying the agitation rate between 100 and 600 rpm (data not shown). This demonstrates that the applied method ensured light saturation and is therefore an accurate method for the determination of the value of $q_{H_2,max}$.

The observed $q_{H_2,max}$ is comparable to values of 0.41 and 0.58 mmol·kg^{-1}·s^{-1} reported for *Rhodopseudomonas palustris* wild type species grown photoheterotrophically on a mixture of acetate and glutamate (Fissler et al. 1994; Vincenzini et al. 1982).

The specific hydrogen production rate purple non sulphur bacteria exhibit while growing on other organic acids is significantly higher. An ammonium limited *Rhodobacter capsulatus* strain grown on lactate at a dilution rate of 0.96 d^{-1} was reported to exhibit a maximal specific hydrogen production rate of 1.24 mmol·kg^{-1}·s^{-1} (Tsygankov et al. 1998a). By genetic modification, the maximal specific hydrogen production rate can be increased even further. Knocking out the uptake hydrogenase or preventing the storage of reducing equivalents in an alternative way, like the accumulation of intracellular polyhydroxy butyric acid, can significantly increase the maximal specific hydrogen production rate. Zorin et al. reported that a *Rhodobacter capsulatus* species deficient in uptake hydrogenase, grown on a mixture of lactate and glutamate, produced hydrogen at a rate of 1.60 mmol·kg^{-1}·s^{-1}, compared to 1.11 mmol·kg^{-1}·s^{-1} for the wild type strain (Zorin et al. 1996).

The maximally achievable yield of hydrogen energy on light energy

By applying the determined parameters to Equation 4.11, $r_{H_2}^u$ can be written as a function of C_x and D. r_{le}^u and f_{heat} also depend on C_x. Therefore, these relationships were fit to the data acquired during the D-stat performed at 410 W·m^{-2} (Figure 4.5), resulting in Equation 4.13 and Equation 4.14. Both curve-fits display a correlation coefficient larger than 0.90.

Equation 4.13 $$r_{le}^u(C_x) = \sqrt{1.84 \cdot 10^8 - \frac{3.51 \cdot 10^7}{(C_x)^2}}$$

Equation 4.14 $$f_{heat}(C_x) = 0.015 \cdot C_x^{0.792} + 0.82$$

The value of $r_{H_2}^u$ can also be described using the maximal hydrogen producing capacity $q_{H_2,max}$ of the biomass that is present in the reactor, according to Equation 4.3. Whichever outcome for $r_{H_2}^u$ is lower is limiting the reactor performance when that

combination of C_x and D is applied. Based on this model, Figure 4.8 was constructed. Figure 4.8A displays the value of $r^u_{H_2}$ as a function of D at constant C_x. Three C_x-values within the applied experimental range of the D-stat performed at 410 W m^{-2} (3, 4 and 5 kg·m^{-3}) were chosen. At 3 and 4 kg·m^{-3}, combined with a sufficiently low dilution rate, the value of $r^u_{H_2}$ is set by the hydrogen production capacity of the biomass, according to Equation 4.3. As the dilution rate is increased, the value of r^u_x in Equation 4.11 increases, resulting in a decrease in $r^u_{H_2}$. This decrease is faster and occurs at a lower dilution rate as the biomass concentration is higher (Figure 4.8A). More and more absorbed light energy must be used for generating additional biomass as the dilution rate is increased further. Finally, all the absorbed light energy is used for the formation of biomass and no absorbed light energy is available for generating hydrogen.

Similarly, the biomass concentration can be increased while keeping the dilution rate constant. This is shown in Figure 4.8B for three values of D (0.1, 0.4 and 0.8 d^{-1}) within the experimental range of the D-stat performed at 410 W·m^{-2}. At low biomass concentrations, the value of $r^u_{H_2}$ is limited by the hydrogen production capacity of the biomass present (Equation 4.3). When its value is increased, $r^u_{H_2}$ increases and reaches a maximum. As C_x is increased further, r^u_x must increase at the expense of $r^u_{H_2}$ (Equation 4.11). This effect is more pronounced as larger values of D are chosen, due to a further increase in r^u_x.

Figure 4.8 Simulation results of the volumetric hydrogen production rate $r^u_{H_2}$ within the flat panel PBR at a constant biomass concentration C_x of 3, 4 and 5 kg·m^{-3} as a function of the dilution rate D (A) and at a constant D of 0.1, 0.4 and 0.8 d^{-1} as a function of C_x (B).

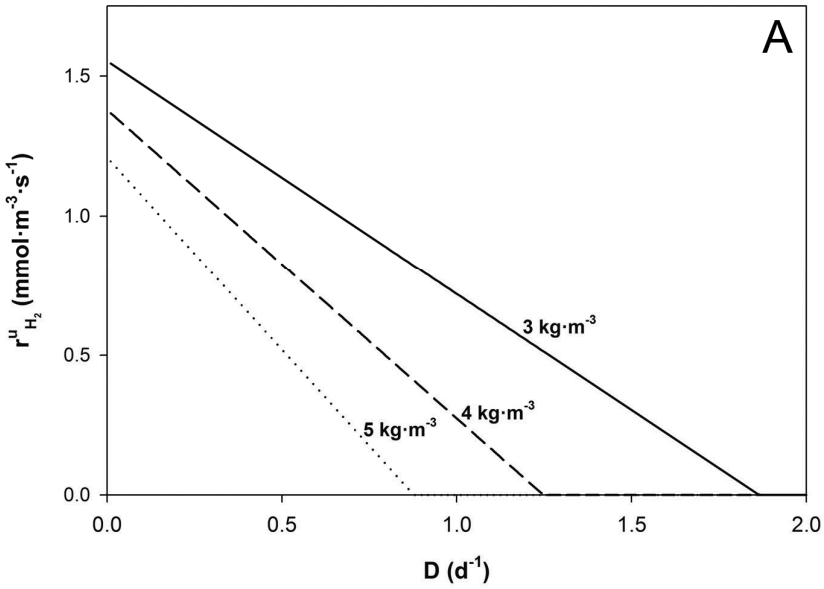
A
1.5
1.0
0.5
0.0
0.0
0.5
1.0
1.5
2.0
$r^u_{H_2}$ (mmol·m^{-3}·s^{-1})
D (d^{-1})
3 kg·m^{-3}
4 kg·m^{-3}
5 kg·m^{-3}

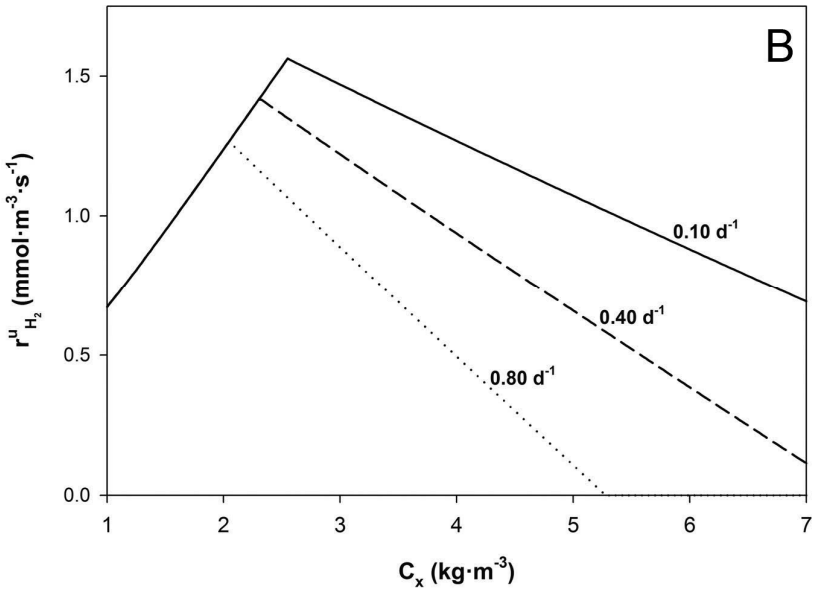
B
1.5
1.0
0.5
0.0
1
2
3
4
5
6
7
$r^u_{H_2}$ (mmol·m^{-3}·s^{-1})
C_x (kg·m^{-3})
0.10 d^{-1}
0.40 d^{-1}
0.80 d^{-1}

From Figure 4.8, it can be seen that the dependency of $r^{u}_{H_2}$ on C_x or D should have a clear maximum. By adjusting the biomass concentration or the dilution rate of a continuous hydrogen producing culture of *Rhodobacter capsulatus*, a significant increase in the value of $r^{u}_{H_2}$ can possibly be achieved, reaching values up to 1.6 mmol·m^{-3}·s^{-1}. This hydrogen production rate corresponds to a photosynthetic efficiency of 3.3% (considering light energy input and hydrogen energy output only), at which 98% of all incident light energy (400 – 950 nm) is absorbed. This maximally achievable efficiency of absorbed light energy to hydrogen energy conversion is expected to take place when a dilution rate of 0.1 d^{-1} is combined with a biomass concentration of 2.55 kg·m^{-3}, as illustrated graphically in Figure 4.8B.

The enthalpy balance for biomass growth and hydrogen production of an ammonium limited *Rhodobacter capsulatus* continuous culture illuminated at 410 W·m^{-2} is illustrated in Figure 4.9C in Appendix I.

Conclusions

The commercial applicability of microbial phototrophic fermentation is limited mainly by its photosynthetic efficiency. In this work we describe a model-based approach to calculate what photosynthetic efficiency can maximally be achieved in a given photobioreactor. A new experimental method to quantify both the biomass yield and maintenance coefficient on light energy of phototrophic cultures in a limited time span was designed and tested. For this an experimental technique called D-stat was used.

The photo production of hydrogen by *Rhodobacter capsulatus* NCIMB 11773 at realistic solar irradiation conditions was taken as a case-study. The yield coefficient of biomass synthesis on light energy was determined to be $3.8 \pm 0.03 \cdot 10^{-8}$ kg·J^{-1} and the biomass maintenance coefficient on light energy was 71.6 ± 11.3 W·kg^{-1} at an incident light intensity of 8.4 W·m^{-2} (400 – 950 nm). The fraction of the light energy that was absorbed by the culture but was not used for either biomass synthesis or maintenance under non-

ammonium limited conditions was dissipated to heat. It varied between 0.80 and 0.88 in the applied photobioreactor, at a light intensity of 410 $W \cdot m^{-2}$ (400 – 950 nm).

The destinations of the absorbed light energy under ammonium limitation are biomass synthesis and maintenance, hydrogen formation and dissipation to heat. They were modelled using the abovementioned parameters. By limiting the extent of biomass synthesis, while retaining a sufficient viable biomass concentration in the photobioreactor, the volumetric hydrogen production rate can possibly be increased up to 1.6 $mmol \cdot m^{-3} \cdot s^{-1}$, at an incident light intensity of 410 $W \cdot m^{-2}$. This hydrogen production rate corresponds to a photosynthetic efficiency of 3.3%. The model predicts this maximally achievable efficiency to occur at a dilution rate of 0.1 d^{-1} combined with a biomass concentration of 2.55 $kg \cdot m^{-3}$. The validation of the described model will be subject of future work.

Erratum

The light intensities at the surface of the PBR that are reported in this chapter are lower than those reported previously (Hoekema et al. 2006). The originally reported light intensities were based on an emission spectrum of the applied halogen-tungsten lamps that was acquired with a spectrometer that was not properly calibrated. More details are provided in Appendix II.

Appendix I

a) Relation between yield factors and the enthalpy balance

Equation 4.15 represents the stoichiometry for *Rhodobacter capsulatus* growth on acetate and ammonium, based on the biomass' elemental composition.

Equation 4.15 $$Y_{ac,x} \cdot CH_3COO^- + Y_{amm,x} \cdot NH_4^+ \xrightarrow{W_{le}} CH_kO_lN_m + Y_{CO_2,x} \cdot CO_2 + Y_{H_2O,x} \cdot H_2O + Y_{OH^-,x} \cdot OH^-$$

The parameters $Y_{a,x}$ represent the yield coefficients of *a* per C-mole biomass and W_{le} is the work exerted on the system in the form of the total light energy absorption. Since biomass growth can be considered to be a constant pressure process, an enthalpy balance can be made according to Equation 4.16.

Equation 4.16 $$\sum \Delta_c H^0_{out} - \sum \Delta_c H^0_{in} + W_{le} + Q_{met} = 0$$

The summations $\sum \Delta_c H^0_{in}$ and $\sum \Delta_c H^0_{out}$ represent the enthalpies of the reactants and products, while Q_{met} is the heat generated during all metabolic processes involved with biomass synthesis, including maintenance. The enthalpy change was calculated using enthalpies of combustion as a reference state (von Stockar et al. 1993). The enthalpy of combustion of the biomass was estimated on the basis of its elemental composition (Spoehr and Milner 1949). The temperature used was 25˚C since temperature influence is negligible (von Stockar et al. 1993).

b) Biomass formation at low light intensity

Considering the process of biomass formation at rate r_x^u to be at steady-state, Equation 4.16 was rewritten to Equation 4.17. The contributions of CO_2(g), H_2O(l) and OH^-(aq) to the enthalpy balance are zero and were left out of Equation 4.17.

Equation 4.17 $$r_x^u \cdot \Delta_c H^0_{x(s)} - Y_{ac,x} \cdot r_x^u \cdot \Delta_c H^0_{ac(aq)} - Y_{amm,x} \cdot r_x^u \cdot \Delta_c H^0_{amm(aq)} + W_{le} + Q_{met} = 0$$

Where $W_{le} = r_{le}^u$

When the experimental results obtained during the D-stat at 8.4 $W \cdot m^{-2}$ are combined with Equation 4.17, the enthalpy balance for biomass synthesis can be calculated. The results are presented in Figure 4.9A. The fraction of the total enthalpy taken up that is recovered as biomass equals 38.2%.

c) Biomass formation at high light intensity

The situation in which the culture is producing biomass at 410 $W \cdot m^{-3}$ is considered. Equation 4.17 is now re-written to Equation 4.18 to include photosynthetic heat dissipation.

Equation 4.18 $$r_x^u \cdot \Delta_c H^0_{x(s)} - Y_{ac,x} \cdot r_x^u \cdot \Delta_c H^0_{ac(aq)} - Y_{amm,x} \cdot r_x^u \cdot \Delta_c H^0_{amm(aq)} + W_{le} + Q_{met} + Q_{phot} = 0$$

Where $W_{le} = r_{le}^u$

$Q_{phot} = -1 \cdot f_{heat}(C_x) \cdot r_{le}^u$

The enthalpy balance for biomass synthesis is presented in Figure 4.9B. The fraction of the total enthalpy uptake that is recovered as biomass equals 10.5%.

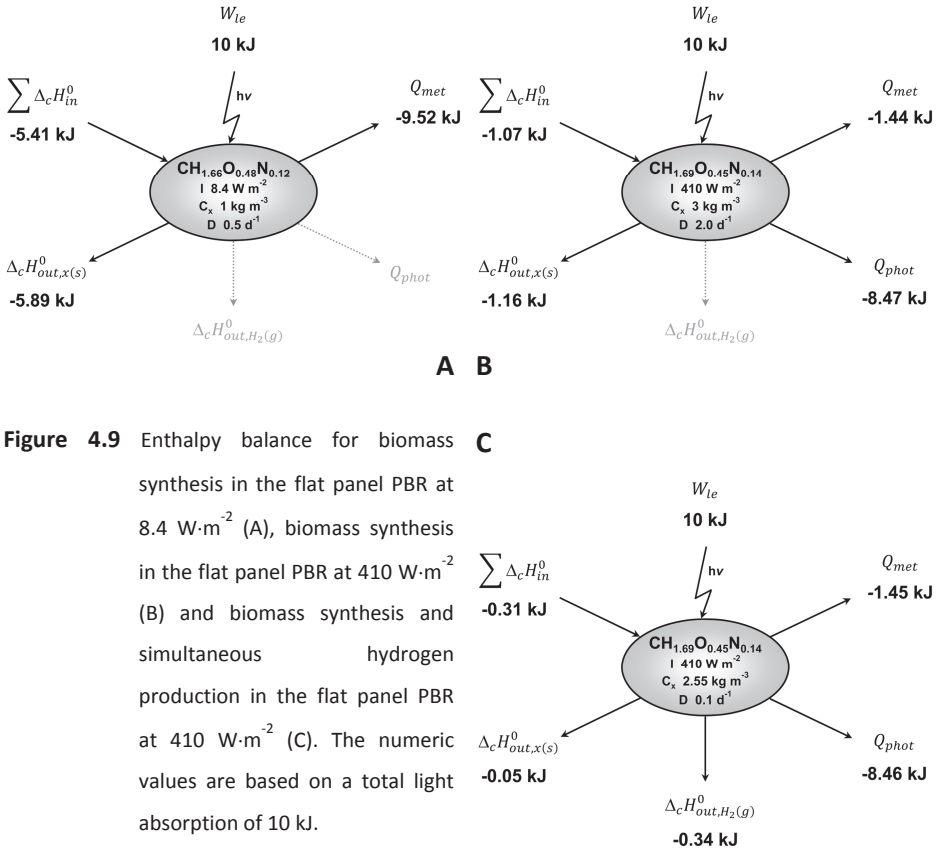

Figure 4.9 Enthalpy balance for biomass synthesis in the flat panel PBR at 8.4 W·m^{-2} (A), biomass synthesis in the flat panel PBR at 410 W·m^{-2} (B) and biomass synthesis and simultaneous hydrogen production in the flat panel PBR at 410 W·m^{-2} (C). The numeric values are based on a total light absorption of 10 kJ.

d) Biomass and hydrogen formation under high light intensity

Finally, the situation in which the culture is illuminated at 410 W·m^{-3} and is actively producing hydrogen is considered. In this situation, the enthalpy balance is written according to
Equation 4.19.

Equation 4.19
$$r_x^u \cdot \Delta_c H^0_{x(s)} + r^u_{H_2} \cdot \Delta H^o_{H_2(g)} - Y_{ac,x} \cdot r_x^u \cdot \Delta_c H^0_{ac(aq)} - Y_{amm,x} \cdot r_x^u \cdot \Delta_c H^0_{amm(aq)} + W_{le} + Q_{met} + Q_{phot} = 0$$

Where $W_{le} = r_{le}^u$

$Q_{phot} = -1 \cdot f_{heat}(C_x) \cdot r_{le}^u$

The enthalpy balance is presented in Figure 4.9C. The fraction of the total enthalpy consumption that is recovered as hydrogen equals 3.3%, while 0.6% is recovered as biomass. The light energy to hydrogen energy conversion efficiency equals 3.8% in this case.

Appendix II

The light intensities at the surface of the PBR reported in this chapter are lower than those reported previously (Hoekema et al. 2006). This is due to an incorrect factory calibration of the spectroradiometer used in this study. The re-calculated light intensities presented in this thesis are significantly lower than reported previously and result in changes in the numeric values of the parameters included in the light energy balance. However, they do not change the general conclusions that were drawn previously from this work.

Below, the correct procedure for the measurement and calculation of the light intensity is explained in detail. The newly calculated light intensities were thus used in this thesis.

First, the spectral composition of the light source (in this case 500 W Philips Halotone R7s halogen-tungsten lamps fitted in Philips QVF 415n reflectors) is measured by using a calibrated fiber optic CCD based spectroradiometer (Avaspec 2048 detector, FC-IR100-1-ME fiber, Avantes, Eerbeek, the Netherlands). Its output in $\mu W \cdot cm^{-2} \cdot nm^{-1}$ is re-calculated to $\mu mol \cdot cm^{-2} \cdot s^{-1} \cdot nm^{-1}$ using Planck's relation. The spectral composition is used to calculate a light energy output in $\mu mol \cdot m^{-2} \cdot s^{-1}$, both the in the 400-700 (PAR) and the 400-950 nm range. Accordingly, a conversion factor can be calculated from $\mu mol\ PAR \cdot m^{-2} \cdot s^{-1}$ to $W \cdot m^{-2}$ (400-950nm).

Second, the light source is positioned in front of the PBR and an average light intensity is measured at the surface of the PBR by means of a LI SA-190 quantum sensor combined with a LI-250 read-out unit (Li-Cor, USA). This device gives a light intensity value in $\mu mol\ PAR \cdot m^{-2} \cdot s^{-1}$. The conversion factor derived from the light spectrum is then used to calculate the light intensity in $W \cdot m^{-2}$ (400-950 nm) from the measurements of the PAR quantum sensor.

The light intensities reported previously were calculated on the basis of a spectral composition that was determined with another spectroradiometer that was not properly calibrated. Both the initial and corrected calibration curves are displayed in Figure 4.10. The application of the old calibration information results in a significant overestimation of the light energy output at wavelengths exceeding 700 nm.

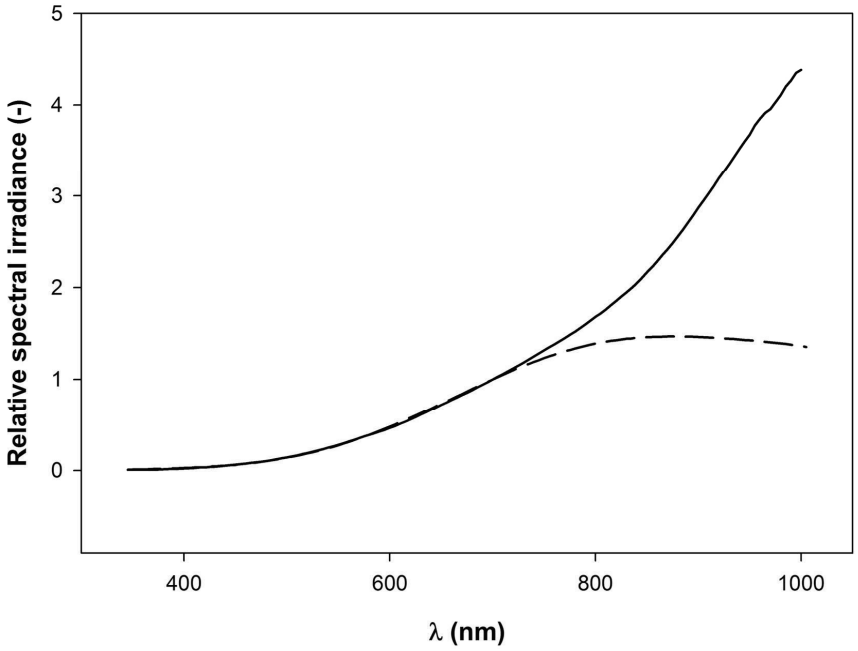

Figure 4.10 Relative spectral irradiance of a Philips Halotone halogen-tungsten lamp using the initial (solid line) and corrected (dashed line) calibration information.

Nomenclature

a	Acceleration rate	[d^{-2}]
A-stat	Acceleration stat	[-]
a^*_{dw}	Specific absorption surface	[$m^2 \cdot kg^{-1}$]
A	Specific surface area	[$m^2 \cdot m^{-3}$]
ADP	Adenosine di-phosphate	[-]
ATP	Adenosine tri-phosphate	[-]
BChl a	Bacteriochlorophyll a	[-]
C_x	Biomass concentration	[$kg \cdot m^{-3}$]
C/N-ratio	Carbon to nitrogen ratio	[-]
d	Deceleration rate	[d^{-2}]
d.w.	Dry weight	[$kg \cdot m^{-3}$]
D	Dilution rate	[d^{-1}]
D-stat	Deceleration stat	[-]
Fd	Ferredoxin	[-]
f_{heat}	Fraction of the total absorbed light dissipated as heat	[-]
f_{bm}	Fraction of the total absorbed light used for biomass synthesis	[-]
f_m	Fraction of the total absorbed light used for biomass maintenance	[-]
LHC	Light harvesting complex	[-]
I	Light intensity	[$J \cdot m^{-2} \cdot s^{-1}$, 400 – 950 nm]
m_{le}	Biomass maintenance coefficient on light energy	[$J \cdot kg^{-1} \cdot s^{-1}$]
NADH	Protonated nicotinamide adenine di-nucleotide	[-]
OP	Optical path	[m]
P_{870}	Primary electron donor in the photosystem of PNS bacteria	[-]
PAR	Photosynthetic Active Radiation	[$\mu mol \cdot m^{-2} \cdot s^{-1}$, 400 – 700 nm]
PBR	Photobioreactor	[-]
PFD	Photon flux density	[$\mu mol \cdot m^{-2} \cdot s^{-1}$]

P_i	Orthophosphate	[-]
PI	Propidium Iodine	[-]
Q_{met}	Heat generation related to metabolic and maintenance processes	[kJ]
Q_{phot}	Heat generation due to photosynthetic heat dissipation	[kJ]
q_{H_2}	Specific hydrogen production rate	[mol·kg^{-1}·s^{-1}]
$q_{H_2,max}$	Maximal specific hydrogen production rate	[mol·kg^{-1}·s^{-1}]
r_{le}^{u}	Volumetric light energy absorption	[J·m^{-3}·s^{-1}, 400 – 950 nm]
$r_{H_2}^{u}$	Volumetric hydrogen production rate	[mol·m^{-3}·s^{-1}]
r_x^{u}	Volumetric biomass production rate	[kg·m^{-3}·s^{-1}]
t	Time	[s]
s.e.	Standard error	[-]
W_{le}	Work exerted onto the system in the form of light energy abs.	[kJ]
$Y_{H_2,le}$	Yield coefficient of hydrogen energy on light energy	[mol·J^{-1}]
$Y_{x,le}$	Yield coefficient of biomass on light energy	[kg·J^{-1}]
ΔH_c^0	Enthalpy of combustion	[kJ·mol^{-1}]
μ	Specific growth rate	[d^{-1}]
μ_{max}	Maximal specific growth rate	[d^{-1}]
$\mu_{max}(I)$	Maximal specific growth rate at light intensity I	[d^{-1}]

Subscripts

0	initial
av	average
aq	aqueous
f	final
i	inorganic
in	ingoing
l	liquid
le	light energy

red	reduced
s	solid
out	outgoing
ox	oxidized
x	biomass

Chapter 5

Exploration of the hydrogen producing potential of *Rhodobacter capsulatus* chemostat cultures: The application of deceleration-stat and gradient-stat methodology

The contents of this chapter have been published as

Hoekema S, van Breukelen, FR, Janssen M, Tramper J, Wijffels RH. 2009. Exploration of the hydrogen producing potential of R*hodobacter capsulatus* chemostat cultures: The application of deceleration-stat and gradient-stat methodology. Biotechnology Progress 25(5):1343-1352.

5. Exploration of the hydrogen producing potential of *Rhodobacter capsulatus* chemostat cultures: The application of deceleration-stat and gradient-stat methodology

Abstract

In this work, the dependency of the volumetric hydrogen production rate of ammonium-limited *Rhodobacter capsulatus* chemostat cultures on their imposed biomass concentration and dilution rate was investigated.

A deceleration-stat experiment was carried out by lowering the dilution rate from 1.0 d^{-1} to zero aimed at a constant biomass concentration of 4.0 $g \cdot L^{-1}$ at constant incident light intensity. The results displayed a maximal volumetric hydrogen production rate of 0.6 $mmol \cdot m^{-3} \cdot s^{-1}$, well below model predictions. Possibly the high cell density limited the average light availability, resulting in a sub-optimal specific hydrogen production rate.

In order to investigate this hypothesis, a gradient-stat experiment was conducted at constant dilution rate of 0.4 d^{-1} at constant incident light intensity. The biomass concentration was increased from 0.7 to 4.0 $g \cdot L^{-1}$ by increasing the influent ammonium concentration. Up to a biomass concentration of 1.5 $g \cdot L^{-1}$, the volumetric hydrogen production rate of the system increased according to model predictions, after which it started to decline. The results obtained provide strong evidence that the observed decline in volumetric hydrogen production rate at higher biomass concentrations was at least partly caused by a decrease in light availability.

Introduction

Limited global fossil fuel reserves and the greenhouse effect have caused a renewed interest in studies on biological systems for the production of renewable energy carriers. Hydrogen is one of them and it can be produced by many different micro-organisms, including chemoheterotrophs like *Caldicellilosiruptor* and *Thermotoga* (fermentative bacterial) species, phototrophs like *Chlamydomonas* (green algal) species and *Rhodobacter* (purple non-sulfur, PNS, bacterial) species. The focus of the current investigation is on hydrogen photoproduction by PNS bacteria.

In PNS bacteria, hydrogen production is catalyzed by the nitrogenase enzyme complex. Significant nitrogenase inhibition in *Rps. capsulata* cultures typically starts at an ammonium concentration of 100 μM (Willison et al. 1983). Thus, PNS bacteria are able to produce hydrogen only under ammonium-limited (< 100 μM) conditions.

Hydrogen production by PNS bacteria is not solely dependent on the ambient ammonium concentration. The application of phototrophic micro-organisms in general is limited by the low efficiency at which light energy conversion takes place. The main reason for this is the excessive dissipation of light energy to heat, resulting from simultaneous light over-saturation in the photic zone and light limitation in the dark zone of a photobioreactor. This self-shading effect can be limited by decreasing the optical path of the applied photobioreactor (PBR) as demonstrated extensively for cyanobacteria (Qiang et al. 1998b).

The light energy expenditure for biomass formation and maintenance, hydrogen production and photosynthetic heat dissipation by *Rba. capsulatus* was measured previously for the PNS bacterium *Rba. capsulatus*, cultivated in a three cm thick flat-panel PBR. These data were used to model the volumetric hydrogen production rate of a *Rba. capsulatus* culture as a function of both its biomass concentration and its dilution rate at fixed incident light intensity (Hoekema et al. 2006). In this paper, data are presented that were obtained using two alternative and fast experimental methods to

generate multiple steady state data in the same flat panel PBR. They are referred to as *deceleration*-stat and *gradient*-stat and are based on the gradual change in either the dilution rate or the concentration of the growth limiting substrate. Their application resulted in the generation of information on wide ranges of process operation.

All experiments described in this work were conducted in order to explore the hydrogen producing potential of ammonium-limited *Rba. capsulatus* cultures and its dependency on both their imposed dilution rate and biomass concentration. The acquired data were used to evaluate the hydrogen producing potential of chemostat cultures and compare them to the model estimations derived previously (Hoekema et al. 2006).

Theory

The D-stat experimental method

During a *Deceleration*-stat (D-stat in short) experiment, the dilution rate (D, d^{-1}) is decreased gradually in time. As a result of the decrease in dilution rate, the biomass concentration (C_x, $kg \cdot m^{-3}$) generally increases (Hoekema et al. 2006). However, when the culture is subjected to growth limitation by applying a constant, limiting ammonium concentration in the influent, its biomass concentration should remain constant. The dilution rate can therefore be changed without a concomitant change in biomass concentration.

The G-stat experimental method

During a gradient-stat (G-stat in short) experiment, a gradient in the concentration of one or more of the substrates in the influent is introduced in time while maintaining a constant dilution rate. A gradual increase in the influent ammonium concentration of an ammonium-limited chemostat culture results in a gradual increase of its biomass

concentration. Thus the biomass concentration can be changed without a concomitant change in dilution rate.

Pseudo steady-state

Both experimental approaches described above yield more information in less experimental time compared to multiple steady state approaches, provided that the D-stat or G-stat remains in pseudo steady-state. According to chemostat theory, a microbial culture is considered to be in steady state when its growth rate (μ, d^{-1}) is equal to its dilution rate (Gottschal 1992). When a step-wise change in one of the culture conditions is imposed on such a steady-state culture (for instance its dilution rate or growth-limiting substrate concentration), the culture's response will eventually result in another steady state, provided that it lies within the physiological capacity of the applied microbe. During the time that is required to reach this second steady state, the culture is not in steady state.

In case the imposed change is not executed step-wise, but slowly and smoothly enough, the microbe can keep up with the imposed change rate. This is the case only when the time the culture requires for metabolic and physiologic adaptation as a result of the change rate is smaller than the imposed change rate itself.

Because the culture is subjected to changing cultivation conditions, this situation cannot be classified as a steady state situation. However, when the change is so slow that no dissimilarity between the culture properties at a discrete time-point during the D- or G-stat experiment and its corresponding steady state can be observed, we refer to this situation as *pseudo* steady-state (Barbosa et al. 2003; Paalme et al. 1995; van der Sluis et al. 2001a).

Calculations

Energy balances were set-up as described before (Hoekema et al. 2006), in which the total light energy absorbed was divided into fractions used for biomass maintenance, biomass

synthesis and hydrogen production and in which the remainder was assumed to be dissipated as heat.

Materials and methods

Bacterial strain and medium composition

The PNS bacterium *Rba. capsulatus* NCIMB 11773 was used in this work. It was selected based on its wide substrate range and its high C-substrate to hydrogen conversion efficiency (Segers and Verstraete 1983). An exponentially growing culture was harvested and stored at -80˚C in aliquots of 1 mL containing 15% glycerol. Prior to starting an experiment, a cryo-vial was thawed and its contents transferred aseptically to a 500 mL flask containing 250 mL of SYA-medium under a nitrogen headspace. This medium is based on the previously reported aSy-medium (Miyake et al. 1984). The culture flasks were incubated at 30˚C, stirred and illuminated continuously at about 90 µmol·m^{-2}·s^{-1} using fluorescent lamps.

During the entire D-stat experiment carried out in the flat panel PBR, modified SYA-medium, designated 'D-stat'-medium was used. It contained macro- and micronutrients, acetate and ammonium. During the G-stat experiment, 'G-stat'-medium was used, containing macro- and micronutrients, vitamins and acetate. The ammonium concentration in the PBR influent was increased in time by increasing a separate concentrated ammonium inflow.

The maximal specific hydrogen production rate ($q_{H_2,max}$, mol·kg^{-1}·s^{-1}) of the cultures was assessed using $q_{H_2,max}$-medium. It contained no ammonium and had a higher buffer capacity. Ammonium was added at a concentration of 1 mM where indicated. The composition of all media described above is displayed in Table 5.1. The media were prepared from concentrated stock solutions, set to pH 7.0 and autoclaved prior to use. Only the stock solution of calcium chloride and magnesium sulfate was autoclaved

separately and added later. The concentrated vitamin stock solution used was filter sterilized (0.2 µm) prior to addition to the medium.

Table 5.1 Composition of all media and stock solutions used to prepare the media.

	Stock Solutions, C/N sources	Medium → Stock g·L^{-1}↓	SYA (µM)	D-stat (µM)	G-stat (µM)	$q_{H_2,max}$ (µM)	pH-regulation D- / G-stat	Nitrogen feed G-stat
Buffer			20 mL·L^{-1}↓	6 mL·L^{-1}↓	6 mL·L^{-1}↓	40 mL·L^{-1}↓	-	-
	KH_2PO_4	86.6	12726	3818	3818	25452		
	K_2HPO_4	73.3	8416	2525	2525	16832		
Macro nutrients			40 mL·L^{-1}↓	40 mL·L^{-1}↓	40 mL·L^{-1}↓	40 mL·L^{-1}↓	-	-
	$MgSO_4$.$7H_2O$	5.00	812	812	812	812		
	$CaCl_2$.$2H_2O$	2.48	674	674	674	674		
Micro nutrients			10 mL·L^{-1}↓	10 mL·L^{-1}↓	10 mL·L^{-1}↓	10 mL·L^{-1}↓	-	-
	$Na_2EDTA.2H_2O$	2.00	53.7	53.7	53.7	53.7		
	$FeSO_4$.$7H_2O$	1.18	42.5	42.5	42.5	42.5		
	H_3BO_3	0.280	45.3	45.3	45.3	45.3		
	$MnSO_4$.$2H_2O$	0.277	16.4	16.4	16.4	16.4		
	Na_2MoO_4.$2H_2O$	0.0750	3.10	3.10	3.10	3.10		
	$ZnSO_4$.$7H_2O$	0.0240	0.835	0.835	0.835	0.835		
	$Cu(NO_3)_2$.$3H_2O$	0.0040	0.166	0.166	0.166	0.166		
Vitamins			10 mL·L^{-1}↓	10 mL·L^{-1}↓	10 mL·L^{-1}↓	10 mL·L^{-1}↓	-	-
	Biotin	0.1	1 mg·L^{-1}	1 mg·L^{-1}	1 mg·L^{-1}	1 mg·L^{-1}		
	Thiamin	0.1	1 mg·L^{-1}	1 mg·L^{-1}	1 mg·L^{-1}	1 mg·L^{-1}		
	p-aminobenzoic acid	0.1	1 mg·L^{-1}	1 mg·L^{-1}	1 mg·L^{-1}	1 mg·L^{-1}		
	vitamin B_{12}	0.1	1 mg·L^{-1}	1 mg·L^{-1}	1 mg·L^{-1}	1 mg·L^{-1}		
	nicotinamide	0.1	1 mg·L^{-1}	1 mg·L^{-1}	1 mg·L^{-1}	1 mg·L^{-1}		
SYA			50 mL·L^{-1}↓	-	-	-	-	-
	Na_2 succinate	81	25 mM					
	Yeast extract	10	500 mg·L^{-1}					
	Na acetate	16.4	10 mM					
Carbon source	Acetic acid	-	-	-	-	-	2.0 / 2.0 M	520 mM
	Na-acetate	-	-	52 mM	20 mM	50 mM	27 / 20 mM	
Nitrogen source	NH_4Cl	-	-	27 mM	-	1 mM[1]	27 / 0 mM	500 mM
	Headspace	-	nitrogen	nitrogen	nitrogen	argon	-	

[1] Where indicated

Experimental procedures

During the D-stat experiment the dilution rate was decreased smoothly from 1.0 to 0 d^{-1} at a fixed influent ammonium concentration of 27 mM in order to find the dilution rate that yields an optimal volumetric hydrogen production rate ($r_{H_2}^u$, $mol \cdot m^{-3} \cdot s^{-1}$) at a constant biomass concentration of 4 $g \cdot L^{-1}$. A D-stat experiment executed previously at similar conditions demonstrated that the application of a deceleration rate (d, d^{-2}) of 0.17 warranted pseudo-steady state. In order to expand the experimental time available to collect the required data, a value of d of 0.1 d^{-2} was chosen. The specific growth rate was calculated as described before (Hoekema et al. 2006).

During the G-stat experiment, the biomass concentration was increased smoothly by increasing the ammonium concentration in the reactor influent using a separate concentrated ammonium flow to which an equimolar concentration of acetate was added for pH compensation (see Table 5.1 for concentrations). The dilution rate was fixed at 0.4 d^{-1} to make sure that steady state could be reached relatively fast. At this dilution rate the model of Hoekema et al. (Hoekema et al. 2006) predicts an optimum in volumetric hydrogen production rate of 1.60 $mmol \cdot m^{-3} \cdot s^{-1}$ at a biomass concentration of 2.55 $kg \cdot m^{-3}$. An experimental biomass concentration range of 0.7 - 4.2 $g \cdot L^{-1}$ was chosen, as it enables the verification of the predicted optimum while a wide range of average light intensities is covered. The experiment was started in chemostat mode at an influent ammonium concentration of 2.7 mM (corresponding to a biomass concentration of 0.7 $g \cdot L^{-1}$). During a D-stat experiment run earlier at identical illumination, pseudo-steady state was maintained at a biomass increment of 0.2 $g \cdot L^{-1} \cdot d^{-1}$ (Hoekema et al. 2006). This increment

was also applied during the G-stat experiment and corresponds to a gradient rate (g, $mM \cdot d^{-1}$) of 0.8[1].

Comparability with steady state conditions was verified experimentally by incorporating a true steady state period into each experiment during which the dilution rate or influent ammonium concentration was kept constant.

Since the focus of this work is on studying the conversion of light energy into hydrogen energy in ammonium-limited *Rba. capsulatus* cultures, the carbon to nitrogen (C/N) ratio in the influent was kept above the C/N ratio of the biomass at all time in order to assure full nitrogenase expression (Dörffler et al. 1998).

During both experiments, pH regulation using acetic acid yielded stable acetate concentrations of 20 - 25 mM in the PBR (data not shown). This acetate concentration range neither limits nor inhibits growth of *Rba. capsulatus* NCIMB 11773 cultures (data not shown).

Experimental configurations

Photobioreactor

Both stat experiments were carried out in the flat-panel PBR described before (Hoekema et al. 2002). It was computer controlled using LabVIEW© 5.1 software (National Instruments, Austin, TX) via an ADAM-5000 data-acquisition and control module (Advantech, Milpitas, CA). It was autoclaved completely prior to use. Mixing was facilitated by sparging 0.85 $nL \cdot L^{-1}$ min^{-1} argon into the culture chamber through 25 hypodermic needles.

[1] An 80% conversion efficiency of NH_4^+-N to biomass-N and a biomass elemental composition of $CH_{1.686}O_{0.469}N_{0.111}$ (based on previous experimental results with an ammonium-limited culture at identical illumination) were used.

The reactor consisted of two compartments, the front one being oriented to the light. Water was circulated through it via a cryostat water bath to maintain the temperature in the culture compartment at 30˚C. The culture compartment had an optical path of 3 cm and a working volume of 2.4 L (total volume 3.6 L). Both a pH and a redox probe were fit into the reactor for control and monitoring purposes. The pH was controlled at 7.0 by dosing acetic acid enriched with acetate to the reactor using a pH-controller (see Table 5.1 for the composition of the pH regulation liquid). This is similar to the carbon substrate feeding methodology described previously (Hoekema et al. 2006).

The reactor was illuminated by two 500 W tungsten halogen lamps (Philips Halotone R7s, fitted in Philips QVF 415n reflectors, Philips, Eindhoven, the Netherlands), placed on one side of the reactor. The lamps were mounted in a frame, on top of each other. The desired incident light intensity was reached by altering the distance between the reactor and the lamp-frame. The average radiation on the inner surface of the culture compartment was measured prior to cultivation, in the empty reactor, with the cooling-water compartment present. The D-stat and G-stat experiments were executed at light intensities of 590 and 410 $W \cdot m^{-2}$ (400-950 nm) respectively.

The medium was pumped into the reactor using a peristaltic pump. The culture was pumped out of the reactor via an L-shaped glass tube with the small leg upwards at the desired liquid level, using a second peristaltic pump. The weight of the effluent vessel was measured continuously in order to calculate the actual dilution rate of the system. A diluted (40 times) 'Antifoam B' Silicone emulsion (J. T. Baker, Deventer, the Netherlands) was automatically dosed into the reactor as a conductivity sensor detected the presence of foam in the reactor headspace.

$q_{H_2,max}$ determination

Glass vessels with an average internal volume of 120 mL were used for the experimental quantification of the maximal specific hydrogen production rate of culture samples from the PBR by applying light-saturated conditions. Stirring was facilitated using magnetic

stirrer bars at 300 rpm. The temperature of the double-jacketed vessels was kept at 30˚C. On top of the vessels light diffusing plates and 50 W tungsten halogen lamps were fitted. Their light intensity was measured at the bottom of the culture compartment in an open vessel, constructed especially for this purpose, and amounted to about 200 $W \cdot m^{-2}$ (400-950 nm).

The vessels were flushed with argon and 10 mL of cell suspension (taken directly from the reactor or washed with the appropriate media where indicated) was added, resulting in an optical light path of 7 mm. Two screw-caps with septa in the vessels' walls facilitated argon flushing and headspace sampling. The increase in the hydrogen concentration in time in the headspace was measured using gas chromatography. The final pressure in the vessels was measured using a Cerabar M PMP41 0-4 bar*a* pressure sensor (Endress+Hauser, Reinach, Switzerland). The value of $q_{H_2,max}$ was calculated from the region with linear kinetics (see Results section). The pH of the applied medium was set to 7.0 initially and was checked after the experiment was ended. It generally increased by 0.7-2.0 units over a six hour incubation period.

Analyses

Sampling

Small samples (up to 20 ml) were withdrawn directly from the PBR using a sampling port. Larger samples (for instance for biomass dry-weight determination) were collected overnight on ice from the PBR effluent.

The ammonium concentration in the culture, the hydrogen concentration in the gas phase, the absorptive properties of the biomass, the light intensity, the spectral composition entering and exiting the PBR, the viability of the biomass, the biomass concentration and the elemental composition of the biomass were determined as described previously (Hoekema et al. 2006).

Specific absorption surface

The light absorptive properties of the biomass were determined using a spectrophotometer equipped with an integrating sphere according to (Hoekema et al. 2006) eliminating the effect of light scattering on the absorption measurement. The specific absorption surface of the biomass (a^*_{dw}, $m^2 \cdot kg^{-1}$) was calculated from the wavelength dependent absorption coefficients measured in the wavelength range between 400 and 950 nm (0.5 nm interval). The wavelength dependent absorption coefficients were first weighed according to the emission spectrum of the tungsten halogen lamps and then averaged. This method of calculation is analogous to the calculation of the average spectral extinction coefficient described previously (Dubinsky et al. 1986).

pH and redox potential

The pH was measured and controlled on-line. The pH value was checked off-line daily and the electrode calibration was adjusted when required. The redox potential was measured on-line to check for anaerobicity, which was always maintained (data not shown).

Acetate

The acetate concentration in the culture medium was determined by gas chromatography. Samples were centrifuged and the supernatant was diluted 1:1 with 3% (v/v) formic acid and stored at -80˚C. The samples were analyzed on an HP 5890 gas chromatograph equipped with a Heliflex AT-Aquawax-DA column (length 30 m, int. diam. 0.32 mm, film thickness 0.25 µm) and an FID (flame-ionization detector). The column temperature was increased from 80-200˚C at a rate of 25˚C·min^{-1}, while the FID was kept at 300˚C. Nitrogen saturated with formic acid was used as the carrier gas at a flow rate of 1.5 mL·min^{-1}.

Results and discussion

In the experiments presented the hydrogen producing potential of ammonium-limited *R. capsulatus* continuous cultures was explored. Its dependency on both the imposed dilution rate and biomass concentration was studied. First a D-stat experiment was conducted in order to determine the volumetric hydrogen production rate at set biomass concentration and variable dilution rate. Then a G-stat experiment was conducted to investigate the extent of light limitation at different biomass concentrations.

D-stat experiment

During the D-stat experiment, the biomass concentration was intended to remain 4.0 $g \cdot L^{-1}$ by applying a constant, limiting ammonium concentration in the influent. This biomass concentration ensures sufficient hydrogen generating capacity in the PBR to direct 3.3% of the light energy input towards hydrogen. The ammonium concentration in the PBR never exceeded 55 µM (data not shown), resulting in nitrogen limitation for the biomass. According to model predictions, a dilution rate of 0.1 d^{-1} should result in a volumetric hydrogen production rate of 1.30 $mmol \cdot m^{-3} \cdot s^{-1}$ at this biomass concentration (Hoekema et al. 2006). The biomass concentration was constant at 4.0 $g \cdot L^{-1}$ during the first 15 days of the experiment. However, as the dilution rate was decreased below 0.8 d^{-1}, the biomass concentration in the PBR increased up to 5.5 $g \cdot L^{-1}$, causing a deviation between the dilution rate and the specific growth rate (Figure 5.1). An increase in the C/N-ratio of the biomass from 7.1 to 9.0 was measured at the point where the increase in biomass concentration was observed (data not shown).

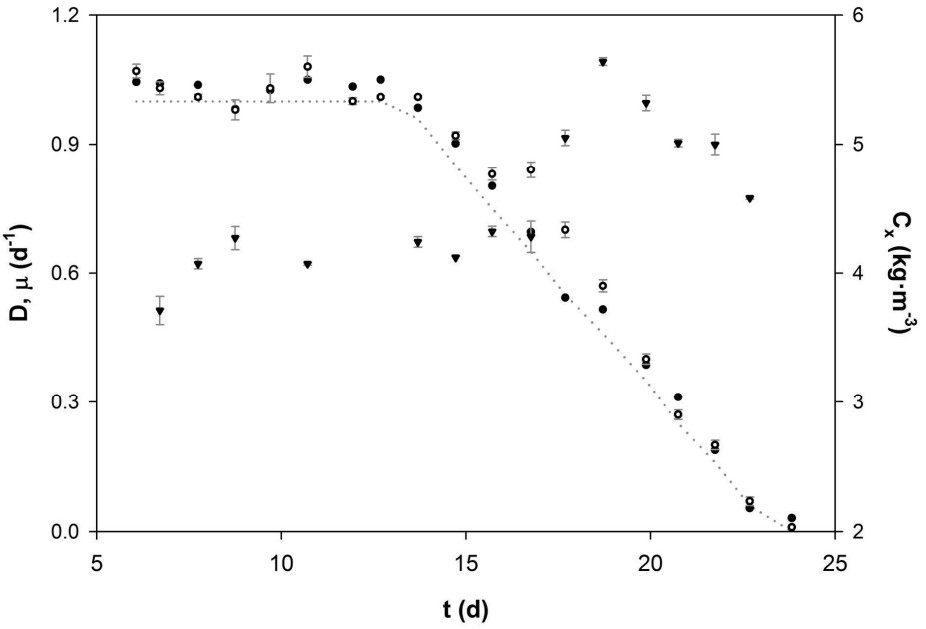

Figure 5.1 Dilution rate (D, ●), resulting growth rate (μ, ○) and biomass concentration (C_x, ▼) during the D-stat experiment. The dotted line represents the set dilution rate. The error bars represent standard errors of the mean.

An unexpected increase in the concentration of several organic acids was observed in the culture medium at this point (Figure 5.2), indicating a shift in the bacterial carbon metabolism. All three observations could be related to the accumulation of carbon storage materials like poly-β-hydroxybutyrate, which is not uncommon for ammonium-limited cultures of PNS bacteria, especially when grown on acetate (Göbel 1978; Khatipov et al. 1998).

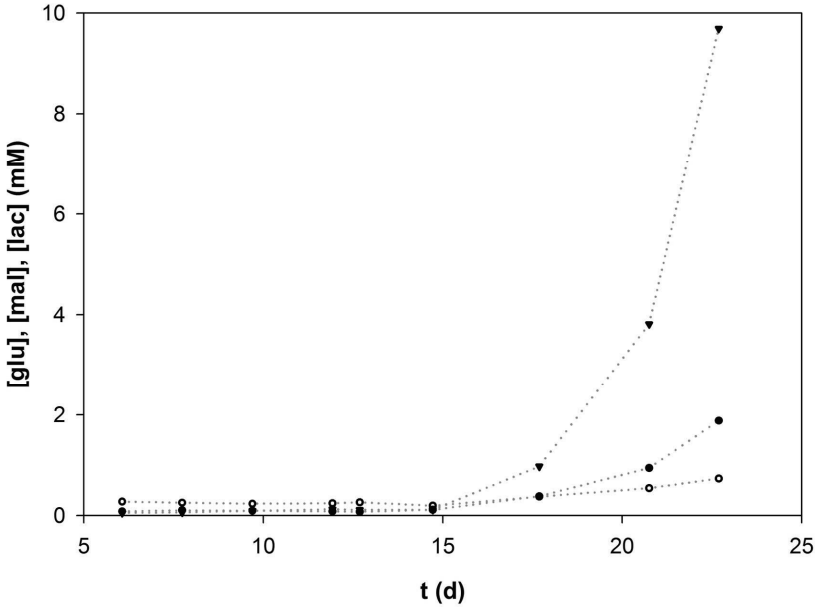

Figure 5.2 Glutamate (glu, ●), malate (mal, ○) and lactate (lac, ▼) concentrations in the PBR culture supernatant during the D-stat experiment.

The volumetric hydrogen production rate $r^{u}_{H_2}$ increased slightly from 0.30 to 0.60 mmol·m^{-3}·s^{-1}, the latter corresponding to a light- to hydrogen energy conversion efficiency of 0.8% at a dilution rate of 0.6 d^{-1} (data not shown). This is significantly lower than the 1.6 mmol·m^{-3}·s^{-1} or 3.3% light to hydrogen energy conversion efficiency that resulted from model calculations at a dilution rate of 0.1 d^{-1} (Hoekema et al. 2006).

The specific hydrogen production rate (q_{H_2}, mmol·kg^{-1}·s^{-1}) in the PBR was constant at 0.11 mmol·kg^{-1}·s^{-1} during the entire experiment. The maximal specific hydrogen production rate was much higher, around 0.40 mmol·kg·s^{-1} (data not shown), but did not reach 0.52 mmol·kg^{-1}·s^{-1} as measured previously (Hoekema et al. 2006). Possibly, light limitation inside the PBR caused the large deviation between the recorded values for q_{H_2}

and $q_{H_2,max}$. Such a severe influence of light limitation on the volumetric hydrogen production rate was unanticipated at this relatively low biomass concentration combined with the short 3 cm optical path of the PBR.

The influence of the biomass concentration on the specific hydrogen production rate was studied next, as the light availability inside the PBR is directly influenced by it.

G-stat experiment

The G-stat experiment was executed at an elevated dilution rate (0.4 d^{-1} instead of 0.1 d^{-1}), in order to prevent the shift in carbon metabolism observed during the D-stat experiment. Both the imposed dilution rate and the resulting specific growth rate are shown in Figure 5.3 and display close resemblance, indicating that steady state was maintained.

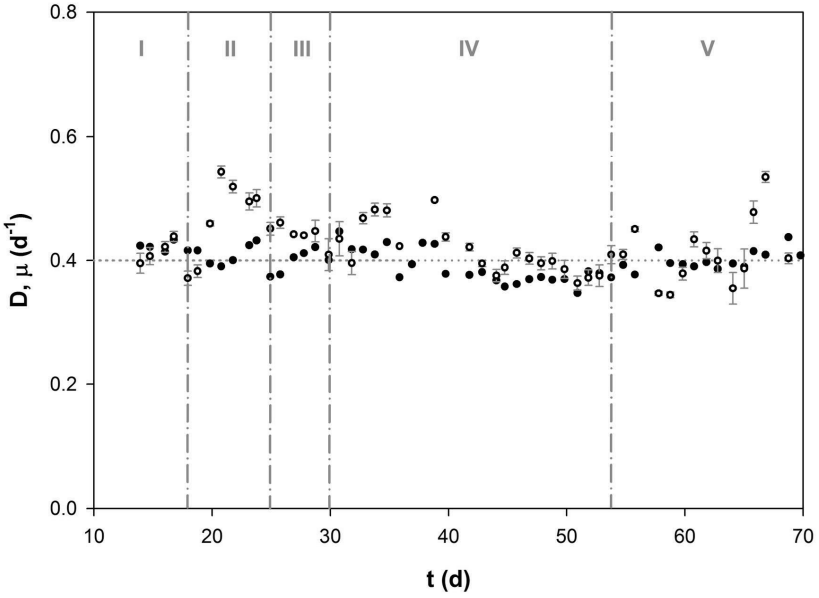

Figure 5.3 Dilution rate (D, ●) and resulting growth rate (μ, ○) during the G-stat experiment. The dotted line represents the set dilution rate. The error bars represent standard errors of the mean.

No accumulation of organic acids was detected (data not shown). After demonstration of initial steady-state (Period I), the influent ammonium concentration was increased gradually at a gradient rate of 0.8 mM·d^{-1}, starting on day 18. This resulted in an increase in biomass concentration and a decrease in light intensity exiting the PBR in time (Period II), as can be seen in Figure 5.4.

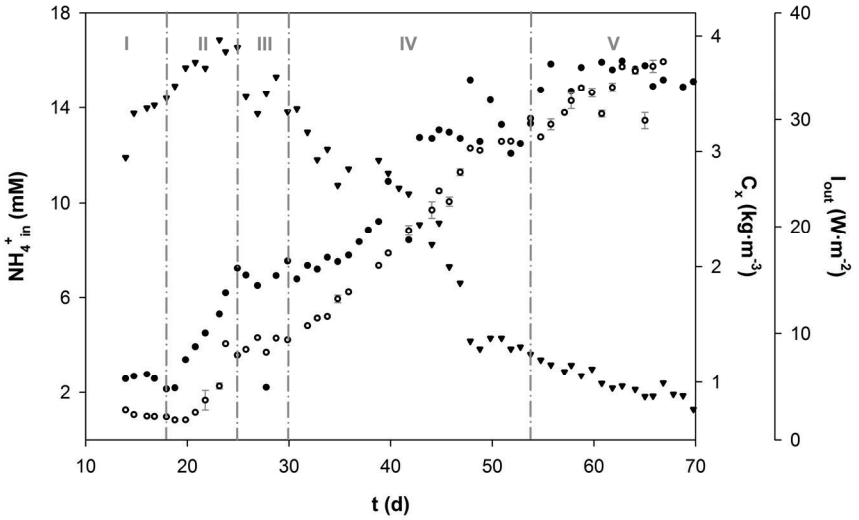

Figure 5.4 Ammonium concentration in the reactor influent (NH_4^+, ●), resulting PBR biomass concentration (C_x, ○) and residual light intensity (I_{out}, ▼) during the G-stat experiment. The error bars represent standard errors of the mean.

The culture was always ammonium-limited, as evidenced by the immediate increase in biomass concentration as the influent ammonium concentration was increased and an ammonium concentration that remained below 10 µM (data not shown). Between days 25 and 30 the increase in influent ammonium concentration was paused (Period III). Comparability between the pseudo-steady state reached and true steady state was demonstrated in this interval because no significant changes in the properties of the culture were observed during this period. On day 30 the increase in influent ammonium concentration was resumed, but at a lower increment of 0.4 instead of 0.8 mM·d^{-1} (Period IV), in order to study the dependency of $r_{H_2}^u$ on C_x with higher resolution.

After day 54 the influent ammonium concentration was kept constant (Period V, see below for an explanation). The five periods identified above are indicated throughout Figures 5.3-5.7.

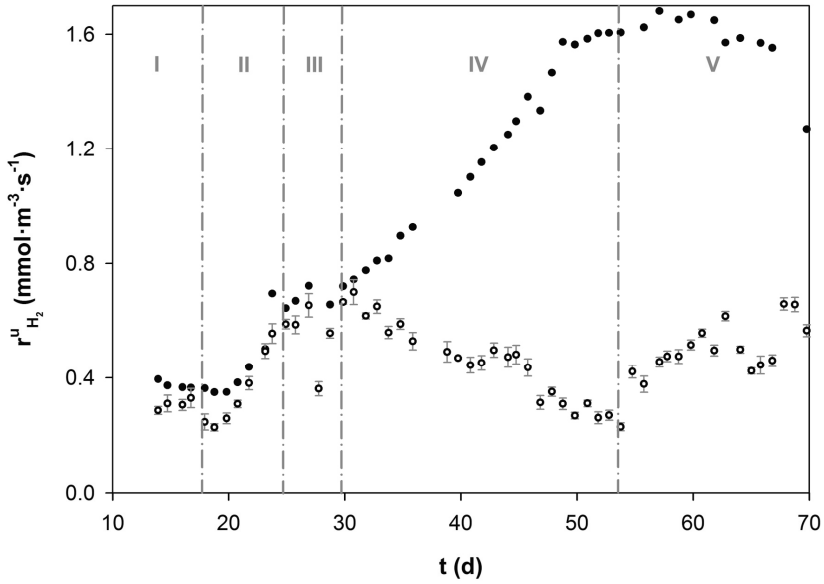

Figure 5.5 Predicted (●) and actual (○) volumetric hydrogen production rate $r^{u}_{H_2}$ during the G-stat experiment. The error bars represent standard errors of the mean.

Both the predicted and actual values of $r^{u}_{H_2}$ as the D-stat experiment progressed are displayed in Figure 5.5. The increase in biomass concentration caused a proportional increase in $r^{u}_{H_2}$, reaching 0.70 mmol·m^{-3}·s^{-1} at 1.5 g·L^{-1}, corresponding to a light to hydrogen conversion efficiency of 1.6%. This value is in good accordance with model predictions. As can also be seen here, a further increase in biomass concentration resulted in a decline in $r^{u}_{H_2}$, while model-predictions suggested a further increase (Hoekema et al. 2006). After day 53 a minor recovery was observed, which will be discussed later.

All light energy absorbed by the bacterial culture is either used for biomass growth, biomass maintenance, hydrogen production or is dissipated as heat. The presented model predictions are based on the assumption that the ratio of fractions of the total absorbed light energy used for biomass synthesis and hydrogen photo production can be influenced

directly by altering the biomass synthesis rate. The results demonstrate that this assumption is only partly true and that a decrease in volumetric biomass synthesis rate does not result in an energetically proportional increase in the volumetric hydrogen production rate. The efficiency of biomass synthesis and maintenance on light energy is unlikely to have changed under these conditions. The absorbed light energy that was neither used for additional biomass nor for additional hydrogen production must have resulted in additional heat dissipation, as the elemental composition of the biomass essentially remained unaltered and no organic acids were observed in the culture medium during the later stage of the exeriment (data not shown).

The specific hydrogen production rate q_{H_2} and the maximal hydrogen production rate $q_{H_2,max}$ are displayed in Figure 5.6. Interestingly, both parameters reach a maximum of 0.50 mmol·kg^{-1}·s^{-1} simultaneously, around day 25 of the G-stat experiment. This value is comparable to literature values for nitrogen-limited *R. palustris* cultures grown on acetate (Fissler et al. 1994; Vincenzini et al. 1982).

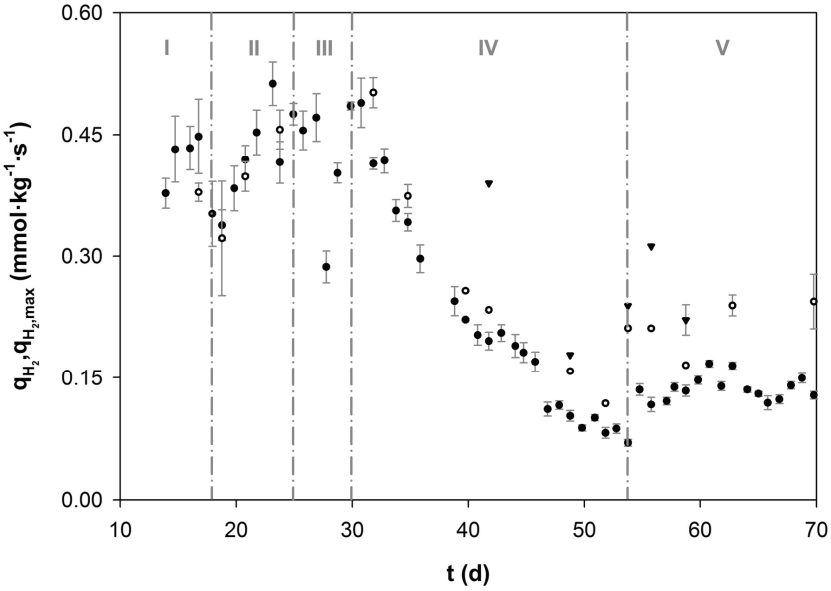

Figure 5.6 Specific hydrogen production rate (q_{H_2}, ●) during the G-stat experiment. Maximal specific hydrogen production rate in the PBR during the G-stat experiment. The medium used contained either no ($q_{H_2,max}$, ○) or 1 mM ($q_{H_2,max}$, ▼) ammonium. The error bars represent standard errors of the mean.

Hydrogen production rate at higher biomass concentrations during the G-stat

As the biomass concentration was increased further, q_{H_2} and $q_{H_2,max}$ declined simultaneously, starting on day 31 at a biomass concentration of 1.5 g·L^{-1}. Several explanations have been given in literature for the variability of the volumetric hydrogen production rate in continuous cultures of PNS bacteria. They will be discussed below in the light of current observations.

The applied growth rate

The volumetric hydrogen production rate of *R. capsulatus* continuous cultures has been reported to increase as the culture is subjected to a lower growth rate, reaching 0.90 mmol·m^{-3}·s^{-1} at 0.96 d^{-1} (Tsygankov et al. 1998a). A volumetric hydrogen production rate of 1.93 mmol·m^{-3}·s^{-1} at a dilution rate of 0.24 d^{-1} was reported previously for a *R. rubrum* chemostat culture (Zürrer and Bachofen 1982). The applied growth rate of 0.4 d^{-1} lies in between these values and since it was kept constant, it is not expected to be related to the observed decline in $r_{H_2}^{u}$.

Product inhibition

The actual rate of hydrogen photoproduction by *Rba. capsulatus* in a PBR might be lower than the potential rate due to product inhibition by hydrogen (Tsygankov et al. 1998a). Since the PBR was continuously flushed with 0.85 L·L^{-1}·min^{-1} argon, it seems unlikely that inhibition by hydrogen played a significant role.

In addition, the value of $q_{H_2,max}$ of washed culture samples (data not shown) yielded results comparable to those for unwashed culture samples and to the q_{H_2} values measured directly in the PBR (Figure 5.6). This observation excludes the possibility of the presence of an extracellular compound exerting a negative influence on the specific hydrogen producing rate of the culture.

Nitrogen limitation

As the extent of nitrogenase derepression was suggested to be correlated with the degree of nitrogen deficiency (Arp and Zumft 1983), the culture's nitrogen deficiency was examined.

According to Monod's chemostat theory, the residual concentration of the growth limiting substrate S depends on the micro-organism's maximal growth rate, the saturation constant for the growth-limiting substrate (K_S, kg·m^{-3}) and the set dilution rate according to Equation 5.1.

Equation 5.1 $S = \frac{D \cdot K_S}{\mu_{max} - D}$

The micro-organism's maximally achievable growth rate in phototrophic culture depends on the available average light intensity, which declines concomitantly with an increase in C_x as a result of increased light limitation (Tsygankov and Laurinavichene 1996b). During the G-stat experiment, the biomass concentration increased, resulting in a decrease in $\mu_{max}(I)$ (resulting from a decreased light availability) and, according to Equation 5.1, a decrease in the extent of nitrogen limitation. The observed increase in supernatant ammonium concentration from 1.3 to 5.8 µM and the increase in dry biomass nitrogen content from 4.1 to 4.9% (data not shown) as the G-stat experiment progressed might be related to this decrease in degree of ammonium limitation. The observed increase in supernatant ammonium concentration is not likely to have had a significant inhibiting effect on the specific hydrogen production rate of the culture, as nitrogenase inhibition in ammonium-limited *Rba. capsulatus* cultures starts at much higher ammonium concentrations of about 100 µM (Willison et al. 1983).

The accumulation of Nif$^-$-mutants

The accumulation of a spontaneous Nif$^-$-mutant in a daily serial transfer of *Rps. capsulata* in time was reported previously, reaching nearly 100% after 8 days (Wall et al. 1984). This Nif$^-$-phenotype was unable to grow with N_2 as the nitrogen source and had no measurable nitrogenase activity.

It is unclear to what extent such Nif$^-$-mutants might have accumulated in the culture during the G-stat experiment. However, both the initially observed increase in volumetric and specific hydrogen production rate (until the end of Period III) and the maximal hydrogen production rate throughout the experiment indicate that the presence of a Nif$^-$-phenotype may not have been significant.

The relationship between light availability and specific nitrogenase activity

As the *G*-stat experiment progressed, the biomass concentration in the PBR increased, resulting in a decrease in the average available light energy (Figure 5.4). Possibly, this decrease in average light intensity caused a decreased synthesis of nitrogenase (Tsygankov and Laurinavichene 1996a), which may have resulted in the decrease in both q_{H_2} and $q_{H_2,max}$ at biomass concentrations higher than 1.5 $g \cdot L^{-1}$. At this biomass concentration, the residual light intensity was still about 50 $W \cdot m^{-2}$, while the specific nitrogenase activity of *Rba. capsulatus* cultures was reported to be already saturated at 22 $W \cdot m^{-2}$ (Tsygankov and Laurinavichene 1996a).

Not only the average light availability but also light quality and -distribution may have contributed to the observed decline in q_{H_2}, as was indicated previously (Tsygankov et al. 1998a). Most probably, the spectral composition of the available light after passing through part of the PBR was not such that it could be used optimally by the bacterial photosystem. Indeed a sharp decline in the fraction of the residual light spectrum leaving the PBR near the absorption maximum of BChl *a* along the optical path could be demonstrated, using the light absorptive properties of the culture and the spectral composition of the light entering the PBR. (data not shown).

The samples taken from the PBR were exposed to a higher and more uniform light intensity during the $q_{H_2,max}$ determinations. The increased light availability possibly resulted in *de novo* synthesis of nitrogenase, resulting in an increased discrepancy between q_{H_2} and $q_{H_2,max}$ (Figure 5.6), as was demonstrated previously (Jouanneau et al. 1985).

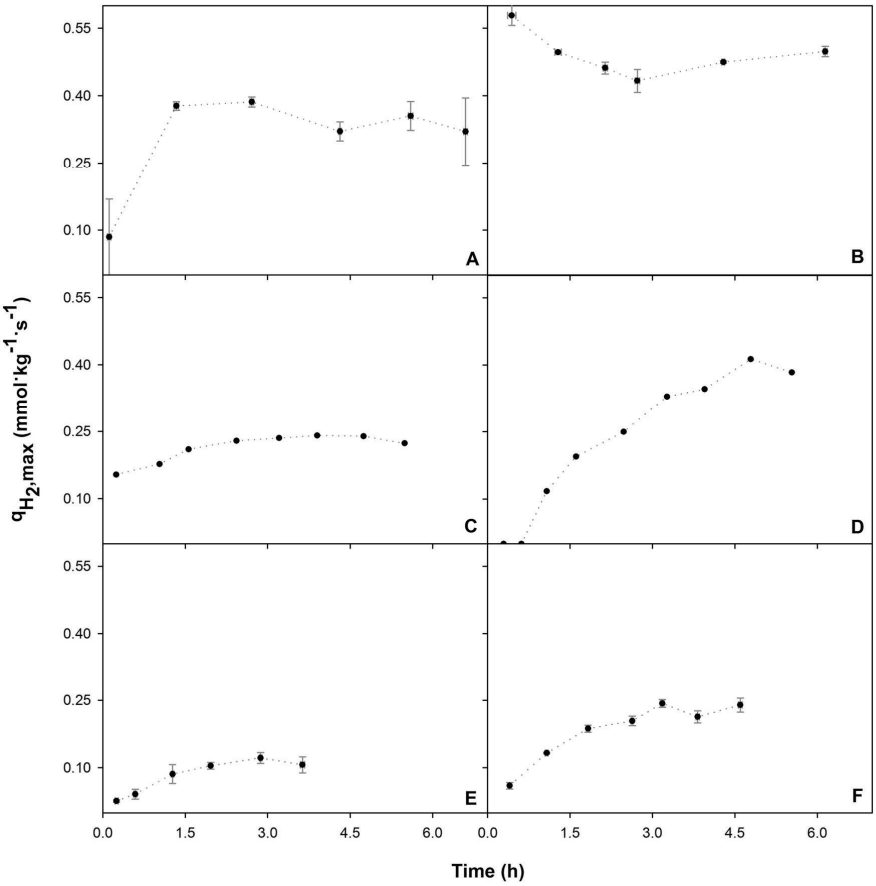

Figure 5.7 Maximal specific hydrogen production rate of the PBR culture after 19 (A), 32 (B), 42 (C without, D with 1 mM NH_4^+ supplied to the medium), 52 (E) and 63 (F) days in the G-stat experiment. The error bars represent standard errors of the mean.

As can be seen in Figure 5.7, an increase in $q_{H_2,max}$ was observed on days 42, 52 and 63. As the G-stat experiment progressed, the final value of $q_{H_2,max}$ was lower and was reached more slowly. Both observations are probably directly related to the decreased value of q_{H_2} (Figure 5.6), which most probably resulted from the decreasing average light availability within the culture as the biomass concentration in the PBR was increased.

The initial lag phase, followed by an increase and a final value of $q_{H_2,max}$ that is much higher than the corresponding value of q_{H_2} in the PBR are most pronounced when ammonium was added to the medium (Figure 5.7C and D). This nitrogen stimulated nitrogenase activity was demonstrated previously (Steinborn and Oelze 1989), who demonstrated that under conditions of energy limitation, nitrogenase activity is indirectly influenced via glutamate consumption.

A limited supply of ammonium was probably required for *de novo* synthesis of additional nitrogenase under high light conditions that facilitated the observed significant increase in specific nitrogenase activity. Based on these results, light availability must have contributed significantly to the observed drop in specific hydrogen production rate.

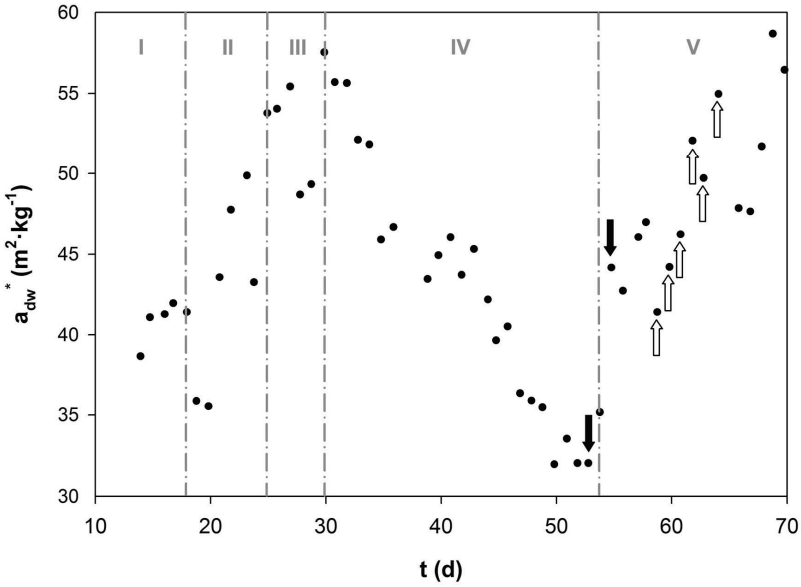

Figure 5.8 Specific absorption surface (a^*_{dw}, ●) during the G-stat experiment. Ammonium spikes and nitrogen flushes are indicated by black and white arrows respectively.

Specific absorption surface of the bacterial culture

The results indicate that light availability within the PBR is a key factor in nitrogenase expression in PNS bacteria and for this reason, the physiological properties of the culture that are related to light absorption were looked into. The specific absorption surface (a^*_{dw}, $m^2 \cdot kg^{-1}$) of the bacterial culture, together with the biomass concentration, determines the average light availability inside a PBR. The specific absorption surface during the G-stat experiment is presented in Figure 5.8. Phototrophic cultures in general respond to a decrease in light availability (and hence a decrease in specific growth rate) by increasing their photosynthetic apparatus (Göbel 1978; Tsygankov and Laurinavichene

1996b), resulting in an increase in specific absorption surface, as is evident throughout Periods I to III in Figure 5.8.

The observed decline in specific absorption surface of the culture as its biomass concentration exceeded 1.5 $g \cdot L^{-1}$ was unanticipated, since the growth rate remained constant and the average light intensity inside the PBR decreased in time. The down regulation of the expression of genes related to nitrogen fixation (nitrogenase) was possibly accompanied by the down regulation of genes related to the expression of the photosynthetic apparatus as reported previously for *Rba. capsulatus* cultures (Masepohl et al. 2002). The prolonged exposure to ammonium limitation could also have caused the unanticipated decline in specific absorption surface of the culture. In the later phase of the G-stat experiment, this possibility was investigated by supplying the culture with additional nitrogen.

Two ammonium spikes were given (1 mM on day 53 and 4 mM on day 59) after which the culture was intermittantly sparged with 0.85 $L \cdot L^{-1} \cdot min^{-1}$ of di-nitrogen instead of argon (6 times per day for 10 minutes from days 60 to 65). The supply of additional nitrogen in Period V did not result in a significant increase in either the calculated specific growth rate (Figure 5.3) or the biomass concentration of the culture (Figure 5.4). It did however result in a small increase in its volumetric hydrogen production rate ($r^{u}_{H_2}$, Figure 5.5), its specific hydrogen production rate and its maximal specific hydrogen production rate (Figure 5.6). Moreover, the culture's specific absorption surface increased significantly (Figure 5.8).

Possibly the co-expression of the photosystem and the nitrogenase enzyme is stimulated separately by both the light availability and the availability of di-nitrogen. Contrary to our observations in this latter phase of the experiment, nitrogen-limited *Rps. palustris* batch cultures were reported to exhibit a four to eight-fold higher specific nitrogenase activity relative to cells sparged with di-nitrogen due to overproduction of nitrogenase (Arp and Zumft 1983). The observed effects of the repeated di-nitrogen flushes are very distinct and unexpected.

Conclusions

In this work, the hydrogen producing potential of nitrogen-limited *Rba. capsulatus* NCIMB 11773 chemostat cultures was explored. Its dependency on both the imposed biomass concentration and the dilution rate was investigated in a flat-panel PBR with an optical path of 3 cm developed previously. Two experimental methods referred to as *Deceleration*-stat and *Gradient*-stat were applied successfully, generating the required data in a reduced time span.

The *Deceleration*-stat experiment was aimed at a constant biomass concentration of 4.0 $g \cdot L^{-1}$ while decelerating the dilution rate starting at 1.0 d^{-1}. The volumetric hydrogen production rate of the culture did not exceed 0.6 $mmol \cdot m^{-3} \cdot s^{-1}$ which is low when compared to 1.3 $mmol \cdot m^{-3} \cdot s^{-1}$ according to model predictions. These low values were probably related to the relatively high biomass concentration resulting in light limitation inside the PBR. The decrease in dilution rate also resulted in a shift in bacterial carbon metabolism.

The *Gradient*-stat experiment demonstrated that the model predictions for $r_{H_2}^{u}$ are rather accurate provided that the biomass concentration does not exceed 1.5 $g \cdot L^{-1}$. While the growth of the culture was nitrogen-limited during the complete experiment, its specific hydrogen production rate most probably was light-limited as the biomass concentration exceeded 1.5 $g \cdot L^{-1}$. Similar observations were made for ammonium-limited *Rps. capsulata* continuous cultures (Jouanneau et al. 1984) and these conditions were referred to as 'double limitation' (Tsygankov et al. 1996).

The unexpected shift in metabolism that was observed during the *Deceleration*-stat experiment at very low dilution rates requires more detailed investigation. Also, the interplay between light and nitrogen availability on the one hand and the expression of the photosystem and the nitrogenase enzyme on the other is not fully understood and should be studied in more detail in order to achieve conditions that facilitate the culture to exhibit a high and stable specific hydrogen production rate.

To study this phenomenon further, the influence of (partial) light limitation on the volumetric hydrogen production rate should be studied in more detail. Possibly a high value of $q_{H_2,max}$ can be maintained up to higher biomass concentrations in reactors with even shorter optical paths. The positive effect of light path reduction on the efficiency of light use was demonstrated for cynobacterial mass cultures (Qiang et al. 1998b). As clearly demonstrated (Qiang and Richmond 1996), a further reduction in optical path should be accompanied with the selection of the optimal biomass density and mixing rate. If the required biomass concentration for an optimal photosynthetic efficiency at a given illumination is 2.3 $g \cdot L^{-1}$, as is the case for the applied system with a 3 cm optical path, a dilution rate of 0.4 d^{-1} and a light intensity of 410 $W \cdot m^{-2}$, a similar areal hydrogen production capacity is reached at 6.9 $g \cdot L^{-1}$ in case the optical path of the PBR is reduced to 1 cm.

This drastically increases the importance of optimal light distribution and -integration. Also, the physiological properties of the applied micro-organisms specific hydrogen production rate is important for future work, because they can significantly reduce the biomass concentration that is required for a certain efficiency of light- to hydrogen energy conversion. Both the fraction of light energy that is converted into biomass energy and the extent to which heat dissipation takes place might be drastically reduced as the specific hydrogen production rate of the culture is higher. For example, a Hup^- mutant of *Rba. sphaeroides* RV displayed a two-fold higher specific hydrogen production rate when compared to the wild type (Franchi et al. 2004). However, at the elevated biomass concentrations still required for good conversion of light energy into hydrogen energy, a certain degree of light limitation cannot be avoided. As such, investigating the influence of light limitation on the volumetric hydrogen production rate is of prime importance to realize breakthroughs in this type of process in the future.

Nomenclature

a^*_{dw}	Specific absorption surface	[$m^2 \cdot kg^{-1}$]
C/N -ratio	Carbon to Nitrogen ratio	[-]
C_x	Biomass concentration	[$kg \cdot m^{-3}$]
d	Deceleration rate	[d^{-2}]
D	Dilution rate	[d^{-1}]
D-stat	*Deceleration*-stat	[-]
g	Gradient rate	[$M \cdot d^{-1}$]
G-stat	*Gradient*-stat	[-]
I	Light intensity	[$W \cdot m^{-2}$, 400 – 950 nm]
K_s	Saturation constant	[$kg \cdot m^{-3}$]
PBR	Photobioreactor	[-]
q_{H_2}	Specific hydrogen production rate	[$mol \cdot kg^{-1} \cdot s^{-1}$]
$q_{H_2,max}$	Maximal specific hydrogen production rate	[$mol \cdot kg^{-1} \cdot s^{-1}$]
$r^u_{H_2}$	Volumetric hydrogen production rate	[$mol \cdot m^{-3} \cdot s^{-1}$]
S	Growth limiting substrate concentration	[$mg \cdot L^{-1}$]
μ	Specific growth rate	[d^{-1}]
μ_{max}	Maximal specific growth rate	[d^{-1}]
$\mu_{max}(I)$	Maximal specific growth rate at light intensity I	[d^{-1}]

Chapter 6

The future of photobiological hydrogen energy

6. The future of photobiological hydrogen energy

Abstract

In this work, an overview is given on the current status of development of photobiological hydrogen production processes using purple non sulfur bacteria and photoautotrophic microorganisms.

The applied cultivation system, the applied microorganism and the mode of operation of the system all play a role in the final efficiency at which light energy is converted into hydrogen energy. For this reason, all three topics are covered, including their interdependencies.

Introduction

It is generally accepted that the final answer to the ever increasing global energy consumption, once fossil energy resources are depleted, lies within solar energy supply (Lewis and Nocera 2006). During the past decades, the application of photosynthesis for the generation of renewable energy from sunlight has received much attention. Several applications are very promising, like the generation of biodiesel that uses microalgal biomass as a source material (Chisti 2007). Another promising process that results in renewable energy derived from photosynthesis generates molecular hydrogen, which can be applied as an intermediate energy carrier. Hydrogen can be produced by phototrophic micro-organisms like purple non sulphur bacteria (or PNS bacteria in short). The required electrons are generated by the dissimilation of organic acids. Also micro-algae are capable of producing molecular hydrogen, when they are subjected to specific conditions, like environmental conditions and/or their growth phase.

Despite the potential of photosynthetic processes as a source for renewable energy and the attention they have received in a time frame of over 4 decades, the commercial viability of large scale application remains to be demonstrated. This is mainly caused by the lack of a competitive efficiency of light energy conversion at larger scales, combined with the high degree of variation in real-life solar light intensities as they are present at ground level on earth (i.e. diurnal variation with variations in the 1000 $W \cdot m^{-2}$ range), as was concluded previously (Adessi et al. 2012; Eroglu and Melis 2011; Tredici 2009). This limited conversion efficiency at larger scales and highly varying light intensity results from the combination of three factors, which are:

(1) the maximal efficiency of photosynthesis
(2) the evolutionary physiological properties of phototrophic organisms and
(3) the design properties of photo-bioreactors (PBRs).

In this chapter, a substantiation of this conclusion is given. Several topics that require further investigation are highlighted, as their study could increase the chance that a process for renewable energy generation based on photosynthesis will become commercially viable in the future.

Theoretical efficiency of photosynthesis

Theoretical efficiency of oxygenic photosynthesis

Photosynthesis is a very efficient process, during which light is harvested and converted to metabolic energy. Microalgae can use radiation between 400 and 700 nm for oxygenic photosynthesis, and for this reason this part of the solar spectrum is referred to as photosynthetic active radiation or PAR in short. Forty-three per cent of all solar irradiation energy reaches the surface of the earth in the PAR region (Thimijan and Heins 1983). The maximal theoretical efficiency of algal photosynthesis (the conversion of light energy into biochemical energy) equals 35% at 600 nm. This efficiency decreases to 27.7% when the entire solar PAR range is included. It decreases even further to 12.4% when the efficiency of photosynthesis over the complete solar spectrum is considered (Tredici 2009).

Theoretical efficiency of anoxygenic photosynthesis

Purple non-sulfur bactera (PNS bacteria in short) have a larger spectral range (400-950 nm) that can be used for anoxygenic photosynthesis. The maximum solar light to hydrogen energy conversion efficiency within this range equals 10.6% in this case, as was calculated previously (see Chapter 4 for the details on this calculation).

Practical efficiency of photosynthesis

Caloric measurements on algal growth, on small scale and at low light intensity, demonstrated a 27% energy conversion efficiency at ~700 nm (Radmer and Kok 1977). These experiments demonstrated that the theoretical maximum photosynthetic efficiency described previously can be approached experimentally.

On a larger scale, at a higher light intensity and using increased biomass densities, the conversion of solar light to biomass in mass cultures of unicellular phototrophic organisms has additional limitations. Several factors, including light reflection at the surface of the PBR, maintenance requirements of the microorganism and a non-uniform distribution of light resulting in both light oversaturation and self-shading (these topics will be adressed in more detail later on in this chapter) can cause additional limitations. Even so, Qiang and Richmond demonstrated that a photosynthetic efficiency of 17.5% on PAR basis could be achieved in dense *Spirulina platensis* cultures when an irradiation of 1800 µmoles PAR was applied (Qiang and Richmond 1996).

These restrictions on the maximal efficiency of oxygenic photosynthesis also hold for anoxygenic photosynthesis by purple non sulfur bacteria.

Light to hydrogen conversion efficiency

The efficiency of the process of molecular hydrogen generation is mostly reported in literature as the light energy to hydrogen energy conversion efficiency. Other substrates (for instance an electron donor) and/or products (for instance biomass) are not considered in this case. Because biomass has to be generated first, after which the photobiological conversion of organic acids to hydrogen can take place, this represents an additional restriction in the conversion efficiency that can be achieved.

Considering the 400-950 nm spectral irradiance of halogen-tungsten lamp (see Figure 1.5B), the maximal light to hydrogen conversion ratio of PNS bacteria equals 25.3% (see the Theory section in Chapter 4). The difference between the maximal and practical light to hydrogen conversion ratio is significant and requires further explanation.

Light to hydrogen conversion efficiencies by photohetertrophs

PNS bacteria contain the enzyme nitrogenase. While this enzymes primary function is to fix molecular nitrogen, it can also catalyse the combination of 2 protons and 2 electrons to form molecular hydrogen in order to control the intra-cellular redox poise (Tabita 1995). The energy requirement of nitrogenase and its dependency on the availability of light (Jouanneau et al. 1985; Tsygankov et al. 1996) causes further restrictions to the light to hydrogen conversion efficiency that can be reached using PNS bacteria.

The highest light to hydrogen conversion ratios reported in literature are presented in Table 6.1 for batch and in Table 6.2 for chemostat experiments. The highest light to hydrogen conversion ratio ever to have been reported to our knowledge is 35% (Yamada et al. 1998). In this specific case, a Xenon light source was applied at non-saturating conditions. Xenon lamps have distinct emission peaks located close to the adsorption maxima of the bacterial photosystem, resulting in a larger fraction of the emitted light that can be used for photosynthesis. Experiments executed with the more commonly applied tungsten lamp gave significantly lower conversion ratios, of which the highest is 10.4% (Kim et al. 2006).

Light to hydrogen conversion efficiencies by photoautotrophs

Several photo-autotrophic organisms are also capable of generating molecular hydrogen. Their highest light to hydrogen conversion ratios reported in literature are presented in Table 6.3. With a PAR based light to hydrogen conversion ratios of 10.4%, Greenbaum demonstrated the large potential of photoautotrophs for converting light to hydrogen (Greenbaum 1988). In general, however, their performance is lower than that of photoheterotrophs, as will be explained later.

Light oversaturation

Table 6.1 to Table 6.3 show that the light to hydrogen conversion efficiency decreases when the applied light intensity increases. For instance, from the data reported by Yamada et al., a drop in light to hydrogen conversion efficiency of 35 to 1.6% can be calculated as the light intensity increases from 13 to 1800 $W \cdot m^{-2}$ (Yamada et al. 1998). Other researchers have reported data that illustrate the same relationship (Hoekema et al. 2009; Jouanneau et al. 1984; Tsygankov et al. 1998a).

Assuming that the larger part of the supplied light was absorbed by the cultures, these observations might be caused by light oversaturation of the reaction centers of the photosystem in question, resulting in a decreased efficiency at which absorbed light is used for photosynthesis. This process, referred to as non-photochemical quenching, acts as a safety valve, protecting the photosystem from photo-oxidative damage in case the light energy absorption capacity exceeds the capacity for light utilization. Most probably, a quencher molecule is formed in the light harvesting complex that dissipates excess absorbed light energy (Cleland et al. 1992; Müller et al. 2001). Non-photochemical quenching results in a fraction of absorbed light that is not used in photosynthesis and it negatively influences the light to hydrogen conversion efficiency.

In our experiments 80 to 90% of all light energy absorbed under high light intensity (410 $W \cdot m^{-2}$), did not result in primary charge separation, but was dissipated as heat instead (Hoekema et al. 2006). Similar values for the dissipation of absorbed by phototrophic microorganisms that are exposed to high light intensities were recorded before (Goldman 1979; Hallenbeck and Benemann 2002).

Self-shading

As light is absorbed by a culture of phototrophic organisms, its intensity is attenuated along the light path of a PBR. The physiological response of a photosynthetic organism to low light intensity is to increase its light harvesting capacity by synthesizing additional light harvesting complex, resulting in additional light attenuation, dark zones and a decreased photosynthetic efficiency.

Table 6.1 to Table 6.3 show that in general, the specific hydrogen production rate decreases as the biomass concentration and/or the optical path of a PBR increases, even at moderate light intensities. This is most probably caused by self-shading, as the part of the culture that is completely deprived of light does not contribute to the specific hydrogen production capacity of the system.

For example, chemostat cultures of *R. capsulatus* with a density of 400 $mg \cdot L^{-1}$ reached a plateau level of nitrogenase activity when exposed to an incident light intensity of 60 $W \cdot m^{2}$ in a PBR with an optical light path of 13 mm (Tsygankov et al. 1996). Jouanneau found comparable results under comparable conditions, also with chemostat cultures of *R. capsulatus* (Jouanneau et al. 1985). These observations illustrate that not only should an optimally constructed PBR for PNS bacterial hydrogen production be void of dark zones, a significant level of light needs to be supplied to each individual cell continuously to safeguard maximal specific nitrogenase activity.

As the biomass concentration of a *R. capsulatus* chemostat culture in a PBR with an optical light path of 3 cm and an incident light intensity of 410 $W \cdot m^{-2}$ was gradually increased, we also found that the specific nitrogenase activity started to decline as a biomass concentration of 1.5 $g \cdot L^{-1}$ was reached (Hoekema et al. 2009).

How to improve the light to hydrogen energy conversion process

Silicon solar cells have already been produced that reach light energy conversion efficiencies of up to 24.4% at elevated light intensities (Zhao et al. 1998). However, the production of solar cells is energy intensive and their lifespan limited. Also, electricity is energy in a form that cannot be stored. The conversion to a storable form will have a negative impact on the overall light conversion efficiency. The comparison does however illustrate that a competitive process based on photosynthesis should have a significant energy conversion efficiency (Blankenship et al. 2011).

The light to hydrogen energy conversion efficiency of a biotechnological process based on unicellular phototrophic organisms results from the interplay between (A) the design of the applied PBR, (B) the physiological properties of the applied unicellular micro-organism and (C) their coupling, resulting in a mode of operation of the process. For this reason, these three essential process constituents and their interdependencies will be discussed here.

(A) PBR design

A properly constructed PBR should facilitate optimal process economy. For this reason, it should create an environment in which the selected organism can generate the desired product the fastest (resulting in a smaller required volume) or the most efficient (resulting in the most efficient use of substrates), depending on the process economics.

In the case of phototrophic processes, the predominant optimization factor is surface area, as it is expensive (Brentner et al. 2011) and its minimization reduces the food versus fuel debate (Lam and Lee 2012; Wijffels and Barbosa 2010). In view of process intensification, many PBRs that have been designed and investigated have a very high surface to volume ratio, as can be seen in Table 6.1 to Table 6.3.

To facilitate a high light to hydrogen conversion efficiency by PNS bacteria, a proper PBR design should adhere to the following three design criteria:

1. It should absorb most of the light impinging on it;
2. It should provide sufficient light to all cells so that they can execute photosynthesis at near maximal photosynthetic efficiency and retain active nitrogenase;
3. It should have limited construction costs and power consumption requirements during process operation (which implies the need for simplicity and process intensification).

As is evident from literature, it is the combination of these pre-requisites that results in a significant engineering challenge. Much progress has been made in understanding the physiological mechanisms of PNS bacteria, microalgae and cyanobacteria that underlie these design criteria. Below the most important aspects will be discussed.

Light energy supply to the individual cell

The use of strong light infers that cells near the illuminated surface of a PBR can suffer cellular damage due to over-exposure to light, resulting in an increase in maintenance requirements up to total inhibition of the photosynthetic system (Adir et al. 2003). Additionally, dark zones develop in a PBR beyond a certain cell concentration and PNS bacteria are not able to execute part of the photosynthetic process. Parts of the culture that are not exposed to light therefore negatively influence the overall light to hydrogen conversion efficiency, as it is not expected that maintenance energy requirements decrease significantly in the absence of light. Dark zones in a culture of PNS bacteria will therefore negatively influence the overall performance of the system, especially at elevated cell concentrations. The PBR optical light path and the applied biomass concentration must be balanced in order to prevent the creation of dark zones but still absorb almost all the light impinging on the PBR surface.

The energy requirements for turbulent mixing

At a certain cell density, a dark zone will develop in a microalgal culture. As a result, the individual cells are exposed to light flashes as part of a light/dark cycle. In case the light/dark cycle is short enough, the productivity of each individual cell can remain close to its maximum, a phenomenon referred to as light integration (Janssen et al. 2000; Kok and Burlew 1953; Qiang et al. 1998b; Vejrazka et al. 2011). Vejrazka et al. postulated that an intracellular pool of reducing equivalents enables light integration, as the dark reaction of photosynthesis can continue during the dark period (Vejrazka et al. 2011) .

Turbulent mixing is needed in order to keep the light/dark cycles short, which translates to a significant required power input. Even though the areal biomass production efficiency and concomitant light conversion efficiency reported by Qiang et al. (Qiang et al. 1998b) is amongst the highest ever reported, the power input required for mixing alone was at least 20% of the generated biomass energy output in this case, assuming a 200 mbar air compression requirement. This example illustrates that even though the light conversion efficiency is an important property of a system based on a phototrophic microorganism, the total energetic efficiency of a process will finally determine its commercial viability.

Dilution of strong light

Strong light can be diluted to levels that prevent oversaturation of the photosynthetic machinery. This does however result in the need for additional surface area. This dilution of light can be achieved for instance by positioning the PBR vertically. Cuaresma et al. demonstrated a 30% increase in photosynthetic efficiency of *Chlorella sorokiniana* cultures upon vertical instead of horizontal PBR placement, resulting from a 78% decrease in light intensity (Cuaresma et al. 2011). Similar results were obtained by Qiang et al., who demonstrated an increase in biomass output by adjusting the tilt angle of the PBR relative to the surface of the earth, depending on the season. In summer, the highest photosynthetic efficiency of *Spirulina platensis* cultures was recorded in PBRs that had a 90° tilt angle (Qiang et al. 1998a).

Alternatively, a light concentration and re-distribution system can be used in order to dilute light. A parabolic mirror was proposed by Janssen et al. for concentrating light, after which an optical fiber light distribution system can be used to distribute the light homogeneously throughout the PBR (Janssen et al. 2003).

The two concepts of adjusting tilt angles and concentrating and re-distributing light can also be combined, as was shown by Zijffers, who designed and built a PBR concept in which a moving Fresnel lens system performs solar tracking and the captured light is re-distributed by a light guide towards an algal suspension (Zijffers 2009). These light dilution strategies may also be applied on PNS bacterial cultures succesfully and should be considered in concert with the need for continuous illumination of each individual cell as described previously.

(B) Physiological properties of the applied unicellular micro-organism

The reduction of protons to molecular hydrogen by PNS bacteria is catalyzed by two classes of enzymes called nitrogenases and hydrogenases. As not all phototrophic hydrogen producing microorganisms contain both classes of enzymes, the choice for the catalyst results in a reduced freedom of choice of the microorganism and vice versa. Microalgae for instance do not contain nitrogenases, while PNS bacteria contain both classes of enzymes.

Nitrogenases

The primary function of nitrogenases in cellular metabolism is to fix molecular nitrogen by reducing it to ammonia. However, this enzyme can also catalyse the reduction of protons to molecular hydrogen. The physiological significance of this side reaction is that the cell is capable of controlling its internal redox state (Tichi and Tabita 2001) and represents an emergency release valve for excess reduction equivalents.

The main advantage of nitrogenase-based photosynthetic hydrogen production systems is the fact that its catalytic activity is irreversible, thus an elevated partial hydrogen pressure

does not affect the hydrogen generating capacity of the culture and hydrogen evolves spontaneously an does not need to be stripped from the system.

There are also drawbacks to the application of nitrogenase-based systems. The energy requirement of nitrogenase activity is very high. The fixation of one molecule of nitrogen takes place at the expense of 16 ATP, while the generation of one molecule of hydrogen costs 4 ATP.

For this reason, nitrogenase activity is tightly regulated. Short-term post-translational nitrogenase-activity downward regulation mechanisms are triggered by the presence of oxygen, nitrogen, ammonium, glutamine, asparagine and urea (Munson and Burris 1969; Zumft and Castillo 1978). Nitrogenase activity is difficult to control, particularly because anaerobic conditions are required and less expensive nitrogen sources like ammonia and urea are more difficult to apply, as in these cases nitrogen limited growth is required due to the inhibitory effect of these nitrogen sources. The activity of the nitrogenase of *Rb. Capsulatus* depended strongly on illumination conditions as well. Under conditions of light limitation, any change in the intensity of illumination is paralleled by a proportional change in nitrogenase activity (Steinborn and Oelze 1989).

During our work on the maximization of the fraction of the absorbed light energy that is directed towards hydrogen (Hoekema et al. 2009), a decrease in specific hydrogen production rate of a *Rb. capsulatus* chemostat culture was observed as the biomass concentration in the bioreactor increased (see Figure 5.6). This observation might well be explained by the progressing level of light limitation the culture experienced.

The exposure of culture samples to saturating light intensities only resulted in a noticeable increase in specific nitrogenase activity in case a low concentration of nitrogen was supplied in the applied medium. This observation could indicate that the increase of nitrogenase activity can only take place after de-novo synthesis of nitrogenase, as indicated previously (Jouanneau et al. 1985).

Maximal specific rate of hydrogen production

The suitability of a phototrophic microorganism for application in a photobiological hydrogen generating system largely depends on its maximal specific hydrogen production rate ($q_{H_2,max}$, mmol·kg^{-1}·s^{-1}). By using a microorganism that has an increased specific hydrogen production rate, there is less need for high biomass at elevated light intensities. This lower biomass requirement in turn decreases the negative effect of self-shading and cellular maintenance on the light to hydrogen conversion ratio. Table 6.1 to Table 6.3 show that the maximal specific hydrogen production rate of the various microorganisms varies a lot. Most evaluated PNS bacteria show a maximal specific hydrogen production rate ranging from 0.2 to 0.7 mmol·kg^{-1}·s^{-1}. From the data reported by Jouanneau et al., a maximal specific hydrogen production rate of 6.9 mmol·kg^{-1}·s^{-1} could be calculated for a chemostat culture of a nitrogen limited wild type species of *Rps. capsulata* (Jouanneau et al. 1984).

A comparable nitrogen limited *Rhodobacter capsulatus* chemostat culture displayed a maximal specific hydrogen production rate of 0.52 ± 0.02 mmol·kg^{-1}·s^{-1} (Hoekema et al. 2006), while also intermediate rates were reported, for instance 1.4 mmol·kg^{-1}·s^{-1} for a nitrogen limited *Rhodobacter capsulatus* wild type culture (Tsygankov et al. 1998a).

How to improve the maximal specific hydrogen production rate?

Several physiological properties of a photosynthetic microorganism determine its maximal specific hydrogen production rate and with it its suitability for application in a phototrophic hydrogen production process. Some of these properties are discussed here, and the reported efforts to change these them in favor of an increase of the specific hydrogen production rate.

The light harvesting complex

The degree of light attenuation increases with the density of a photosynthetic micro-organism in a PBR. This can seriously limit the overall photosynthetic efficiency, as part of

the culture will not be able to execute photosynthesis or maintain a high specific nitrogenase activity. This negative influence on the overall performance can be reduced by genetically modifying the properties of the light harvesting complex.

Melis reported on random tag mutagenesis and subsequent screening resulting in a *Chlamydomonas reinhardtii* strain having a light harvesting Chl antenna with a size that is reduced by 60%. As a result, the half saturation light intensity of the pertinent strain is 117% as compared to the wild type. When these results are extrapolated to PBR scale, the improved half saturation light intensity translates to a 45% increase in productivity and therefore in photosynthetic efficiency (Melis 2009). Formighieri et al. recently presented modelling predictions that indicate a similar improvement in PE when a *Chlamydomomas reinhardtii* strain that has an 80% reduced chlorophyll concentration is cultivated in a PBR that has a 50 mm optical path and is exposed to strong light (Formighieri et al. 2012).

Kondo et al. reported on a *Rhodobacter sphaeroides* strain that shows a 40-50% decrease in the concentration of the complete light harvesting complex after UV exposure mutagenesis. The mutant displayed a 50% increase in specific hydrogen production capacity when compared to the wild type, which can be ascribed to the increase in average light availability within the mutant strain cultures (Kondo et al. 2002).

Hydrogenases

A second class of hydrogen-generating enzymes, named hydrogenases, is present in both PNS bacteria and green algae. Hydrogenases also function to maintain intracellular redox poise, but do not require metabolic energy for their catalytic activity. Their catalytic rates are also much higher than those of nitrogenases (McKinlay and Harwood 2010). The main drawback of systems based on hydrogenases is the reversibility of their catalytic activity (Kosourov et al. 2012; Vignais and Billoud 2007), limiting the hydrogen partial pressure in the system that can be applied.

Several hydrogenases are so-called uptake hydrogenases. Their catalytic activity contributes to the recycling of electrons to nitrogenase (Willison et al. 1983) and with it

reduces the net hydrogen producing capacity of the micro-organism and hence the light to hydrogen conversion efficiency of the system.

The efficiency of light to hydrogen conversion can be improved in case the uptake hydrogenase (Hup) genes are knocked out. Yamada et al. demonstrated a significant increase in the photosynthetic efficiency of *Rhodovulvum sulfidophilum* when its uptake-hydrogenase gene was removed from 26 to 35% (Yamada et al. 1998). The process details are presented in Table 6.1. Kern et al. (Kern et al. 1994) also reported a 40% increase in hydrogen production capacity of their *Rhodospirillum rubrum* strain after its *Hup*-activity was genetically removed.

PHB accumulation

PNS bacteria accumulate PHB (poly (3-hydroxy) butyric acid) when carbon (preferentially acetate) and energy sources are present in excess, while growth is limited by the availability of nitrogen, sulphur or phosphorus. The metabolic routes that lead to either PHB or H_2 compete for reducing equivalents. Hustede et al. demonstrated that various PNS bacteria accumulate PHB up to 70% of their dry weight, while their PHB^- mutants did not accumulate any PHB and displayed a better substrate to hydrogen conversion ratio (Hustede et al. 1993).

Combinations of genetic modifications

Several examples of PNS bacteria that have multiple genetic modifications directed towards improving the hydrogen production capacity or the substrate to hydrogen conversion ratio can be found in literature. For example, Kim et al. constructed a *R. sphaeroides* mutant that displayed a 38% increase in hydrogen production rate and photosynthetic efficiency when compared to the wild type upon knocking out both the uptake hydrogenase and the PHB synthase genes (Kim et al. 2006).

Alternative micro-organisms to PNS bacteria for application in a phototrophic hydrogen production process

The maximal efficiency of the conversion of solar light to hydrogen energy by means of PNS bacteria using a nitrogenase is restricted to 10.5% (Hoekema et al. 2006). Other photosynthetic micro-organisms, like the cyanobacterial genera *Anabaena* and *Nostoc*, can also produce hydrogen by both their nitrogenase and hydrogenases activity. As can be seen in Table 6.3, cyanobacteria have been produced that are deficient in uptake hydrogenases, aiming at an increased specific hydrogen production rate.

As can be seen from Table 6.3, these cyanobacterial strains do not display a high light to hydrogen energy conversion ratio, even at low light intensities. One of the main factors restricting the maximal light to hydrogen conversion efficiency is the high energy requirement of the nitrogenase enzyme and the inhibition of its activity due to the release of molecular oxygen by photosystem II in the photosynthetic process.

Microalgae have the potential for being more efficient hydrogen producers than PNS bacteria, as they only contain hydrogenases (Miura et al. 1982). The algal species that has received the most attention in the field of photosynthetic hydrogen production is *Chlamydomonas reinhardtii*. (see Table 6.3) As a result of oxygenic photosynthesis, algae produce hydrogen as well as the hydrogenase inhibitor oxygen.

A hydrogen production process in which a micro-alga or cyanobacterium is used as efficiently as possible requires two phases. In the first phase, the microorganism executes oxygenic photosynthesis and accumulates intracellular storage compounds. In the second stage, these storage compounds are digested and an excess of electrons is vented by means of hydrogenase activity (Markov et al. 1996; Melis et al. 2007). The application of algae has the advantage that only the catalytic activity of hydrogenase results in the emission of hydrogen, and no additional metabolic energy is required. The light to hydrogen conversion efficiency of a hydrogen-generating process using micro algae can theoretically reach 12.4% based on the complete solar spectrum. A photosynthetic efficiency approaching this value has already been reached. Greenbaum demonstrated a

PE of 10.3% (considering the complete solar spectrum), using a thin layer of *Chlamydomonas moewusii* cells trapped on filter-paper, combined with a very low light intensity of 9.1 $\mu W \cdot cm^{-2}$ (Greenbaum 1988). As the hydrogenase mediated hydrogen generation is reversible, an increased hydrogen concentration in the gas phase results in significant inhibition of hydrogen generation (Kosourov et al. 2012).

Unfortunately, this range of photosynthetic efficiencies has not been demonstrated at light intensities exceeding 70 $\mu mol \cdot m^{-2} \cdot s^{-1}$ (PAR). At increased light intensity, the photosynthetic efficiency generally drops well below 1% (Ghirardi 2006; Giannelli et al. 2009; Kosourov et al. 2012). In Table 6.3, an overview of the highest reported light to hydrogen conversion efficiencies is given during algal phototrophic hydrogen production.

(C) Mode of operation of a PBR

Apart from the properties of the applied PBR and micro-organism, the mode of operation of a PBR is the third factor that plays a key role in the efficiency of a phototrophic process. As phototrophic hydrogen is generated due to a specific catalytic activity of the applied micro-organism, the growth and maintenance expenditures of this micro-organism should be as low as possible. This situation requires a biomass concentration that still safeguards a sufficient catalytic activity in the PBR for (near) complete light absorption, but which is not too high, as this would result in increased maintenance losses. At the same time, the dilution rate should be as low as possible, as higher dilution rates result in increased losses due to biomass generation.

Light energy balance

A light energy balance in which these contributions are quantified as a function of operating conditions can be a valuable tool to predict the mode of operation that will result in the highest attainable photosynthetic efficiency. In order to do so, the growth and maintenance expenditures of the microorganism in question need to be determined experimentally. Once these parameters have been determined, a light energy balance can

be set up, dividing the absorbed light energy into fractions used for maintenance, growth and hydrogen production (Hoekema et al. 2006). The light energy balance can be used to predict the dilution rate and biomass concentration that yield the maximal light to hydrogen conversion efficiency during chemostat cultivation. A light to hydrogen conversion efficiency of 3.3% was predicted to be achievable by a chemostat culture of *R. capsulatus* in a 3 cm flat panel PBR illuminated at 410 $W \cdot m^{-2}$ (400-950 nm). The settings at which this efficiency was predicted were a biomass concentration of 2.55 $kg \cdot m^{-3}$ combined with a dilution rate of 0.1 d^{-1} (Hoekema et al. 2006).

Predicted versus experimental results

The predicted light to hydrogen conversion efficiency using the light energy balance was checked in a G-stat experiment. During this experiment a nitrogen limited *Rhodobacter capsulatus* culture was fed an increasing amount of ammonium in time, resulting in a gradual increase in culture biomass density.

Up to a biomass concentration of 1.5 $g \cdot L^{-1}$, the culture produced molecular hydrogen near its maximal specific rate, which was experimentally determined to be 0.52 ± 0.02 $mmol \cdot kg^{-1} \cdot s^{-1}$. At a dilution rate of 0.4 d^{-1}, a light to hydrogen energy conversion efficiency of 1.6% was predicted and demonstrated. A further increase in biomass concentration resulted in a lower maximal specific hydrogen production rate. This observation may well have coincided with the on-set of light limitation, resulting in a limitation for both nitrogen and light, referred to as a double limitation (Tsygankov et al. 1996).

Much higher specific hydrogen production rates could be calculated from literature data, as can be seen in Table 6.1 and Table 6.2. As argued before, a higher specific hydrogen production rate decreases the requirement for high cell densities at increased light intensities and with it the risk of self-shading, resulting in the loss of specific nitrogenase activity.

At a higher specific hydrogen production capacity, the predicted 3.3% light to hydrogen energy conversion efficiency would have been more easily achieved in the applied system, due to the lower required biomass concentration and the concomitant lower fraction of the absorbed light that is not used for photosynthesis due to over-saturation and subsequent non-photochemical quenching (Hoekema et al. 2006). This fraction could be reduced even further by applying a PBR design that facilitates the dilution of the incident light, as discussed previously.

D-Stat experimental approach

Both the determination of the parameters that are included in the light energy balance $Y_{x,le}$, m_{le} and f_{heat} as well as the experimental validation of the balance require a vast amount of chemostat experiments. The application of stat technologies can be an efficient alternative, as in this way the required information can be acquired much faster (Hoekema et al. 2006; Hoekema et al. 2009). The application of stat technologies can result in a significant reduction of experimental time required for process optimization when compared to the more traditional series of chemostat experiments approach (Hoekema et al. 2014). To validate this approach a model was set up to describe and simulate both D-stat and chemostat cultivations of the diatoms *Thalassiosira pseudonana* and *Phaeodactylum tricornutum* in a flat panel PBR with an optical light path of 3 cm.

When optimizing these cultures for biomass output rate, a reduction in required experimental time ranging between 85 and 94% is calculated, depending on both the applied microorganism and light intensity on the surface of the PBR (Hoekema et al. 2014), in favor of the D-stat experimental approach.

Conclusions

Light to hydrogen energy conversion by microorganisms is a concept that has been studied for decades. During this time, a lot of knowledge was gained on the required characteristics of the applied cultivation system, the physiological responses of the applied microorganisms and the way the activities of the key enzymes in the process are regulated.

Due to light oversaturation on the illuminated side of a photo bioreactor system and self-shading on the other, practical light to hydrogen conversion efficiencies are much lower than can be calculated based on theory. For this reason, photobiological hydrogen generating systems are not commercially viable at this moment.

Related to the applied photo bioreactor, it can be concluded that its construction should be as simple as possible. A high efficiency of light to hydrogen energy conversion requires a photobioreactor design in which strong light is diluted, at the cost of additional surface area. The PBR should facilitate illumination of all microorganism present above the compensation point in case of photo autotrophs or above the light intensity that safeguards full nitrogensase expression in case of PNS bacteria. This can be achieved by controlling for instance the biomass concentration, either by the imposed dilution rate or by nitrogen limitation.

As far as the applied microorganism is concerned, there are several possibilities for improving its performance by means of genetic modification. A reduced light harvesting complex results in reduced light gradients and self-shading of the culture. Other genetic modifications that have proven their effectiveness aim at directing a larger fraction of the total available reducing power towards hydrogen, by knocking out the routes that facilitate the recycling of hydrogen or the intracellular accumulation of reducing power in storage compounds like PHB. Mutant strains that have multiple modifications that are all intended to improve the light to hydrogen conversion efficiency have also been

constructed and have demonstrated an increased capacity for light to hydrogen conversion or an increased specific rate of hydrogen production.

Despite this knowledge-base, a limited amount of pilot studies using solar irradiation for the production of molecular hydrogen have been reported. A pilot scale study was executed by Adessi et al. with *Rp. palustris* in a tubular PBR at 50L scale. (Adessi et al. 2012). The light to hydrogen conversion efficiency that could be achieved did not exceed 1% (see Table 6.1).

Given the effort that has been invested in investigating processes for phototrophic light to hydrogen conversion, and considering their complexity and the requirement for a simple system, the future of photobiological hydrogen is by no means certain. The present study demonstrates that in this field of research, stat experiments are very useful. Their use has been demonstrated both during the determination of model parameters and both the optimization and validation of the process. Also a light energy balance for absorbed light is very useful in order to gain process insight and to make rational process optimization decisions.

Nomenclature

C_x	Biomass concentration	[kg·m^{-3}]
Hup	Hydrogenase Uptake	[-]
OP	Optical path	[mm]
PAR	Photosynthetic Active Radiation	[µmol·m^{-2}·s^{-1}, 400 – 700 nm]
PBR	Photo Bio Reactor	[-]
PHB	poly(3-hydroxy) butyric acid	[-]
PNSB	Purple Non-Sulphur Bacteria	[-]
PS	Photo System	[-]
$q_{H_2,max}$	Maximal specific H_2 production rate	[mol·kg^{-1}·s^{-1}]
$q_{H_2,max,Chla}$	Maximal Chl a specific H_2 production rate	[µmol·mg Chla^{-1}·h^{-1}]
S	Surface area	[m^2]
UV	Ultra violet	[-]
V	Volume	[m^3]
$\eta_{light \rightarrow H_2}$	Light to hydrogen conversion efficiency	[%]

Table 6.1 Batch photoheterotrophic hydrogen production processes from literature[1].

Process specifics → Applied organism ↓	I_{in}[3] ($W\ m^{-2}$) + Type	S/V Ratio (m^{-1})	C_x ($kg\ m^{-3}$)	$\eta_{light \rightarrow H_2}$[2] (%)	$q_{H_2,max}$ ($mmol\ kg^{-1}\ s^{-1}$)	Scale (L)	References
R. sulfidophilum Hup$^-$	13 Xenon	33*	3.1	35	0.5*	0.012	(Yamada et al. 1998)
R.sphaeroides KD131 Phb$^-$ Hup$^-$	30* Halogen tungsten	57*	1.8	10.4*	0.4*	0.05	(Kim et al. 2006)
R. sphaeroides WT	50 Xenon	160*	3.3*	9.1*	0.3*	0.015	(Miyake and Kawamura 1987)
R. sphaeroides WT	267* Tungsten	100*	-	8.9*	-	0.3	(El-Shishtawy et al. 1997)
R. sphaeroides GL	287* Tungsten	500	-	8.1*	-	0.005	(Tsygankov et al. 1998b)
R. sphaeroides WT	33* Tungsten	20*	0.3	8.1*	0.7*	1	(Sasaki 1998)
R. sphaeroides WT	76* Tungsten	160*	-	7.7*	-	0.015	(Zhu et al. 1999)
R.sphaeroides KD131	30* Halogen tungsten	57*	1.8	7.6*	0.3*	0.05	(Kim et al. 2006)
Rhodopseudomonas WT	100* Tungsten	20*	0.3*	7.2*	0.5*	0.7	(Kim et al. 1981)
R. sphaeroides RV	44* Tungsten	9*	0.4	7.0*	0.3*	0.2	(Nagamine et al. 1996)
Rhodospirillaceae sp. WT	95* Tungsten	33*	3.0	6.4*	0.2*	0.07	(Matsumoto et al. 1998)
Rhodopseudomonas sp. WT	22* Tungsten	95*	0.3	6.2	0.004*	0.15	(Barbosa et al. 2001)
R. capsulatus Hup$^-$	57 Tungsten	67*	1.0	6.0*	0.7*	0.005	(Ooshima et al. 1998)
R. sulfidophilum Hup$^-$	34* Unknown	57*	3.1	4.4*	0.1*	0.5	(Matsunaga and Takeyama 2000)
R. sulfidophilum Hup$^-$	1800 Xenon	33*	3.1*	1.6	3.0*	0.012	(Yamada et al. 1998)
R. capsulatus WT	206 Halogen tungsten	141	4.8	1.0	0.5	0.01	(Hoekema et al. 2009)
R. capsulatus WT	77* Tungsten	534*	1.0	1.0*	1.4*	0.002	(Tsygankov et al. 1998a)
R. palustris WT	1000 Solar	30.5	3.0*	0.9	0.1*	50	(Adessi et al. 2012)

[1] Values that were calculated from the reported data are indicated with an asterisk.
[2] Based on a 400-950 nm spectral range. Light and hydrogen are the only substrate and product considered.
[3] Incident light energy based on the 400-950 nm spectral range.

Table 6.2 Chemostat photoheterotrophic hydrogen production processes from literature[1].

Process specifics → Applied organism ↓	I_{in}[3] (W m^{-2}) + Type	S/V Ratio (m^{-1})	C_x (kg m^{-3})	$\eta_{light \rightarrow H_2}$[2] (%)	$q_{H_2,max}$ (mmol kg^{-1} s^{-1})	Scale (L)	References
R. sphaeroides	96* Tungsten	14*	0.5	8.8*	0.9*	1	(Fascetti and Todini 1995)
R. rubrum WT	378* Tungsten	33*	3.5*	4.4*	0.6*	1	(Zürrer and Bachofen 1982)
R. sphaeroides PHA$^-$ Hup$^-$	57* Tungsten	43*	7.4*	4.2*	1.2*	0.93	(Franchi et al. 2004)
R. palustris WT	90* Tungsten	67*	7.0	2.4*	0.1*	0.8	(Chen and Chang 2006)
R. capsulata WT	150* Tungsten	54*	0.5*	2.0*	2.6*	0.45	(Jouanneau et al. 1984)
R. capsulata WT	150 Tungsten	54*	0.1*	1.6*	6.9*	0.45	(Jouanneau et al. 1984)
R. capsulatus WT	236* Tungsten	69*	1.0	1.6*	0.9*	1	(Tsygankov et al. 1998a)
R. capsulatus WT	410 Tungsten	33	1.5	1.6	0.5	2.4	(Hoekema et al. 2009)
R. capsulata Nif$^-$ (80%)	300 Tungsten	54*	1.0	1.0*	0.6*	0.45	(Allibert et al. 1984)

[1] Values that were calculated from the reported data are indicated with an asterisk.
[2] Based on a 400-950 nm spectral range. Light and hydrogen are the only substrate and product considered.
[3] Incident light energy based on the 400-950 nm spectral range.

Table 6.3 Batch photoautotrophic hydrogen production processes from literature[1].

Process specifics → Applied organism ↓	I_{in}[3] (W m^{-2}) + Type	S/V Ratio (m^{-1})	[Chla] (mg Chla L^{-1})	$\eta_{light \rightarrow H_2}$[2] (%)	$q_{H_2,max,Chla}$ (µmol·mg Chla^{-1}·h^{-1})	Scale (L)	References
C. moewusii	0.1* Unknown	-	-	24.0	-	-	(Greenbaum 1988)
C. reinhardtii WT	13.8 Fluorescent	-	-	9.4*	-	0.5	(Laurinavichene et al. 2004)
Nostoc sp. Hup$^-$	14.3* Fluorescent	-	1	3.7	100	0.001	(Yoshino et al. 2007)
A. variabilis WT	8.4 Fluorescent	500*	-	3.2	8.2	0.002	(Markov et al. 1996)
C. reinhardtii WT	24 Fluorescent	38*	25	3.2*	12.5	0.5	(Kosourov et al. 2012)
C. reinhardtii WT	14* Fluorescent	32*	24	1.6	9.0*	1	(Giannelli et al. 2009)
Anabaena sp. Hup$^-$	22 Fluorescent	290*	22	1.4	45	5	(Kumazawa and Asakawa 1995)

[1] Values that were calculated from the reported data are indicated with an asterisk.
[2] Based on a 400-700 nm spectral range (PAR). Light and hydrogen are the only substrate and product considered.
[3] Incident light energy based on the 400-700 nm spectral range (PAR).

References

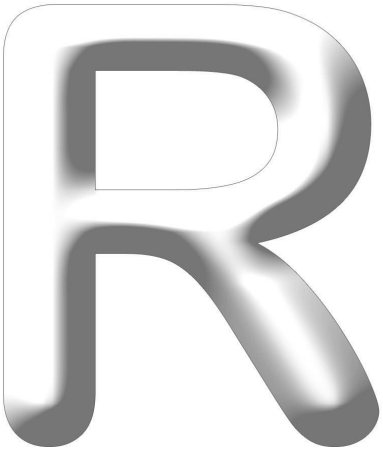

References

Adessi A, Torzillo G, Baccetti E, De Philippis R. 2012. Sustained outdoor H_2 production with *Rhodopseudomonas palustris* cultures in a 50 L tubular photobioreactor. International Journal of Hydrogen energy 37(10):8840-8849.

Adir N, Zer H, Shochat S, Ohad I. 2003. Photoinhibition a historical perspective. Photosynthesis Research 76(1-3):343-370.

Albers H, Gottschalk G. 1976. Acetate metabolism in Rhodopseudomonas gelatinosa and several other Rhodospirillacae. Archives of Microbiology 111:45-49.

Alef K, Arp DJ, Zumft WG. 1981. Nitrogenase switch-off by ammonia in Rhodopseudomonas palustris : loss under nitrogen deficiency and independence from the adenylylation state of glutamine synthetase. Archives of Microbiology 130 138 - 142

Allen JF. 2003. Cyclic, pseudocyclic and noncyclic photophosphorylation: new links in the chain. Trends in Plant Science 8(1):15-19.

Allibert P, Odom JM, Wall JD, Vignais P. 1984. Phenotypic changes in hydrogen evolving chemostat cultures of *Rhodopseudomonas capsulata* FEMS Microbiology Letters 23:221-226.

Apt KE, Behrens PW. 1999. Commercial developments in microalgal biotechnology. Journal of Phycology 35:215-226.

Armaroli N, Balzani V. 2011. The hydrogen issue. ChemSusChem 4(1):21-36.

Arp DJ, Zumft WG. 1983. Overproduction of nitrogenase by nitrogen-limited cultures of *Rhodopseudomonas palustris*. Journal of Bacteriology 153(3):1322-1330.

Asada Y, Miyake J. 1999. Photobiological hydrogen production. Journal of Bioscience and Bioengineering 88(1):1-6.

ASTM. 2005. Reference Solar Spectral Irradiance ASTM G-173 - 03.

Balat M. 2009. Possible methods for hydrogen production. Energy Sources, Part A: Recovery, Utilization and Environmental Effects 31(1):39-50.

Barbosa MJ, Hoogakker J, Wijffels RH. 2003. Optimization of cultivation parameters in photobioreactors for microalgae cultivation using the A-stat technique. Biomolecular Engineering 20(4-6):115-123.

Barbosa MJ, Rocha JMS, Tramper J, Wijffels RH. 2001. Acetate as a carbon source for hydrogen production by photosynthetic bacteria. Journal of Biotechnology 85:25-33.

Barbosa MJ, Zijffers JW, Nisworo A, Vaes W, van Schoonhoven J, Wijffels RH. 2005. Optimisation of biomass, vitamins, and carotenoid yield on light energy in a flat-panel reactor using the A-stat technique. Biotechnology and Bioengineering 89(2):233-242.

Benemann JR. 1996. Hydrogen biotechnology: progress and prospects. Nature Biotechnology 14:1101-1103.

Birol F. 2010. World energy outlook 2010. Priddle R, editor. Paris: OECD/IEA.

Blankenship RE, Tiede DM, Barber J, Brudvig GW, Fleming G, Ghirardi M, Gunner MR, Junge W, Kramer DM, Melis A and others. 2011. Comparing photosynthetic and photovoltaic efficiencies and recognizing the potential for improvement. Science 332(6031):805-809.

Blasco R, Cardenas J, Castillo F. 1991. Regulation of isocitrate lyase in Rhodobacter capsulatus E1F1. Current Microbiology 22(1):73-76.

Boatman ES. 1964. Observations on the fine structure of spheroplasts of *Rhodospirillum rubrum*. The Journal of cell biology 20(2):297-311.

Borghese R, Borsetti F, Foladori P, Ziglio G, Zannoni D. 2004. Effects of the Metalloid Oxyanion Tellurite (TeO32−) on Growth Characteristics of the Phototrophic Bacterium *Rhodobacter capsulatus*. Applied and Environmental Microbiology 70(11):6595-6602.

Bregoff HM, Kamen MD. 1951. Studies on the metabolism of photosynthetic bacteria. XIV. Quantitative relations between malate dissimilation, photoproduction of hydrogen, and nitrogen metabolism in *Rhodospirillum rubrum*. Archives of Biochemistry and Biophysics 36:202-220.

Brentner LB, Eckelman MJ, Zimmerman JB. 2011. Combinatorial Life Cycle Assessment to Inform Process Design of Industrial Production of Algal Biodiesel. Environmental Science & Technology 45(16):7060-7067.

Bryant DA, Frigaard NU. 2006. Prokaryotic photosynthesis and phototrophy illuminated. Trends in Microbiology 14(11):488-496.

Bunthof CJ, Bloemen K, Breeuwer P, Rombouts FM, Abee T. 2001. Flow cytometric assessment of viability of lactic acid bacteria. Applied and Environmental Microbiology 67(5):2326-2335.

Chalk SG, Miller JF. 2006. Key challenges and recent progress in batteries, fuel cells, and hydrogen storage for clean energy systems. Journal of Power Sources 159(1 SPEC. ISS.):73-80.

Chang PK, Lu CH, Yeh CH, Houng MP. 2012. High efficiency a-Si:H/a-Si:H solar cell with a tunnel recombination junction and a n-type μc-Si:H layer. Thin Solid Films 520(9):3684-3687.

Chen CY, Chang JS. 2006. Enhancing phototrophic hydrogen production by solid-carrier assisted fermentation and internal optical-fiber illumination. Process Biochemistry 41:2041-2049.

Chen CY, Yang MH, Yeh KL, Liu CH, Chang JS. 2008. Biohydrogen production using sequential two-stage dark and photo fermentation processes. International Journal of Hydrogen energy 33(18):4755-4762.

Chisti Y. 2007. Biodiesel from microalgae. Biotechnology Advances 25:294-306.

Claassen PAM, van Lier JB, Lopez Contreras AM, van Niel EWJ, Sijtsma L, Stams AJM, de Vries SS, Weusthuis RA. 1999. Utilisation of biomass for the supply of energy carriers. Applied Microbiology and Biotechnology 52:741-755.

Cleland RE, Rees D, Horton P. 1992. Light-induced fluorescence quenching and loss of photochemistry in chromatophores of photosynthetic purple bacteria. Journal of Photochemistry and Photobiology B: Biology 13:253-265.

Cuaresma M, Janssen M, Vílchez C, Wijffels RH. 2009. Productivity of *Chlorella sorokiniana* in a short light-path (SLP) panel photobioreactor under high irradiance. Biotechnology and Bioengineering 104(2):352-359.

Cuaresma M, Janssen M, Vílchez C, Wijffels RH. 2011. Horizontal or vertical photobioreactors? How to improve microalgae photosynthetic efficiency. Bioresource Technology 102:5129-5137.

Dalton H, Mortenson LE. 1972. Dinitrogen (N_2) fixation (with a biochemical emphasis). Bacteriological Reviews 36(2):231-260.

David E. 2005. An overview of advanced materials for hydrogen storage. Journal of Materials Processing Technology 162-163(SPEC. ISS.):169-177.

Dörffler M, Steindorf A, Oelze J. 1998. Determination of C/N ratios required for de-repression of nitrogenase in *Rhodobacter capsulatus* Zeitschrift für Naturforschung 53 c:961-967.

Dubinsky Z, Falkowski PG, Wyman K. 1986. Light harvesting and utilization by phytoplankton. Plant and Cell Physiology 27(7):1335-1349.

Dubinsky Z, Stambler N. 2009. Photoacclimation processes in phytoplankton: mechanisms, consequences, and applications. Aquatic Microbial Ecology 56(2-3):163-176.

Dudley B. 2011. BP statistical review of world energy june 2011.

El-Shishtawy RMA, Kawasaki S, Morimoto M. 1997. Biological H_2 production using a novel light-induced and diffused photobioreactor. Biotechnology Techniques 11(6):403-407.

Eroglu E, Melis A. 2011. Photobiological hydrogen production: Recent advances and state of the art. Bioresource Technology 102(18):8403-8413.

Evers EG. 1991. A model for light-limited continuous cultures: growth, shading, and maintenance. Biotechnology and Bioengineering 38:254-259.

Fajer J, Brune DC, Davis MS. 1975. Primary charge separation in bacterial photosynthesis: oxidized chlorophylls and reduced pheophytin. Proceedings of the National Academy of Sciences of the United States of America 72(12):4956-4960.

Fascetti E, Addario E, Todini O, Robertiello A. 1998. Photosynthetic hydrogen evolution with volatile organic acids derived from the fermentation of source selected municipal solid wastes. International Journal of Hydrogen energy 23(9):753-760.

Fascetti E, Todini O. 1995. *Rhodobacter sphaeroides* RV cultivation and hydrogen production in a one- and two-stage chemostat. Applied Microbiology and Biotechnology 44:300-305.

Fedorov AS, Laurinavichene TV, Tsygankov AA. 1999. Factors influencing nitrogenase switch-off by ammonium in the purple bacterium *Rhodobacter capsulatus*. Microbiology-USSR 68(4):379-386.

Ferguson SJ, Jackson JB, McEwan AG. 1987. Anaerobic respiration in the Rhodospirillaceae: characterisation of pathways and evaluation of roles in redox balancing during photosynthesis. FEMS Microbiology Reviews 46:117-143.

Fissler J, Schirra C, Kohring GW, Giffhorn F. 1994. Hydrogen production from aromatic acids by *Rhodopseudomonas palustris* Applied Microbiology and Biotechnology 41:395-399.

Formighieri C, Franck F, Bassi R. 2012. Regulation of the pigment optical density of an algal cell: Filling the gap between photosynthetic productivity in the laboratory and in mass culture. Journal of Biotechnology.

Franchi E, Tosi C, Scolla G, Della Penna G, Rodriguez F, Pedroni PM. 2004. Metabolically engineered *Rhodobacter sphaeroides* RV strains for improved biohydrogen photoproduction combined with disposal of food wastes. Marine Biotechnology 6:552-565.

Geider RJ, Macintyre HL, Kana TM. 1996. A dynamic model of photoadaptation in phytoplankton. Limnology and Oceanography 41(1):1-15.

Ghirardi ML. 2006. Hydrogen production by photosynthetic green algae. Indian Journal of Biochemistry and Biophysics 43(4):201-210.

Giannelli L, Scoma A, Torzillo G. 2009. Interplay between light intensity, chlorophyll concentration and culture mixing on the hydrogen production in sulfur-deprived *Chlamydomonas reinhardtii* cultures grown in laboratory photobioreactors. Biotechnology and Bioengineering 104(1):76-90.

Gibson JL, Tabita FR. 1976. Different molecular forms of D-ribulose-1,5-bisphosphate carboxylase from *Rhodopseudomonas sphaeroides*. The Journal of Biological Chemistry 252(3):943-949.

Göbel F. 1978. Quantum efficiencies of growth. In: Clayton RK, Sistrom WR, editors. The Photosynthetic Bacteria. New York: Plenum Press. p 907-925.

Goldman JC. 1979. Outdoor algal mass cultures - II. Photosynthetic yield limitations. Water Research 13:119-136.

Gottschal JC. 1992. Continuous culture. In: Lederberg J, editor. Encyclopedia Of Microbiology. San Diego: Academic Press, Inc. p 559-572.

Greenbaum E. 1988. Energetic efficiency of hydrogen photoevolution by algal water splitting. Biophysical Journal 54:365-368.

Hallenbeck PC, Benemann JR. 2002. Biological hydrogen production; fundamentals and limiting processes. International Journal of Hydrogen energy 27:1185-1193.

Hoekema S, Bijmans M, Janssen M, Tramper J, Wijffels RH. 2002. A pneumatically agitated flat-panel photobioreactor with gas-recirculation: anaerobic photoheterotrophic cultivation of a purple non-sulphur bacterium. International Journal of Hydrogen energy 27:1331-1338.

Hoekema S, Douma RD, Janssen M, Tramper J, Wijffels RH. 2006. Controlling light-use by *Rhodobacter capsulatus* continuous cultures in a flat-panel photobioreactor. Biotechnology and Bioengineering 95(4):613-626.

Hoekema S, Rinzema A, Tramper J, Wijffels RH, Janssen M. 2014. Deceleration-Stats Save Much Time During Phototrophic Culture Optimization. Biotechnology and Bioengineering 111(4):792-802.

Hoekema S, Van Breukelen FR, Janssen M, Tramper J, Wijffels RH. 2009. Exploration of the hydrogen producing potential of *Rhodobacter capsulatus* chemostat cultures: The application of deceleration-stat and gradient-stat methodology. Biotechnology Progress 25(5):1343-1352.

Hustede E, Steinbüchel A, Schlegel HG. 1993. Relationship between the photoproduction of hydrogen and the accumulation of PHB in non-sulphur purple bacteria. Applied Microbiology and Biotechnology 39:87-93.

Hwang JC, Burris RH. 1972. Nitrogenase-catalyzed reactions. BBA - Bioenergetics 283(2):339-350.

Ivanovskii RN, Krasil'nikova EN, Berg IA. 1997. The mechanism of acetate assimilation in the purple nonsulfur bacterium Rhodospirillum rubrum lacking isocitrate lyase. Microbiology 66(6):621-626.

Janssen M, de Winter M, Tramper J, Mur LR, Snel JFH, Wijffels RH. 2000. Efficiency of light utilization of *Chlamydomonas reinhardtii* under medium-duration light/dark cycles. Journal of Biotechnology 78:123-137.

Janssen M, Slenders P, Tramper J, Mur LR, Wijffels RH. 2001. Photosynthetic efficiency of *Dunaliella tertiolecta* under short light/dark cycles. Enzyme and Microbial Technology 29(4-5):298-305.

Janssen M, Tramper J, Mur LR, Wijffels RH. 2003. Enclosed outdoor photobioreactors: light regime, photosynthetic efficiency, scale-up and future prospects. Biotechnology and Bioengineering 81(2):193-210.

Jouanneau Y, Lebecque S, Vignais PM. 1984. Ammonia and light effect on nitrogenase activity in nitrogen-limited continuous cultures of *Rhodopseudomonas capsulata*. Role of glutamine synthetase. Archives of Microbiology 139:326-331.

Jouanneau Y, Wong B, Vignais P. 1985. Stimulation by light of nitrogenase synthesis in cells of *Rhodopseudomonas capsulata* growing in N-limited continuous cultures. Biochimica et Biophysica Acta 808:149-155.

Kask S, Laht T-M, Pall T, Paalme T. 1999. A study on growth characteristics and nutrient consumption of *Lactobacillus plantarum* in A-stat culture. Antonie Van Leeuwenhoek International Journal Of General And Molecular Microbiology 75(4):309-320.

Kern M, Klipp W, Klemme JH. 1994. Increased nitrogenase-dependent H_2 photoproduction by *hup* mutants of *Rhodospirillum rubrum* Applied and Environmental Microbiology 60(6):1768-1774.

Khatipov E, Miyake M, Miyake J, Asada Y. 1998. Accumulation of poly-β-hydroxybutyrate by *Rhodobacter sphaeroides* on various carbon and nitrogen substrates. FEMS Microbiology Letters 162 39 - 45

Kim JS, Ito K, Takahashi H. 1981. Production of molecular hydrogen by *Rhodopseudomonas* sp. Journal of Fermentation Technology 59(3):185-190.

Kim MS, Baek JS, Lee JK. 2006. Comparison of H_2 accumulation by *Rhodobacter sphaeroides* KD131 and its uptake hydrogenase and PHB synthase deficient mutant. International Journal of Hydrogen energy 31(1):121-127.

Kirmaier C, Holten D. 1987. Primary photochemistry of reaction centers from the photosynthetic purple bacteria. Photosynthesis Research 13(3):225-260.

Kliphuis AMJ, Klok AJ, Martens DE, Lamers PP, Janssen M, Wijffels RH. 2011. Metabolic modeling of *Chlamydomonas reinhardtii*: energy requirements for photoautotrophic growth and maintenance. Journal of Applied Phycology 24(2):253-266.

Kok B, Burlew JS. 1953. Experiments on photosynthesis by Chlorella in flashing light. Algal Culture. Washington: Carnegie Institution of Washington, Pub 600. p 63-75.

Kondo T, Arakawa M, Hirai T, Wakayama T, Hara M, Miyake J. 2002. Enhancement of hydrogen production by a photosynthetic bacterium mutant with reduced pigment. Journal of Bioscience and Bioengineering 93(2):145-150.

Kosourov SN, Batyrova KA, Petushkova EP, Tsygankov AA, Ghirardi ML, Seibert M. 2012. Maximizing the hydrogen photoproduction yields in *Chlamydomonas reinhardtii* cultures: The effect of the H_2 partial pressure. International Journal of Hydrogen energy 37(10):8850-8858.

Koyama Y. 1991. Structures and functions of carotenoids in photosynthetic systems. Journal of Photochemistry and Photobiology B: Biology 9:265-280.

Kumazawa S, Asakawa H. 1995. Simultaneous production of H_2 and O_2 in closed vessels by marine *cyanobacterium Anabaena* sp. TU37-1 under high-cell-density conditions. Biotechnology and Bioengineering 46(4):396-398.

Lam MK, Lee KT. 2012. Microalgae biofuels: A critical review of issues, problems and the way forward. Biotechnology Advances 30(3):673-690.

Lascelles J. 1960. The formation of Ribulose 1:5-diphosphate carboxylase by growing cultures of Athiorhodaceae. Journal of General Microbiology 23(3):499-510.

Laurinavichene TV, Tolstygina I, Tsygankov AA. 2004. The effect of light intensity on hydrogen production by sulfur-deprived Chlamydomonas reinhardtii Journal of Biotechnology 114:143-151.

Lee CM, Chen PC, Wang CC, Tung YC. 2002. Photohydrogen production using purple nonsulfur bacteria with hydrogen fermentation reactor effluent. International Journal of Hydrogen energy 27:1309-1313.

Lewis NS, Nocera DG. 2006. Powering the planet: Chemical challenges in solar energy utilization. Proceedings of the National Academy of Sciences of the United States of America 103(43):15729-15735.

Li Z, Wakao S, Fischer BB, Niyogi KK. 2009. Sensing and Responding to Excess Light. Annual Review of Plant Biology 60:239-260.

Lipman TE. 2004. What will power the hydrogen economy? Present and future sources of hydrogen energy. Davis: Energy and resources group, Institute of transportation studies, University of California - Berkeley

Institute of transportation studies, University of California - Davis. Report nr UCD-ITS-RR-04-10.

Luo HP, Al-Dahhan MH. 2012. Airlift column photobioreactors for Porphyridium sp. culturing: Part II. verification of dynamic growth rate model for reactor performance evaluation. Biotechnology and Bioengineering 109(4):942-949.

Ma F, Hanna MA. 1999. Biodiesel production: A review. Bioresource Technology 70(1):1-15.

MacIntyre HL, Kana TM, Anning T, Geider RJ. 2002. Photoacclimation of photosynthesis irradiance response curves and photosynthetic pigments in microalgae and cyanobacteria. Journal of Phycology 38(1):17-38.

Madigan MT, Cox SS, Stegeman RA. 1984. Nitrogen fixation and nitrogenase activities in members of the family *Rhodospirillaceae* Journal of Bacteriology 157(1):73-78.

Madigan MT, Gest H. 1979. Growth of the photosynthetic bacterium Rhodopseudomonas capsulata chemoautotrophically in darkness with H2 as the energy source. Journal of Bacteriology 137(1):524-530.

Markov SA, Bazin MJ, Hall DO. 1996. Efficiency of light energy conversion in hydrogen production by cyanobacterium Anabaena variabilis Journal of Marine Biotechnology 4:57-60.

Marshall HL, Geider RJ, Flynn KJ. 2000. A mechanistic model of photoinhibition. New Phytologist 145(2):347-359.

Masepohl B, Drepper T, Paschen A, Groá S, Pawlowski A, Raabe K, Riedel KU, Klipp W. 2002. Regulation of nitrogen fixation in the phototrophic purple bacterium Rhodobacter capsulatus Journal of Molecular Microbial Biotechnology 4 (3):243 - 248

Matsumoto H, Yoza B, Radway J-AC, Zaborsky OR. 1998. Photosynthetic bacteria of Hawaii. In: Zaborsky OR, editor. Biohydrogen I. New York: Plenum Press. p 163-166.

Matsunaga T, Takeyama H. 2000. Screening of marine photosynthetic microorganisms and hydrogen production. In: Miyake J, Matsunaga T, San Pietro A, editors. Biohydrogen II. Oxford: Elsevier Science. p 185-194.

McKinlay JB, Harwood CS. 2010. Photobiological production of hydrogen gas as a biofuel. Current Opinion in Biotechnology 21(3):244-251.

Meister M, Saum S, Alber BE, Fuchs G. 2005. L-malyl-coenzyme A/β-methylmalyl-coenzyme A lyase is involved in acetate assimilation of the isocitrate lyase-negative bacterium Rhodobacter capsulatus. Journal of Bacteriology 187(4):1415-1425.

Melis A. 2009. Solar energy conversion efficiencies in photosynthesis: Minimizing the chlorophyll antennae to maximize efficiency. Plant Science 177(4):272-280.

Melis A, Seibert M, Ghirardi ML, León R, Galván A, Fernández E. 2007. Hydrogen Fuel Production by Transgenic Microalgae

Transgenic Microalgae as Green Cell Factories. Springer New York. p 110-121.

Minkevich IG, Laurinavichene TV, Tsygankov AA. 2004. Theoretical and experimental quantum efficiencies of the growth of anoxygenic phototrophic bacteria. Process Biochemistry 39(8):939-949.

Miura Y, Yagi K, Shoga M, Miyamoto K. 1982. Hydrogen production by a green alga, *Chlamydomonas reinhardtii*, in an alternating light/dark cycle. Biotechnology and Bioengineering 24:1555-1563.

Miyake J, Kawamura S. 1987. Efficiency of light energy conversion to hydrogen by the photosynthetic bacterium *Rhodobacter sphaeroides* International Journal of Hydrogen energy 12(3):147-149.

Miyake J, Mao XY, Kawamura S. 1984. Photoproduction of hydrogen from glucose by a co-culture of a photosynthetic bacterium and *Clostridium butyricum* Journal of Fermentation Technology 62(6):531-535.

Miyake J, Zaborsky OR. 1998. The science of biohydrogen; An energetic view. Biohydrogen. New York: Plenum Press. p 7-18.

Molina Grima E, García Camacho F, Sánchez Pérez JA, Acién Fernández FG, Fernández Sevilla JM. 1997. Evaluation of photosynthetic efficiency in microalgal cultures using averaged irradiance. Enzyme and Microbial Technology 21(5):375-381.

Mortenson LE. 1964. Ferredoxin and ATP, Requirements for nitrogen fixation in cell-free extracts of *Clostridium pasteurianum*. Proceedings of the National Academy of Sciences of the United States of 52:272-279.

Morweiser M, Kruse O, Hankamer B, Posten C. 2010. Developments and perspectives of photobioreactors for biofuel production. Applied Microbiology and Biotechnology 87(4):1291-1301.

Müller P, Li XP, Niyogi KK. 2001. Non-photochemical quenching. A response to excess light energy. Plant.Physiol. 125(4):1558-1566.

Müller RH, Bley T, Babel W. 1995. Transient state cultivation as a means for determining maximum growth rates of microorganism in inhibition kinetics. Journal of Microbiological Methods 22(3):209-219.

Munson TO, Burris RH. 1969. Nitrogen fixation by *Rhodospirillum rubrum* grown in nitrogen-limited continuous culture. Journal of Bacteriology 97(3):1093-1098.

Muradov NZ, Veziroğlu TN. 2008. “Green” path from fossil-based to hydrogen economy: An overview of carbon-neutral technologies. International Journal of Hydrogen energy 33(23):6804-6839.

Nagamine Y, Kawasugi T, Miyake M, Asada Y, Miyake J. 1996. Characterization of photosynthetic bacterium *Rhodobacter sphaeroides* RV for hydrogen production. Journal of Marine Biotechnology 4:34-37.

Nielsen AM, Sojka GA. 1979. Photoheterotrophic utilization of acetate by the wild type and an acetate-adapted mutant of Rhodopseudomonas capsulata. Archives of Microbiology 120(1):39-42.

Nitschke W, Dracheva SM. 1995. Reaction center associated cytochromes. In: Blankenship RE, Madigan MT, Bauer CE, editors. Anoxygenic Photosynthetic Bacteria. Dordrecht: Kluwer Academic Publishers. p 775-805.

Ooshima H, Takakuwa S, Katsuda T, Okuda M, Shirasawa T, Azuma M, Kato J. 1998. Production of hydrogen by a hydrogenase-deficient mutant of *Rhodobacter capsulatus* Journal of Fermentation and Bioengineering 85(5):470-475.

Ormerod JG. 1956. The use of radioactive carbon dioxide in the measurement of carbon dioxide fixation in *Rhodospirillum rubrum*. Biochemical Journal 64 373 - 380

Ormerod JG, Gest H. 1962. Symposium on metabolism of inorganic compounds: IV. Hydrogen photosynthesis and alternative metabolic pathways in photosynthetic bacteria. Bacteriological Reviews 26:51-66.

Otsuki T, Uchiyama S, Fujiki K, Fukunaga S, Zaborsky OR. 1998. Hydrogen production by a floating-type photobioreactor. Biohydrogen. New York: Plenum Press. p 369-374.

Paalme T, Elken R, Vilu R, Korhola M. 1997. Growth efficiency of *Saccharomyces cerevisiae* on glucose/ethanol media with a smooth change in the dilution rate (A-stat). Enzyme and Microbial Technology 20(3):174-181.

Paalme T, Kahru A, Elken R, Vanatalu K, Tiisma K, Vilu R. 1995. The computer-controlled continuous culture of *Escherichia coli* with smooth change of dilution rate (A-stat). Journal of Microbiological methods 24(2):145-153.

Paddock ML, Chang C, Xu Q, Abresch EC, Axelrod HL, Feher G, Okamura MY. 2005. Quinone (QB) reduction by B-branch electron transfer in mutant bacterial reaction centers from Rhodobacter sphaeroides: Quantum efficiency and X-ray structure. Biochemistry 44(18):6920-6928.

Paddock ML, Feher G, Okamura MY. 2003. Proton transfer pathways and mechanism in bacterial reaction centers. FEBS Letters 555(1):45-50.

Parson WW. 1969. The reaction between primary and secondary electron acceptors in bacterial photosynthesis. BBA - Bioenergetics 189(3):384-396.

Paschinger H. 1974. A changed nitrogenase activity in *Rhodospirillum rubrum* after substitution of tungsten for molybdenum. Archives of Microbiology 101(4):379-389.

Payne J, Morris JG. 1969. Acetate utilisation by Rhodopseudomonas spheroides. FEBS Letters 4(1):52-54.

Perram JW. 1973. Relaxation times in bacteriological culture and the approach to steady state. Journal of Theoretical Biology 38(3):571-578.

Pruvost J, Van Vooren G, Le Gouic B, Couzinet-Mossion A, Legrand J. 2011. Systematic investigation of biomass and lipid productivity by microalgae in photobioreactors for biodiesel application. Bioresource Technology 102(1):150-158.

Pulz O, Scheibenbogen K, Groá W, Rehm HJ, Reed G, P hler A, Stadler P. 2001. Biotechnology with cyanobacteria and microalgae. Biotechnology Volume 10: Special Processes. Weinheim: Wiley-VCH. p 107-136.

Qiang H, Faiman D, Richmond A. 1998a. Optimal tilt angles of enclosed reactors for growing photoautotrophic microorganisms outdoors. Journal of Fermentation and Bioengineering 85(2):230-236.

Qiang H, Guterman H, Richmond A. 1996. A flat inclined modular photobioreactor for outdoor mass cultivation of photoautotrophs. Biotechnology and Bioengineering 51(1):51-60.

Qiang H, Richmond A. 1996. Productivity and photosynthetic efficiency of *Spirulina platensis* as affected by light intensity, algal density and rate of mixing in a flat plate photobioreactor. Journal of Applied Phycology 8(2):139-145.

Qiang H, Zarmi Y, Richmond A. 1998b. Combined effects of light intensity, light-path and culture density on output rate of *Spirulina platensis* (Cyanobacteria). European Journal of Phycology 33(2):165-171.

Radmer R, Kok B. 1977. Photosynthesis: Limited yields, unlimited dreams. BioScience 27(9):599-605.

Richmond A. 2000. Microalgal biotechnology at the turn of the millennium: A personal view. Journal of Applied Phycology 12:441-451.

Rodolfi L, Zittelli GC, Bassi N, Padovani G, Biondi N, Bonini G, Tredici MR. 2009. Microalgae for oil: Strain selection, induction of lipid synthesis and outdoor mass cultivation in a low-cost photobioreactor. Biotechnology and Bioengineering 102(1):100-112.

Ross DK. 2006. Hydrogen storage: The major technological barrier to the development of hydrogen fuel cell cars. Vacuum 80(10):1084-1089.

Sasaki K. 1998. Hydrogen and 5-aminolevulinic acid production by photosynthetic bacteria. In: Zaborsky OR, editor. Biohydrogen. New York: Plenum Press. p 133-142.

Sasikala K, Ramana CV, Raghuveer Rao P, Kovács KL. 1993. Anoxygenic phototrophic bacteria: physiology and advances in hydrogen production technology. Advances in Applied Microbiology 38:211-295.

Schulten K. 1999. From simplicity to complexity and back: function, architecture, and mechanism of light-harvesting systems in photosynthetic bacteria. In: Frauenfelder H, Deisenhofer J, Wolynes PG, editors. Simplicity and Complexity in Proteins and Nucleic Acids: Dahlem University Press. p 227-253.

Segers L, Verstraete W. 1983. Conversion of organic acids to H_2 by *Rhodospirillaceae* grown with glutamate or dinitrogen as nitrogen source. Biotechnology and Bioengineering 25:2843-2853.

Şener MK, Olsen JD, Hunter CN, Schulten K. 2007. Atomic-level structural and functional model of a bacterial photosynthetic membrane vesicle. Proceedings of the National Academy of Sciences of the United States of America 104(40):15723-15728.

Sojka GA. 1978. Metabolism of nonaromatic organic compounds. In: Clayton RK, Sistrom WR, editors. The Photosynthetic Bacteria. New York: Plenum Press. p 707-718.

Spoehr HA, Milner HW. 1949. The chemical composition of Chlorella ; effect of environmental conditions. Plant Physiology 24:120-149.

Steinborn B, Oelze J. 1989. Nitrogenase and photosynthetic activities of chemostat cultures of *Rhodobacter capsulatus* 37b4 grown under different illuminations. Archives of Microbiology 152:100-104.

Sundström V, van Grondelle R. 1995. Kinetics of excitation transfer and trapping in purple bacteria. In: Blankenship RE, Madigan MT, Bauer CE, editors. Anoxygenic Photosynthetic Bacteria. Dordrecht: Kluwer Academic Publishers. p 349-372.

Tabita FR. 1995. The biochemistry and metabolic regulation of carbon metabolism and CO_2 fixation in purple bacteria. In: Blankenship RE, Madigan MT, Bauer CE, editors. Anoxygenic Photosynthetic Bacteria. Dordrecht: Kluwer Academic Publishers. p 885-914.

Takache H, Pruvost J, Cornet J-F. 2012. Kinetic modeling of the photosynthetic growth of *Chlamydomonas reinhardtii* in a photobioreactor. Biotechnology Progress 28(3):681-692.

Tang CK, Williams JC, Taguchi AKW, Allen JP, Woodbury NW. 1999. P+H(A)- charge recombination reaction rate constant in Rhodobacter sphaeroides reaction centers is independent of the P/P+ midpoint potential. Biochemistry 38(27):8794-8799.

Thauer RK, Jungermann K, Decker K. 1977. Energy conservation in chemotrophic anaerobic bacteria. Bacteriological Reviews 41(1):100-180.

Thiele HH. 1968. Assimilation of simple organic compounds by Thiorhodaceae. Die Verwertung einfacher organischer Substrate durch Thiorhodaceae 60(2):124-138.

Thimijan RW, Heins RD. 1983. Photometric, radiometric, and quantum light units of measure: A review of procedures for interconversion. HortScience 18(6):818-822.

Tichi MA, Tabita FR. 2001. Interactive control of *Rhodobacter capsulatus* redox-balancing systems during phototrophic metabolism. Journal of Bacteriology 183(21):6344-6354.

Tredici MR. 2009. Photobiology of microalgae mass cultures: understanding the tools for the next green revolution. Biofuels 1(1):143-162.

Tredici MR, Zittelli GC. 1998. Efficiency of sunlight utilization: Tubular versus flat photobioreactors. Biotechnology and Bioengineering 57(2):187-197.

Trissl HW, Breton J, Deprez J, Dobek A, Leibl W. 1990. Trapping kinetics, annihilation, and quantum yield in the photosynthetic purple bacterium *Rps. viridis* as revealed by electric measurement of the primary charge separation. Biochimica et Biophysica Acta - Bioenergetics 1015(2):322-333.

Tsygankov AA, Fedorov AS, Laurinavichene TV, Gogotov IN, Rao KK, Hall DO. 1998a. Actual and potential rates of hydrogen photoproduction by continuous culture of the purple non-sulphur bacterium *Rhodobacter capsulatus* Applied Microbiology and Biotechnology 49:102-107.

Tsygankov AA, Fedorov AS, Talipova IV, Laurinavichene TV, Miyake J, Gogotov I. 1998b. Use of immobolized phototrophic microorganisms for waste water treatment and simultaneous production of hydrogen. Applied Biochemistry and Microbiology 34(4):398-402.

Tsygankov AA, Laurinavichene TV. 1996a. Effects of illumination and pH on the growth rate and nitrogenase activity of *Rhodobacter capsulatus* grown with or without molybdenum. Microbiology-USSR 65(4):436-441.

Tsygankov AA, Laurinavichene TV. 1996b. Influence of the degree and mode of light limitation on growth characteristics of the Rhodobacter capsulatus continuous cultures. Biotechnology and Bioengineering 51:605-612.

Tsygankov AA, Laurinavichene TV, Gogotov I, Asada Y, Miyake J. 1996. Switching from light limitation to ammonium limitation in chemostat cultures of *Rhodobacter capsulatus* grown in different types of photobioreactor. Journal of Marine Biotechnology 4:43-46.

van der Sluis C, Westerink BH, Dijkstal MM, Castelein SJ, Boxtel AJB, Giuseppin MLF, Tramper J, Wijffels RH. 2001a. Estimation of steady-state culture characteristics during acceleration-stats with yeasts. Biotechnology and Bioengineering 75(3):267-275.

van der Sluis C, Westerink BH, Dijkstal MM, Castelein SJ, van Boxtel AJB, Giuseppin MLF, Tramper J, Wijffels RH. 2001b. Estimation of steady-state culture characteristics during acceleration-stats with yeasts. Biotechnology and Bioengineering 75(3):267-275.

Van Groenestijn JW, Hazewinkel JHO, Nienoord M, Bussmann PJT. 2002. Energy aspects of biological hydrogen production in high rate bioreactors operated in the thermophilic temperature range. International Journal of Hydrogen energy 27(11-12):1141-1147.

van Niel EWJ, Budde MAW, de Haas GG, van der Wal FJ, Claassen PAM, Stams AJM. 2002. Distinctive properties of high hydrogen producing extreme thermophiles, *Caldicellulosiruptor saccharolyticus* and *Thermotoga elfii*. International Journal of Hydrogen energy 27 1391 - 1398

Vejrazka C, Janssen M, Streefland M, Wijffels RH. 2011. Photosynthetic efficiency of *Chlamydomonas reinhardtii* in flashing light. Biotechnology and Bioengineering 108(12):2905-2913.

Vignais PM, Billoud B. 2007. Occurrence, classification, and biological function of hydrogenases: An overview. Chemical Reviews 107(10):4206-4272.

Vincenzini M, Materassi R, Tredici MR, Florenzano G. 1982. Hydrogen production by immobilized cells - I. Light dependent dissimilation of organic substances by *Rhodopseudomonas palustris* International Journal of Hydrogen energy 7(3):231-236.

von Stockar U, Gustafsson L, Larsson C, Marison I, Tissot P, Gnaiger E. 1993. Thermodynamic considerations in constructing energy balances for cellular growth. Biochimica et Biophysica Acta 1183:221-240.

Wall JD, Love J, Quinn SP. 1984. Spontaneous Nif$^-$ mutants of *Rhodopseudomonas capsulata* Journal of Bacteriology 159 (2):652 - 657

Webb WL, Newton M, Starr D. 1974. Carbon dioxide exchange of *Alnus rubra* - A mathematical model. Oecologia 17(4):281-291.

Weckesser J, Mayer H, Schulz G. 1995. Anoxygenic phototrophic bacteria: model organisms for studies on cell wall macromolecules. In: Blankenship RE, Madigan MT, Bauer C, editors. Anoxygenic phototrophic bacteria. Dordrecht: Kluwer. p 207-230.

Wijffels RH, Barbosa MJ. 2010. An outlook on microalgal biofuels. Science 329(5993):796-799.

Wilhelm C, Jakob T. 2011. From photons to biomass and biofuels: evaluation of different strategies for the improvement of algal biotechnology based on comparative energy balances. Applied Microbiology and Biotechnology 92(5):909-919.

Williams PJlB, Laurens LML. 2010. Microalgae as biodiesel & biomass feedstocks: Review & analysis of the biochemistry, energetics & economics. Energy and Environmental Science 3(5):554-590.

Willison JC, Jouanneau Y, Colbeau A, Vignais P. 1983. H_2 metabolism in photosynthetic bacteria and relationship to N_2 fixation. Annales de Microbiologie 134 B:115-135.

Wormit M, Dreuw A. 2007. Quantum chemical insights in energy dissipation and carotenoid radical cation formation in light harvesting complexes. Physical Chemistry Chemical Physics 9(23):2917-2931.

Wraight CA, Clayton RK. 1974. The absolute quantum efficiency of bacteriochlorophyll photooxidation in reaction centres of *Rhodopseudomonas spheroides*. Biochimica et Biophysica Acta 333(2):246-260.

Wu X, Merchuk JC. 2001. A model integrating fluid dynamics in photosynthesis and photoinhibition processes. Chemical Engineering Science 56:3527-3538.

Yagi K, Maeda I, Idehara K, Miura Y, Akano T, Fukatu K, Ikuta Y, Nakamura K. 1994. Removal of inhibition by ammonium ion in nitrogenase dependent hydrogen evolution of a marine photosynthetic bacterium, *Rhodopseudomona*s sp. strain W-1S. Applied Biochemistry and Biotechnology 45/46:429-436.

Yakunin AF, Hallenbeck PC. 1998. Short-term regulation of nitrogenase activity by NH_4^+ in *Rhodobacter capsulatus* : multiple in vivo nitrogenase responses to NH_4^+ addition Journal of Bacteriology 180 (23):6392 - 6395

Yamada A, Hatano T, Matsunaga T, Zaborsky OR. 1998. Conversion efficiencies of light energy to hydrogen by a novel Rhodovulvum sp. and its uptake-hydrogenase mutant. Biohydrogen. London: Plenum Press. p 167-172.

Yee L, Blanch HW. 1993. Defined media optimization for growth of recombinant *Escherichia coli* X90. Biotechnology and Bioengineering 41(2):221-230.

Yoch DC. 1978. Nitrogen fixation and hydrogen metabolism by photosynthetic bacteria. In: Clayton RK, Sistrom WR, editors. The photosynthetic bacteria. New York: Plenum Press. p 657-676.

Yoch DC, Arnon DI. 1975. Comparison of two ferredoxins from *Rhodospirillum rubrum* as electron carriers for the native nitrogenase. Journal of Bacteriology 121(2):743-745.

Yoshino F, Ikeda H, Masukawa H, Sakurai H. 2007. High photobiological hydrogen production activity of a *Nostoc* sp. PCC 7422 uptake hydrogenase-deficient mutant with high nitrogenase activity. Marine Biotechnology 9(1):101-112.

Zajic JE, Kosaric N, Brosseau JD. 1978. Microbial production of hydrogen. Adv Biochem Eng 9:57-109.

Zhao J, Wang A, Green MA, Ferrazza F. 1998. 19.8% efficient "honeycomb" textured multicrystalline and 24.4% monocrystalline silicon solar cells. Applied Physics Letters 73(14):1991-1993.

Zhu H, Wakayama T, Suzuki T, Asada Y, Miyake J. 1999. Entrapment of *Rhodobacter sphaeroides* RV in cationic polymer/agar gels for hydrogen production in the presence of NH_4^+ Journal of Bioscience and Bioengineering 88(5):507-512.

Zijffers JW, Schippers KJ, Zheng K, Janssen M, Tramper J, Wijffels RH. 2010. Maximum photosynthetic yield of green microalgae in photobioreactors. Marine Biotechnology 12(6):708-718.

Zijffers JWF. 2009. The Green Solar Collector: optimization of microalgal areal productivity [PhD thesis]. Wageningen: Wageningen University. 156 p.

Zorin NA, Lissolo T, Colbeau A, Vignais PM. 1996. Increased hydrogen photoproduction by *Rhodobacter capsulatus* strains deficient in uptake hydrogenase. Journal of Marine Biotechnology 4:28-33.

Zou N, Richmond A. 2000. Light-path length and population density in photoacclimation of Nannochloropsis sp. (Eustigmatophyceae). Journal of Applied Phycology 12:349-354.

Zumft WG, Castillo F. 1978. Regulatory properties of the nitrogenase from *Rhodopseudomonas palustris* Archives of Microbiology 117 53 - 60

Zürrer H, Bachofen R. 1979. Hydrogen production by the photosynthetic bacterium *Rhodospirillum rubrum* Applied and Environmental Microbiology 37(5):789-793.

Zürrer H, Bachofen R. 1982. Aspects of growth and hydrogen production of the photosynthetic bacterium *Rhodospirillum rubrum* in continuous culture. Biomass 2:165-174.

Summary

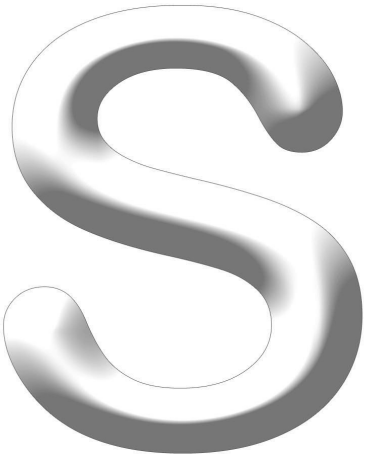

Summary

The rising global energy demand, depleting fossil fuel reserves and the negative impact of the combustion of fossil fuels on our environment increase the need for clean and renewable energy sources. These clean and renewable energy sources will most probably be based on solar energy. One of the possibilities for applying solar energy for the generation of clean and renewable energy is the conversion of sugars from energy crops like *Sorghum* into the energy carrier hydrogen. For the complete conversions of sugars from biomass to hydrogen, a two–step biological process was proposed. In the first step, fermentative microorganisms convert the sugars that are liberated from the biomass by enzymatic treatment to hydrogen and organic acids. In the second step, these organic acids are converted into additional hydrogen by phototrophic fermentation.
This thesis describes the process development of the second step, the conversion of acetate and light energy to molecular hydrogen by the purple non sulfur bacterium *Rhodobacter capsulatus*.

The development of the process of photobiological hydrogen production requires a substantial amount of information on the bacterium and its response to variations in process conditions. This information was acquired mostly by continuously illuminated chemostat cultivations. Traditionally, continuous bioprocesses are studied by chemostat experiments. During each chemostat, the level of the parameter under investigation is changed. After each change, a new steady state needs to be established, which is time consuming. Another method for studying the influence of the dilution rate on a continuous process is a D-stat. During a D-stat, the dilution rate is slowly decreased in time.
With the aim of finding the maximum biomass output rate, both experimental methods were simulated in a mathematical model that describes photo-acclimation and biomass productivity as a function of the local light intensity in a photobioreactor. The

physiological properties of the diatoms *Thalassiosira pseudonana* and *Phaeodactylum tricornutum* were used for generating the model output.

Even at higher change rates of the dilution rate, when the culture was clearly not in steady state, D-stats simulations still resulted in the successful determination of the maximum biomass output rate, resulting in a reduction of required time of up to 94%.

Having confirmed the applicability of the D-sat approach a fully controlled flat panel photobioreactor was designed and constructed as the cultivation system for purple non sulfur bacteria. The limited optical path (30 mm), combined with turbulent mixing, facilitates the proper illumination of the entire culture, which is required in order to prevent non-productive dark zones. Additionally, the mathematical description of light transfer towards a flat panel photobioreactor is easier than alternative geometries.

The PBR was constructed from a stainless steel frame and transparent polycarbonate sheets, facilitating autoclaving for axenic culturing.

A light energy balance was constructed for photobiological hydrogen production by *R. capsulatus* continuous cultures in the flat panel photobioreactor. The required kinetic parameters in the light energy balance were determined by the use of the D-stat method, as it saves significant amounts of time. The balance allocates the total absorbed light to biomass synthesis, biomass maintenance, non-photochemical quenching and hydrogen production.

In order to determine the four fractions in the balance, the biomass yield on light energy and the maintenance coefficient were determined to be $3.8 \pm 0.03 \cdot 10^{-8}$ kg·J^{-1} and 71.6 ± 11.3 W·kg^{-1}. This experiment was done at low light intensity at the reactor surface (8.4 W·m^{-2}) and under non-hydrogen producing conditions, using acetate as the electron donor. Subsequently, the fraction of light that was absorbed by the culture but not used for photosynthesis was determined to be 0.85 - 0.90, increasing with increasing biomass concentration. This experiment was executed at high light intensity at the reactor surface (410 W·m^{-2}), under non-hydrogen producing conditions.

The maximal specific hydrogen production rate of nitrogen limited continuous cultures of *R. capsulatus* was required to do predictions for the light to hydrogen conversion efficiency of the system. The maximal specific hydrogen production rate was determined to be 0.52 ± 0.02 mmol·kg^{-1}·s^{-1}.

The biomass yield on light energy, the maintenance coefficient, the fraction of the absorbed light that was not used for the photosynthetic process and the maximal specific hydrogen production rate were used to predict the light to hydrogen conversion efficiency at a given mode of operation (a combination of the dilution rate and the biomass concentration). A peak in predicted conversion efficiency was found at the combination of a dilution rate of 0.1 d^{-1} with a biomass concentration of 2.55 kg·m^{-3}, in which case the system should be capable of converting light energy to hydrogen with an efficiency of 3.3% at high light intensity at the reactor surface (410 W·m^{-2}). Only the light to hydrogen conversion efficiency is considered here, excluding the energy content of the other (organic) substrates.

The potential of *R. capsulatus* chemostat cultures for converting light energy into hydrogen energy was then investigated in the developed photobioreactor, at high light intensity at the reactor surface (410 W·m^{-2}), in order to validate the light energy balance developed previously.

First, a D-stat was executed that had an initial dilution rate of 1.0 d^{-1} and a final dilution rate of 0 d^{-1} (ending as a batch cultivation), aiming at a constant biomass concentration of 4.0 kg·m^{-3}. The maximal specific hydrogen production rate never exceeded 0.11 mmol·kg^{-1}·s^{-1}, a much lower value than measured previously (0.52 ± 0.02 mmol·kg^{-1}·s^{-1}). Probably, the high biomass concentration limited the average availability of light, and with it the maximal specific hydrogen production rate. This resulted in a volumetric hydrogen production rate remaining at 0.6 mmol·m^{-3}·s^{-1}, which is well below the predicted 1.3 mmol·m^{-3}·s^{-1}.

In order to investigate this discrepancy further, a gradient (G)-stat was executed in which the supply of the nitrogen source (ammonium) was slowly increased in a nitrogen limited culture. The initial specific hydrogen production rates were comparable to results obtained previously. The biomass concentration increased from 0.7 to 4.0 $g \cdot L^{-1}$ during the course of the experiment, at a constant dilution rate of 0.4 d^{-1}. Up to a biomass concentration of 1.5 $g \cdot L^{-1}$, the volumetric hydrogen production rate of the system increased according to model predictions. At this point, the system converted light energy into hydrogen energy at an efficiency of 1.6%. At higher culture densities, the volumetric hydrogen production rate commenced to decline, due to a decline in the specific hydrogen production rate.

The obtained results provide strong evidence that the observed decline in volumetric hydrogen production rate at higher biomass concentrations was at least partly caused by a decrease in light availability.

During the optimization of a photobiological hydrogen production using purple non-sulfur bacteria, several factors need to be considered as they directly influence the economic feasibility of such a process.

First, the construction of the photobioreactor should be inexpensive and simple, but at the same time facilitate light transfer to the entire culture. This can be achieved by a system that dilutes the incident light intensity to a level that can be adsorbed by the culture without oversaturation near the surface and light limitation along the optical light path.

Second, the applied micro-organism should retain its (near) maximal specific hydrogen production rate under the proposed mode of operation. Because the maximal specific hydrogen production rate decreases as the local light intensity decreases below a certain level, this level should be investigated and culture densities should be chosen that support this level in the complete photobioreactor. The maximal specific hydrogen production rate of a purple non-sulfur bacterium is mainly caused by its nitrogenase activity. The

nitrogenase activity of a purple non sulfur bacterium can be influenced by genetic engineering. This goal can be achieved by increasing the availability of light, as a result of a decrease in the size of the light harvesting complex. Another approach is to take away alternative routes the microorganism has to vent reducing equivalents (for instance the intracellular storage of PHB) or to recycle molecular hydrogen once it has been produced (for instance the activity of uptake hydrogenases). Several cyanobacterial and algal species have been shown to produce hydrogen photoautotrophically. These microorganisms produce hydrogen by hydrogenases. As, contrary to nitrogenases, hydrogenases have no energy requirement for their catalytic activity, their application has a great potential.

Finally, the mode of operation in terms of dilution rate and biomass concentration should be chosen using a light energy balance. With it, light expenditures for biomass production and maintenance, as well as light absorption that does not result in photosynthetic activity can be taken into account during the process optimization for the light to hydrogen conversion efficiency of the system.

Although photobiological systems for the conversion of light to hydrogen energy have shown great potential, their commercial viability has not been demonstrated and their future remains uncertain. The present study demonstrates that in this field of research, stat experiments are very useful. Their use has been demonstrated both during the determination of model parameters and both the optimization and validation of the process. Also a light energy balance for absorbed light is very useful in order to gain process insight and to make rational process optimization decisions.

Samenvatting

Samenvatting

De stijgende globale energiebehoefte, de uitgeput-rakende fossiele brandstofreserves en de negatieve invloed die de verbranding van fossiele brandstoffen heeft op ons milieu vergroten de behoefte aan schone en hernieuwbare energie bronnen. Deze schone en hernieuwbare energiebronnen zullen hoogstwaarschijnlijk gebaseerd zijn op zonne-energie. Een van de mogelijkheden van toepassing van zonne-energie voor het opwekken van schone en hernieuwbare energie is de conversie van suikers uit energiegewassen zoals *Sorghum* in de energiedrager waterstof. De volledige conversie van suikers uit biomassa naar waterstof kan worden uitgevoerd met een proces dat uit twee stappen bestaat. In de eerste stap worden de suikers die zijn vrijgekomen na enzymatische behandeling van de biomassa door fermentatieve micro-organismen omgezet in waterstof en organische zuren. In de tweede stap worden deze organische zuren ook nog omgezet in waterstof door middel van fototrofe fermentatie.
In dit proefschrift wordt de ontwikkeling van de tweede processtap, de conversie van acetaat en licht energie naar moleculaire waterstof door de paarse niet-zwavelbacterie *Rhodobacter capsulatus*, beschreven.

De ontwikkeling van het proces van foto-biologische waterstof productie vereist een aanzienlijke hoeveelheid informatie over de bacterie en zijn reactie op variaties in de procesomstandigheden. Deze informatie is hoofdzakelijk verkregen met behulp van continu-belichte chemostaat kweken. Continue bioprocessen worden van oudsher bestudeerd met behulp van chemostaat experimenten. Tijdens elke chemostaat wordt de ingestelde waarde van de te onderzoeken parameter gewijzigd. Na iedere wijziging moet een nieuwe steady state worden bereikt, wat tijdrovend is. Een andere manier om de invloed van de verdunningssnelheid op een continu proces te bestuderen is een D-stat. Tijdens een D-stat wordt de verdunningssnelheid gedurende het experiment langzaam verlaagd.

Een mathematisch model dat foto-acclimatie en biomassa productiviteit als functie van de plaatselijke lichtintensiteit in een fotobioreactor beschrijft werd gebruikt om beide experimentele methoden, chemostaat en D-stat, te simuleren. Het doel van deze simulaties was vast te stellen wat de maximale biomassa productie snelheid van het systeem is en hoeveel tijd het kost om deze maximale biomassa productie snelheid experimenteel vast te stellen. De fysiologische eigenschappen van de diatomeeën *Thalassiosira pseudonana* en *Phaeodactylum tricornutum* werden gebruikt om de model resultaten te genereren.

Zelfs als de verdunningssnelheid snel werd veranderd, waarbij de cultuur duidelijk niet in steady state was, kon de maximale biomassa productiesnelheid toch nog succesvol bepaald worden. Dit resulteerde in een verlaging van de benodigde tijd tot wel 94%.

Nadat de toepasbaarheid van de D-stat experimentele methode was bevestigd werd een volledig geautomatiseerde vlakke plaat fotobioreactor ontworpen en gebouwd. Deze werd gebruikt als kweeksysteem voor paarse niet-zwavel bacteriën. Het beperkte optische pad (30 mm), gecombineerd met turbulente menging, maakte belichting van de gehele cultuur mogelijk. Dit is van belang ter voorkoming van niet-productieve donkere zones in de fotobioreactor. Daarnaast is de overdracht van licht naar een vlakke plaat eenvoudiger te beschrijven dan in het geval van andere geometrieën.

De fotobioreactor bestond uit een roestvaststalen frame en transparante polycarbonaat platen, waardoor het systeem kon worden geautoclaveerd en gebruikt voor steriele cultivaties.

Een lichtenergiebalans is opgesteld voor foto-biologische waterstofproductie door continu cultures van *R. capsulatus* in de vlakke-plaat fotobioreactor. De benodigde kinetische parameters in de lichtenergiebalans zijn bepaald met behulp van de D-stat methode, omdat op die manier veel tijd bespaard kon worden. De balans verdeelt het geabsorbeerde licht over biomassasynthese, biomassaonderhoud, niet-fotochemische uitdoving en waterstofproductie.

Om de vier fracties in de balans te kunnen kwantificeren, werden de coëfficiënten voor biomassaopbrengst ($3.8 \pm 0.03 \cdot 10^{-8}$ kg·J^{-1}) en biomassaonderhoud (71.6 ± 11.3 W·kg^{-1}) bepaald. Dit experiment werd uitgevoerd bij lage lichtintensiteit aan het reactoroppervlak (8.4 W·m^{-2}) en onder niet-waterstof-producerende condities, met acetaat als elektrondonor. Vervolgens werd de fractie geabsorbeerd licht die door de cultuur werd geabsorbeerd, maar niet werd gebruikt voor fotosynthese, bepaald. Deze fractie bedroeg 0.85-0.90 en nam toe met de biomassaconcentratie. Dit experiment werd uitgevoerd bij hoge licht intensiteit aan het reactor oppervlak (410 W·m^{-2}), onder niet-waterstof-producerende condities.

De maximale specifieke waterstofproductiesnelheid van stikstof-gelimiteerde continu cultures van *R. capsulatus* was benodigd om de licht naar waterstof conversie-efficiëntie van het systeem te voorspellen en werd vastgesteld op 0.52 ± 0.02 mmol·kg^{-1}·s^{-1}.

De biomassaopbrengst op lichtenergie, de biomassaonderhoudscoëfficiënt, de fractie geabsorbeerd licht die niet gebruikt wordt voor fotosynthese en de maximale specifieke waterstofproductiesnelheid werden vervolgens gebruikt om de licht naar waterstof conversie-efficiëntie te voorspellen, als functie van de opgelegde verdunningssnelheid en biomassaconcentratie. Deze conversie-efficiëntie vertoont een piek bij een verdunningssnelheid van 0.1 d^{-1} en een biomassa concentratie van 2.55 kg·m^{-3}. In deze situatie zou het systeem in staat moeten zijn om bij hoge lichtintensiteit (410 W·m^{-2}) lichtenergie naar waterstofenergie om te zetten met een efficiëntie van 3.3%. De energie-inhoud van andere (organische) substraten en producten is hier buiten beschouwing gelaten.

De werkelijke capaciteit van *R. capsulatus* chemostaat cultures om lichtenergie om te zetten in waterstof energie is vervolgens onderzocht in de eerder ontwikkelde fotobioreactor, bij hoge lichtintensiteit aan het reactoroppervlak (410 $W \cdot m^{-2}$), ten behoeve van validatie van de lichtenergiebalans.

Eerst werd hiertoe een D-stat uitgevoerd met een initiële verdunningssnelheid van 1.0 d^{-1} en een uiteindelijke verdunningssnelheid van 0 d^{-1} (uitlopend in een batch cultivatie) bij een constante biomassa concentratie van 4.0 $kg \cdot m^{-3}$. De maximale specifieke waterstofproductiesnelheid kwam niet boven de 0.11 $mmol \cdot kg^{-1} \cdot s^{-1}$, een veel lagere waarde dan eerder gemeten (0.52 ± 0.02 $mmol \cdot kg^{-1} \cdot s^{-1}$). Waarschijnlijk veroorzaakte de hoge biomassaconcentratie een beperking in de beschikbaarheid van licht, en daarmee ook in de maximale specifieke waterstofproductiesnelheid. Deze observatie resulteerde in een volumetrische waterstofproductiesnelheid van 0.6 $mmol \cdot m^{-3} \cdot s^{-1}$, hetgeen ook ruim onder de voorspelde 1.3 $mmol \cdot m^{-3} \cdot s^{-1}$ is.

Om deze discrepantie verder te onderzoeken werd een gradiënt (G)-stat uitgevoerd waarbij de toevoer van de stikstof bron (ammonium) aan een stikstof-gelimiteerde cultuur langzaam werd verhoogd. De initiële specifieke waterstofproductiesnelheid was vergelijkbaar met eerder verkregen resultaten. Gedurende het experiment steeg de biomassaconcentratie van 0.7 tot 4.0 kg m^{-3}, bij een constante verdunningssnelheid van 0.4 d^{-1}. Tot aan een biomassaconcentratie van 1.5 $kg \cdot m^{-3}$ steeg de volumetrische waterstof productie snelheid conform de modelvoorspellingen. Op dit moment zette het systeem lichtenergie om in waterstofenergie met een efficiëntie van 1.6%. Bij hogere biomassaconcentraties begon de volumetrische waterstofproductiesnelheid af te nemen, door een afname in de specifieke waterstofproductiesnelheid.

De verkregen resultaten verschaffen sterk bewijs dat de waargenomen afname in volumetrische waterstofproductiesnelheid bij hogere biomassaconcentraties, op zijn minst ten dele, veroorzaakt werd door een afname in beschikbaarheid van licht.

Bij de optimalisatie van foto-biologische waterstofproductie met behulp van paarse niet-zwavel bacteriën moeten diverse factoren beschouwd worden, omdat ze de economische haalbaarheid van een dergelijk proces direct beïnvloeden.

Allereerst moet de constructie van de fotobioreactor goedkoop en eenvoudig zijn, maar tegelijkertijd moet ervoor worden gezorgd dat de gehele cultuur goed wordt belicht. Dit zou kunnen worden bereikt door toepassing van een systeem dat het licht verdunt tot een niveau waarbij adsorptie door de cultuur niet leidt tot oververzadiging bij het oppervlak en lichtlimitatie dieper in de fotobioreactor.

Ten tweede moet het toegepaste micro-organisme dicht bij zijn maximale specifieke productiesnelheid waterstof kunnen produceren bij de gekozen procesomstandigheden. Omdat de maximale specifieke waterstofproductiesnelheid beneden een bepaalde lichtintensiteit afneemt, moet worden bepaald bij welke lichtintensiteit dit gebeurt en vervolgens moet de biomassaconcentratie zo gekozen worden dat deze lichtintensiteit in de volledige fotobioreactor gegarandeerd is. De maximale specifieke waterstofproductiesnelheid van een paarse niet-zwavelbacterie wordt vooral bepaald door zijn nitrogenase-activiteit. Deze nitrogenase-activiteit kan worden verhoogd door middel van genetische modificatie. Dit doel kan worden bereikt door verkleining van het licht-invangend complex, wat resulteert in een verhoging van de beschikbaarheid van licht. Een andere benadering is het wegnemen van alternatieve routes die het micro-organisme ter beschikking heeft om reductie-equivalenten kwijt te raken (bijvoorbeeld intracellulaire opslag van PHB) of om juist waterstof te recyclen als het al is geproduceerd (bijvoorbeeld de activiteit van opname hydrogenases). Voor enkele cyanobacteriën en algen is aangetoond dat zij in staat zijn om foto-autotroof waterstof te produceren. Deze micro-organismen produceren waterstof met behulp van hydrogenases. Omdat hydrogenases, in tegenstelling tot nitrogenases, geen energie nodig hebben voor hun katalytische activiteit, hebben hun toepassing veel potentie.

Als laatste dient de manier waarop het proces wordt bedreven (de keuze voor een verdunningssnelheid en biomassaconcentratie) te zijn gebaseerd op een lichtenergiebalans. Met behulp van een dergelijke balans kan bij de procesoptimalisatie

van de licht naar waterstof conversie-efficiëntie van een systeem rekening worden gehouden met de fracties van het geabsorbeerde licht die worden gebruikt voor productie en onderhoud van biomassa en het licht dat geabsorbeerd wordt maar niet resulteert in fotosynthetische activiteit.

Alhoewel foto-biologische systemen voor de conversie van licht- naar waterstofenergie hun potentie hebben laten zien, is hun commerciële levensvatbaarheid nog niet aangetoond en blijft hun toekomst onzeker. De huidige studie laat zien dat stat-experimenten in dit werkveld erg nuttig zijn. Hun toepasbaarheid is aangetoond bij het bepalen van modelparameters en bij de optimalisatie en validatie van het proces. Ook een lichtenergiebalans is erg nuttig om inzicht in het proces te verkrijgen en om op rationele wijze procesoptimalisatie-beslissingen te kunnen nemen.

Dankwoord

Het is inmiddels een behoorlijke tijd geleden dat ik in het Biotechnion op de zesde verdieping bij Proceskunde bezig was met mijn promotie onderzoek. Evengoed kijk ik (ver) terug op een uitdagende maar vooral leuke tijd, waarin ik heel erg veel heb geleerd, zowel tijdens het doen van het onderzoek als tijdens het schrijven van het proefschrift. Beide waren enkel mogelijk met de hulp van en samenwerking met een boel personen. Hiervoor ben ik onbeschrijfelijk dankbaar, maar toch zal ik hier, volgens de consensus, een poging wagen.

René, zoals je weet had ik vooral met het richting geven aan wat er moest gebeuren in vier jaar, op weg naar een proefschrift, veel moeite. Ik denk dat jij meer vertrouwen had in een goede afloop dan ikzelf. Met alle positieve energie van jouw pep talks kon ik altijd wel weer even vooruit! Eind goed, al goed.
Marcel, jouw geduld, kennis, inzicht en enthousiasme hebben mij heel erg goed vooruit geholpen, ik heb door de jaren heen bijzonder veel waardering voor jou gekregen. Met een kritische en positieve blik was jouw commentaar op mijn werk en artikelen vrijwel altijd zeer nuttig. Bedankt voor je vertrouwen!
Hans, ook jij hebt veel ondernomen om mijn motivatie het proefschrift af te ronden op peil te houden, vooral in de laatste fase. Ook bij het schrijven (met quotes als ‘sorry maar dit begrijp ik echt niet’) wist je me altijd uit te dagen om meer te verduidelijken en meer structuur aan te brengen.
Arjen, dankzij jou ben ik natuurlijk bij proceskunde komen werken als onderzoeker op vaste stof fermentatie; ik was blij met die mogelijkheid. Ik heb jouw hulp bij het tot stand brengen van het tweede hoofdstuk van mijn proefschrift ook bijzonder gewaardeerd.

Ik deelde eerst een kamer met Marcel en Maria, en later met Eduard, Tim, Mohammad en Jan-Willem. Er was altijd tijd voor een goed gesprek, en een grap op zijn tijd. Mede

daardoor heb ik me altijd erg thuis gevoeld bij proceskunde. Ook alle gezellige activiteiten, zoals de filmavonden, kerstdiners, labuitjes en borrels die georganiseerd werden, hebben daar zeker aan bijgedragen, het was altijd een gezellige boel!

En dan niet te vergeten de andere mariene biotechnologen van de vakgroep uit die tijd: Rouke, Ronald, Detmer, Mohammad, Eira en Wim. Dank voor jullie enthousiasme! Ronald en Detmer: dank voor de proceskunde squashladder en de 'squashles' die ik van jullie kreeg. Rouke, dank voor jouw tomeloze enthousiasme en bereidheid mee te denken als ik weer eens met lichtdistributie modellen bezig was.

Hylke en Olivier, bedankt voor de vele technisch inhoudelijke lunch wandelingen door het arboretum.

Pieter, wat wist jij altijd een gevatte opmerkingen te produceren bij vrijwel elke gelegenheid. Met Rouke op de kamer vormden jullie een zeer geslaagd humoristisch koppel. Chapeau!

Er gaat ook veel dank uit naar de studenten die ik met veel plezier heb mogen begeleiden: Martijn, David, Simon, Tom, Rutger en Frank. Dank voor jullie tomeloze inzet tijdens het bedenken en uitvoeren van velerlei experimenten, ik vond het zeer plezierig om met jullie samen te werken en ik heb er een boel van opgestoken.

Jan en André van de werkplaats, Frans, Rouke, Fred, Maurice en Sebastiaan: dank dat jullie altijd klaar stonden en meedachten bij alle uitdagingen tijdens het bouwen van reactoren en opstellingen en het opzetten van diverse analyses.

Jan en Stan, ik ben blij dat jullie bij de verdediging van dit proefschrift samen met mij op het podium plaats willen nemen. Dank voor jullie vriendschap, enthousiasme en vertrouwen.

Erik, jij had goed door dat ik het proefschrift graag af wilde ronden maar daar, gezien een drukke baan bij MSD, te weinig tijd voor had. Dank voor jouw steun, de extra tijd die jij voor me regelde in onze tijd bij TCB was cruciaal voor de tot stand koming van dit proefschrift.

En uiteraard - *last but not least* - mijn familie. Aan mijn ouders: ik wil jullie op deze plek graag bedanken voor de stimulans te gaan studeren en alle steun, vertrouwen en interesse tijdens mijn studie. Jullie uitspraak 'als het goed gaat en je wilt verder, dan ga je gewoon door', gaf mij een goede stimulans zonder enige verplichting. Aan mijn broers Jeroen en Tjeerd: dank voor jullie interesse. Tjeerd, jou wil ik in het bijzonder bedanken voor het ontwerpen van de mooie kaft van dit proefschrift.

Publications

Hoekema S, Bijmans M, Janssen M, Tramper J, Wijffels RH. 2002. A pneumatically agitated flat-panel photobioreactor with gas re-circulation: anaerobic photoheterotrophic cultivation of a purple non-sulfur bacterium. International Journal of Hydrogen Energy 27:1331-1338.

Hoekema S, Douma, RD, Janssen M, Tramper J, Wijffels RH. 2006. Controlling light-use by *Rhodobacter capsulatus* continuous cultures in a flat-panel photobioreactor. Biotechnology and Bioengineering 95(4):613-626.

Hoekema S, van Breukelen, FR, Janssen M, Tramper J, Wijffels RH. 2009. Exploration of the hydrogen producing potential of R*hodobacter capsulatus* chemostat cultures: The application of deceleration-stat and gradient-stat methodology. Biotechnology Progress 25(5):1343-1352.

Hoekema S, Rinzema A, Tramper J, Wijffels RH, Janssen M. 2014. Deceleration-stats save much time during phototrophic culture optimization. Biotechnology and Bioengineering 111(4):792-802.

Training activities

Discipline specific

Courses

Matlab (the Mathsoft corp., 2001)

A unified approach to mass transfer (OSPT, 2002)

Advanced statistics (PE&RC, 2003)

Bio information technology (VLAG, 2004)

Meetings

Biohydrogen congress (process engineering, 2002)

OSPT meeting (OSPT, 2002)

Marine biotechnology: basics and applications (process engineering, 2003)

Bio-H meeting (2003)

International hydrogen energy congress and exhibition (IHEC, 2005)

COST meeting (COST, 2005)

General

Scientific writing (WUR, 2001)

Thesis supervision (WUR, 2001)

VLAG PhD week (VLAG, 2002)

Basic statistics (PE&RC, 2002)

Career perspectives (VLAG, 2005)

Optionals

Preparing PhD research proposal (2001)

PhD study trips to South Africa (2002) and Canada (2004)

Curriculum Vitae

Sebastiaan Hoekema was born on the 4th of May 1974 in The Hague. After spending his youth there, he got his diploma for secondary education in 1993. He started his BSc studies in environmental technology in Delft, for which he got his diploma in 1997. Right after that, he started on his MSc studies in bioprocess engineering at Wageningen University, for which he got his diploma in 2000.
His first real job started in 2000, as an added researcher at the department of process engineering at Wageningen University. One year later he started his PhD research at the same department.

Sebastiaan Hoekema werd op 4 mei 1974 geboren in Den Haag. Na zijn jeugd in Den Haag doorgebracht te hebben werd daar ook in 1993 het VWO diploma behaald. Hierna volgde de HBO studie milieutechnologie in Delft die hij in 1997 afrondde, waarna hij startte aan de studie bioprocestechnologie aan Wageningen Universiteit. Deze studie werd in 2000 afgerond.
Zijn eerste echte baan volgde in 2000, als toegevoegd onderzoeker bij de vakgroep proceskunde aan Wageningen Universiteit. Een jaar later startte hij aan zijn promotieonderzoek bij dezelfde vakgroep.

This work was financially supported by the Dutch Programme EET (Economy, Ecology and Technology), a joint initiative of the Ministries of Economic Affairs, Education, Culture and Sciences and of Housing, Spatial Planning and the Environment (project numbers EETK99116 and EETK03028).

Printed by GildePrint, Enschede, the Netherlands.

Cover design by Tjeerd Hoekema.